

A PARAMETRIC COMPARATIVE STUDY OF ELECTROCOAGULATION  
AND COAGULATION OF AQUEOUS SUSPENSIONS OF KAOLINITE AND  
QUARTZ POWDERS

A THESIS SUBMITTED TO  
THE GRADUATE SCHOOL OF NATURAL AND APPLIED SCIENCES  
OF  
MIDDLE EAST TECHNICAL UNIVERSITY

BY

MEHTAP GÜLSÜN KILIÇ

IN PARTIAL FULFILLMENT OF THE REQUIREMENTS  
FOR  
THE DEGREE OF DOCTOR OF PHILOSOPHY  
IN  
MINING ENGINEERING

DECEMBER 2009

Approval of the thesis:

**A PARAMETRIC COMPARATIVE STUDY OF ELECTROCOAGULATION  
AND COAGULATION OF AQUEOUS SUSPENSIONS OF KAOLINITE  
AND QUARTZ POWDERS**

submitted by **MEHTAP GÜLSÜN KILIÇ** in partial fulfillment of the requirements  
for the degree of **Doctor of Philosophy in Mining Engineering Department,**  
**Middle East Technical University** by,

Prof. Dr. Canan Özgen  
Dean, Graduate School of Natural and Applied Sciences \_\_\_\_\_

Prof. Dr. Ali İhsan Arol  
Head of Department, Mining Engineering \_\_\_\_\_

Prof. Dr. Çetin Hoşten  
Supervisor, Mining Engineering Dept., METU \_\_\_\_\_

**Examining Committee Members:**

Prof. Dr. Mustafa Ümit Atalay  
Mining Engineering Dept., METU \_\_\_\_\_

Prof. Dr. Çetin Hoşten  
Mining Engineering Dept., METU \_\_\_\_\_

Prof. Dr. Şahinde Demirci  
Chemistry Dept., METU \_\_\_\_\_

Prof. Dr. Ali İhsan Arol  
Mining Engineering Dept., METU \_\_\_\_\_

Dr. Nuray Karapınar  
General Directorate of Mineral Research and  
Exploration Technology Department \_\_\_\_\_

**Date:** 28.12.2009

**I hereby declare that all information in this document has been obtained and presented in accordance with academic rules and ethical conduct. I also declare that, as required by these rules and conduct, I have fully cited and referenced all material and results that are not original to this work.**

Name, Last name: Mehtap Gülsün KILIÇ

Signature :

## **ABSTRACT**

### **A PARAMETRIC COMPARATIVE STUDY OF ELECTROCOAGULATION AND COAGULATION OF AQUEOUS SUSPENSIONS OF KAOLINITE AND QUARTZ POWDERS**

Kılıç, Mehtap Gülsün

Ph.D., Department of Mining Engineering

Supervisor: Prof. Dr. Çetin Hoşten

December 2009, 139 pages

Mineral treatment processes generally produce wastewaters containing ultrafine and colloidal particles that cause pollution upon their discharge into environment. It is essential that they should be removed from the wastewater before discharge. This study was undertaken by using synthetic turbid systems containing kaolinite and quartz particles in water with the amount of 0.20 g/L and 0.32 g/L, respectively. Removal of the turbidity was tried in two ways; electrocoagulation with aluminum anode and conventional coagulation with aluminum sulfate. Several key parameters affecting the efficiency of electrocoagulation and coagulation were investigated with laboratory scale experiments in search of optimal parameter values. Optimal values of the parameters were determined on the basis of the efficiency of turbidity removal from ultrafine suspensions. The parameters investigated in the study were suspension pH, electrical potential, current density, electrocoagulation time, and

aluminum dosage. This study was also performed to compare electrocoagulation and conventional coagulation regarding the pH ranges under investigation and coagulant dosages applied.

A comparison between electrocoagulation and coagulation was made on the basis of total dissolved aluminum, revealing that electrocoagulation and coagulation were equally effective at the same aluminum dosage for the removal of ultrafine particles from suspensions. Coagulation was more effective in a wider pH range (pH 5-8) than electrocoagulation, which yielded optimum effectiveness in a relatively narrower pH range around 9. In both methods, these pH values corresponded to near-zero zeta potentials of coagulated kaolinite and quartz particles. The mechanism for both coagulation methods was aggregation through charge neutralization and/or enmeshment in aluminum hydroxide precipitates. Furthermore, the experimental results confirmed that electrocoagulation could display some pH buffering capacity. The kinetics of electrocoagulation was very fast (<10 min) in approaching a residual turbidity, which could be modeled with a second-order rate equation.

Keywords: Electrocoagulation, conventional coagulation, zeta potential, kaolinite suspension, quartz suspension, turbidity.

## ÖZ

### İNCE TANELİ KAOLİNİT VE KUVARS SÜSPANSİYONLARININ ELEKTROKOAGÜLASYONU VE KOAGÜLASYONU ÜZERİNE KARŞILAŞTIRMALI PARAMETRİK BİR ÇALIŞMA

Kılıç, Mehtap Gülsün

Doktora, Maden Mühendisliği Bölümü

Tez Yöneticisi: Prof. Dr. Çetin Hoşten

Aralık 2009, 139 sayfa

Cevher hazırlama işlemleri genellikle ince taneli ve koloidal maddeler içeren atıksular üretmekte ve bunlarda çevresel problemlere yol açmaktadırlar. Bu maddelerin çevreye atılmadan önce atıksulardan uzaklaştırılması gerekmektedir. Bu çalışmada, bir litre suda 0.20 g kaolinit ve yine 1 litre suda 0.32 gr kuvarsın kolloid olarak dağıtılmasıyla, sentetik olarak bulanık çözeltiler hazırlanmıştır. Hazırlanan çözeltilerdeki bulanıklık iki yolla giderilmeye çalışılmıştır. Birinde, alüminyum metali anot olarak kullanılıp alüminyum iyonları elde edilmiş ve bulanıklık yapan tanecikler koagüle edilmiş; diğerinde, alüminyum sülfat çözeltisi kullanılarak bulanıklık yaratan tanecikler koagüle edilmiştir. Elektrokoagülasyon ve koagülasyon yöntemlerinin verimliliklerini etkileyen parametreler laboratuvar çaplı deneyler ile araştırılmıştır. Çalışmada, süspansiyon pH'si, elektrik potansiyeli, akım yoğunluğu, elektrokoagülasyon zamanı ve alüminyum miktarları gibi değişkenlerin

etkileri incelenmiştir. Bu çalışmada aynı zamanda, çalışılan pH aralıkları ve uygulanan alüminyum miktarları göz önüne alınarak, elektrokoagülasyon ile konvansiyonel koagülasyon yöntemleri karşılaştırılmıştır.

Elektrokoagülasyon ve koagülasyon arasındaki karşılaştırma sistemde çözünen alüminyum miktarına göre yapılmış ve aynı alüminyum miktarlarında, süspansiyonlardan ince taneli maddelerin giderilmesinde, elektrokoagülasyon ve koagülasyonun aynı derecede etkili olduğu bulunmuştur. Bulanıklığın giderilmesinde, koagülasyon geniş bir pH aralığında (pH 5-8) etkilidir. Elektrokoagülasyon yönteminde bulanıklığın en fazla giderilmesi pH 9'da sağlanmıştır. Her iki yöntemde, bulanıklığın en çok giderilmesini sağlayan pH'lerde kaolinit ve kuvars taneciklerinin zeta potansiyelinin sıfıra yaklaştığı bulunmuştur. Elektrokoagülasyon ve koagülasyon mekanizması, yüzey yükünün nötralizasyonu ve/veya alüminyum hidroksit çökeleğinin oluşması ile açıklanmıştır. Deneysel sonuçlar, elektrokoagülasyonda pH tamponlama olayının olduğu görülmüştür. Elektrokoagülasyon kinetiği, çok hızlı bulunmuş (<10 dk) ve ikinci derece hız denklemi ile modellenmiştir.

Anahtar Kelimeler: Elektrokoagülasyon, koagülasyon, zeta potansiyel, kaolinit süspansiyonu, kuvars süspansiyonu, bulanıklık.

*To My Parents and My Husband*



## ACKNOWLEDGEMENTS

I would like to express my deepest gratitude to Prof. Dr. Çetin Hoşten for his guidance, advice, criticism, encouragement and insight throughout the research. I would like to thank the Prof. Dr. Ali İhsan Arol for his constructive suggestions and helpful discussions.

I also would like to express my sincere appreciation to Prof. Dr. Şahinde Demirci for her steady help, remarks, suggestions and sincere friendship during my study.

I would like to thank to Tahsin Işıksal, İsmail Kaya, Mehmet Çakır for their help during laboratory work.

I am particularly indebted to my friends, especially E. Pekpak, N. and K. Gedik, S. and Ş. Özün, S. Şalap, H. Mertürek, M. Çırak, B. Kıran, T. Tuzcu, and N. Zayım for their invaluable help, encouragement and support. I wish to express my thanks to all my colleagues in the Mining Engineering Department for their assistance, guidance, and support during this research.

I wish to express my special thanks to my mother Nilgün Gülsün, my father Nihat Gülsün, my sister Ebru, my nephew Mustafa, and Kılıç and Ünal families for their patience, support and love in every moment throughout my education.

And, with all my heart, I would also like to thank my beloved husband Bora Kılıç for his encouragement and support. It would not be possible for me to achieve this goal without his patience, understanding and unconditional support.

This study was supported by the BAP-2006-07-02-00-01.

## TABLE OF CONTENTS

ABSTRACT .....	iv
ÖZ .....	vi
ACKNOWLEDGEMENTS .....	ix
TABLE OF CONTENTS .....	x
LIST OF TABLES .....	xiii
LIST OF FIGURES.....	xiv
CHAPTERS	
1. INTRODUCTION.....	1
1.1 General Aspects of Wastewater Treatment .....	1
1.1.1 Coagulation .....	2
1.1.2 Electrocoagulation.....	3
1.2 Aim of the Study.....	6
2. PHYSICO-CHEMICAL PROPERTIES OF COLLOIDAL SYSTEMS .....	10
2.1 Particles in Aquatic Environment.....	10
2.2 Light Scattering and Turbidity .....	13
2.3 Origin of Charge on Particles .....	15
2.3.1 Electrical Double Layer .....	15
2.3.2 Effect of Electrolyte on the Electrical Double Layer.....	17
2.4 Interaction between Particles.....	19
2.4.1 Repulsion.....	20
2.4.2 The van der Waals Attraction.....	20
2.4.3 The Net Interaction Curve and Stability of Dispersed System .....	25
2.4.4 Zeta Potential.....	25
2.4.5 Coagulation .....	27

2.4.5.1 Hydrolyzing metal coagulants.....	29
2.4.6 Electrocoagulation.....	35
2.4.6.1 Description of the Technology.....	39
2.4.6.2 Previous Studies .....	43
3. MATERIALS AND METHODS.....	48
3.1 Materials and Characterization.....	48
3.2 Experimental Methods.....	52
4. RESULTS AND DISCUSSION .....	57
4.1 Material Characteristics.....	57
4.1.1 Kaolinite.....	57
4.1.2 Quartz.....	66
4.2 Electrocoagulation and Coagulation of Kaolinite and Quartz in Suspensions .....	73
4.2.1 Preliminary Testwork.....	75
4.2.1.1 The Effect of Stirring Rate, Electrode Distance and Ultrasonic Treatment on Electrocoagulation .....	75
4.2.1.2 The Effect of Time on Coagulation.....	78
4.2.1.3 Relationship between Current Density, Conductivity, Energy Consumption, Turbidity Removal Efficiency and Amount of Aluminum... ..	79
4.3 Effect of Initial pH on Electrocoagulation and Coagulation .....	83
4.3.1 Change in the Suspension pH during Electrocoagulation.....	89
4.4 Effect of Voltage on Electrocoagulation .....	91
4.5 Effect of Current Density and Time on Electrocoagulation .....	94
4.5.1 Effect of Current Density on Electrocoagulation.....	94
4.5.2 Effect of Time on Electrocoagulation .....	98
4.6 Effect of Aluminum Dosage on Electrocoagulation and Coagulation .....	103
5. CONCLUSIONS AND RECOMMENDATIONS .....	108
REFERENCES.....	112

## APPENDICES

A. PHYSICAL, CHEMICAL AND BIOLOGICAL CONSTITUENTS OF WASTEWATER.....	120
B. THE HYDROLYSIS OF ALUMINUM .....	124
C. ASTM C-837-81- STANDARD TEST METHOD FOR METHYLENE BLUE INDEX OF CLAY .....	130
D. PARTICLE SIZE DISTRIBUTION, XRD AND ZETA POTENTIAL DATA	132
CURRICULUM VITAE .....	138

## LIST OF TABLES

### TABLES

Table 3.1 Experimental variables for electrocoagulation and coagulation experiments. ....	55
Table 4.1 BET surface analysis of kaolinite. ....	59
Table 4.2 Elemental composition (%) of kaolinite. ....	59
Table 4.3 BET surface analysis of quartz. ....	67
Table 4.4 Elemental composition (as % of oxides) of quartz. ....	68
Table 4.5 Concentration of NaCl added (g/L) and the resultant changes in current density and conductivity in kaolinite suspension. ....	95
Table 4.6 The concentration of NaCl added (g/L) and the resultant changes in current density and conductivity in quartz suspension. ....	95
Table 4.7 Comparison of electrocoagulation and conventional coagulation in terms of aluminum added or produced and turbidity removal efficiency for kaolinite and quartz suspension. ....	107
Table A.1 Common analyses used to assess the constituents found in wastewater. ....	121
Table B.1 Calculation log concentration of aluminum species. ....	127
Table D.1 Particle size distribution data for kaolinite sample. ....	133
Table D.2 Kaolinite XRD data and ICDD card. ....	134
Table D.3 Kaolinite zeta potential data. ....	135
Table D.4 Particle size distribution data for quartz sample. ....	136
Table D.5 Quartz XRD data and ICDD card. ....	137
Table D.6 Quartz zeta potential data. ....	137

## LIST OF FIGURES

### FIGURES

Figure 2.1 Diffuse electrical double layer model according to Stern-Gouy-Chapman.....	18
Figure 2.2 Compression of double layer under the effect of electrolyte. $n_1 < n_2 < n_3$ . $n_1, n_2, n_3$ – electrolyte concentration. ....	19
Figure 2.3 Repulsive and attractive energy as a function of particle separation at three electrolyte concentrations.....	22
Figure 2.4 Net interaction energy as a function of particle separation. ....	24
Figure 2.5 The structure and the potential profile in a double layer of flat surface..	27
Figure 2.6 Destabilization and aggregation of particles.....	29
Figure 2.7 Hydrolysis of $Al^{3+}$ . (a) Hydrated aluminum cation. (Note: only 4 of 6 water molecules shown) (b) After loss of $H^+$ to give $Al(OH)^{2+}$ .....	31
Figure 2.8 Solubility diagram of aluminum hydroxide $Al(OH)_{3(s)}$ considering only monomeric aluminum species.....	33
Figure 2.9 Bench-scale electrocoagulation reactor with monopolar electrodes in parallel connection. ....	40
Figure 2.10 Bench-scale electrocoagulation reactor with monopolar electrodes in series connection .....	41
Figure 2.11 Bench-scale electrocoagulation reactor with bipolar electrodes in parallel connection. ....	42
Figure 3.1 Schematic diagram of electrocoagulation experimental setup (1) Power supply, (2) Magnetic stirrer, (3) Conductivity meter, (4) Voltmeter, (5) Ampermeter, (6) pH meter, (7) Turbidimeter, (8) Electrocoagulation cell, (9) Aluminum electrodes, (10) Stainless steel electrodes.....	54

Figure 3.2 Coagulation Unit (1) Magnetic Stirrer, (2) pH meter, (3) Conductivity meter, (4) Turbidimeter. ....	55
Figure 4.1 Particle size distribution of kaolinite. ....	58
Figure 4.2 XRD pattern of kaolinite sample (air dried). K: kaolinite, Q: quartz. ....	61
Figure 4.3 Infrared spectrum of the kaolinite. ....	62
Figure 4.4 The SEM micrograph kaolinite particles before coagulation. ....	63
Figure 4.5 The SEM micrograph of kaolinite particles after electrocoagulation. ....	63
Figure 4.6 The SEM micrograph of kaolinite particles after coagulation. ....	64
Figure 4.7 Zeta potential measurements of kaolinite sample at different pH. ....	66
Figure 4.8 Particle size distribution of quartz. ....	67
Figure 4.9 XRD pattern of quartz. ....	69
Figure 4.10 Infrared spectrum of quartz. ....	70
Figure 4.11 The SEM micrograph of quartz particles before coagulation. ....	71
Figure 4.12 The SEM micrograph of quartz particles after electrocoagulation. ....	71
Figure 4.13 The SEM micrograph of quartz particles after coagulation. ....	72
Figure 4.14 Zeta potential measurements of quartz sample at different pH. ....	73
Figure 4.15 The effect of stirring rate (rpm) on turbidity removal efficiency (pH: 9, 40 V; 10 min). ....	76
Figure 4.16 The effect of electrode distance (mm) between the electrodes on turbidity removal efficiency (pH: 9, 40 V; 10 min). ....	77
Figure 4.17 The effect of ultrasonic treatment on the electrocoagulation (pH: 9, 40 V; 10 min). ....	77
Figure 4.18 The effect of coagulation time on turbidity removal efficiency of kaolinite and quartz from suspension (15 mg Al/L; pH: 6.5). ....	78
Figure 4.19 The effect of conductivity on turbidity removal efficiency (pH: 9; 40 V; 10 min). ....	79
Figure 4.20 The effect of current density ( $A/m^2$ ) and conductivity ( $\mu S/cm$ ) on energy consumption and total dissolved aluminum ( $g\ Al/m^2$ ) in kaolinite suspension (pH:9; 40 V; 10 min). ....	81

Figure 4.21 The effect of current density ( $\text{A/m}^2$ ) and conductivity ( $\mu\text{S/cm}$ ) on energy consumption ( $\text{kwh/m}^3$ ) and amount of aluminum ( $\text{g Al/m}^2$ ) in quartz suspension (pH:9; 40 V; 10 min). ....	82
Figure 4.22 The effect of initial pH on the turbidity removal efficiency for kaolinite suspension (electrocoagulation: 40V; 10 min; coagulation 15 mg Al/L; 10 min)....	83
Figure 4.23 Zeta potential measurements after electrocoagulation (40 V; 10 min) and coagulation (15 mg Al/L; 10 min) of kaolinite suspension as a function of initial pH.....	85
Figure 4.24 Turbidity removal efficiency for electrocoagulation (40 V; 10 min) and coagulation (15 mg Al/L; 10 min) experiments at different initial pHs for quartz suspension. ....	86
Figure 4.25 Zeta potential measurements after electrocoagulation (40 V; 10 min) and coagulation (15 mg Al/L; 10 min) experiments at different initial pHs for quartz suspension. ....	87
Figure 4.26 pH change after electrocoagulation of kaolinite and quartz suspensions (40 V; 10 min). ....	91
Figure 4.27 The effect of applied voltage on current density and turbidity removal efficiency in the kaolinite suspension. ....	93
Figure 4.28 The effect of applied voltage on current density and turbidity removal efficiency in quartz suspension. ....	94
Figure 4.29 The effect of current density on turbidity removal efficiency for kaolinite and quartz suspensions (pH: 9; 40 V; 10 min). ....	97
Figure 4.30 The effect of electrocoagulation time on the turbidity removal efficiency of kaolinite from suspension and kaolinite concentration (g/L) in the suspension (pH: 9; 40 V; 20 $\text{A/m}^2$ ). ....	99
Figure 4.31 The effect of electrocoagulation time on the turbidity removal efficiency of kaolinite from suspension and kaolinite concentration (g/L) in the suspension (pH: 9; 40 V; 87 $\text{A/m}^2$ ). ....	100



Figure 4.32 The effect of electrocoagulation time on the turbidity removal efficiency of quartz from suspension and quartz concentration (g/L) in the suspension (pH: 9; 40 V; 20 A/m <sup>2</sup> ). .....	101
Figure 4.33 The effect of electrocoagulation time on the turbidity removal efficiency of quartz from suspension and quartz concentration (g/L) in the suspension (pH: 9; 40 V; 87 A/m <sup>2</sup> ). .....	102
Figure 4.34 The effect of aluminum dosage (mg/L) on kaolinite removal by electrocoagulation (pH: 9; 40 V; 10 min) and coagulation (pH: 6; 10 min). .....	104
Figure 4.35 The effect of aluminum dosage (mg/L) on quartz removal by electrocoagulation (pH: 9; 40 V; 10 min) and coagulation (pH: 6; 10 min). .....	105
Figure 4.36 Zeta potential measurement after kaolinite and quartz suspension coagulation as a function of aluminum dosage (pH: 6-6.5; coagulation time: 10 min). .....	106

# **CHAPTER 1**

## **INTRODUCTION**

### **1.1 General Aspects of Wastewater Treatment**

The materials in waters and wastewaters stem from land erosion, the mineral dissolution, the vegetation decay, and domestic and industrial waste discharges. Such materials may contain suspended and/or dissolved organic and/or inorganic materials, and various biological forms such as bacteria, algae, and viruses (Bratby, 2006). The main physical properties and the chemical and biological constituents of wastewater, and their sources, are reported in Appendix A. Total solid content, composed of floating, settleable, colloidal matters, and matter in solution, is the most important physical feature of wastewater (Tchobanoglous et al., 2003).

Wastewater treatment techniques include biological processes for nitrification, denitrification, and phosphorous removal and physico-chemical treatment processes for filtration, air stripping, ion-exchange, chemical precipitation, oxidation, carbon adsorption, ultrafiltration, reverse osmosis, electrodialysis, volatilization and gas stripping. The common physico-chemical processes such as coagulation and flocculation require addition of chemicals. Electrochemical technologies which include electrocoagulation, electroflotation, and electrodecantation do not require chemical additions (Mollah et al., 2001).

Mineral treatment processes generally produce wastewaters including suspended and colloidal particles, such as clay particles. Dewatering of waste clay mineral tailings is an important part of mining and mineral processing activities worldwide. For instance, clay tailings which arise from hydrometallurgical processing of mineral ores are always seen but cause problems in waste treatment and disposal (McFarlane et al., 2006). Dewatering of the clay tailings is commonly achieved through flocculated, gravity-assisted thickening processes (Mpofu et al., 2005).

Most colloidal particles are stable and remain in suspension, and thus lead to pollution in water into which they are discharged or degrade re-circulation water in processing plants (Rubio et al., 2002). The mutual repulsion among colloidal particles owing to the same sign of their surface charges is the main reason for the stability of the system. It is difficult to remove colloidal particles in gravitational sedimentation ponds or devices without any size enlargement treatment. Size enlargement treatment may involve destabilization of particles or collision of particles to form aggregates. Destabilization means either a rise in ionic strength of the medium or a neutralization of the surface charge of particles by the addition of chemicals called coagulants or flocculants. These chemicals promote different processes involved in the charge destabilization as they increase ionic strength, and adsorb on the surface of colloidal particle compensating its former electrical charge, and they can promote the formation of precipitates. An alternative to the use of solutions containing the coagulant salts, which causes secondary pollution when added at high concentrations, is the in-situ generation of coagulants by electrolytic oxidation of an appropriate anode material (e.g. iron or aluminum). This process is called electrocoagulation and has many advantages over conventional coagulation (Canizares et al., 2007).

### **1.1.1 Coagulation**

Coagulation is the most widespread and practical method of removing colloidal solids from wastewater. This is a process of destabilizing colloids, aggregating them, and joining them together for ease of sedimentation. It entails the formation

of chemical flocs that adsorb, entrap, or otherwise bring together suspended matter, more particularly suspended matter that is so finely divided as to be colloidal. The chemicals used are: aluminum sulfate,  $\text{Al}_2(\text{SO}_4)_3 \cdot 18\text{H}_2\text{O}$ ; ferrous sulfate,  $\text{FeSO}_4 \cdot 7\text{H}_2\text{O}$  (copperas); ferric sulfate,  $\text{Fe}_2(\text{SO}_4)_3$ ; ferric chloride,  $\text{FeCl}_3$ . Aluminum sulfate is commonly used for coagulation. The use of chemical coagulants, able to act as either negatively or positively charged ions, has highly improved the effectiveness of removal of colloids by coagulation (Nemerow and Agardy, 1998).

The coagulation mechanisms, depending on the physical and chemical properties of the solution, pollutant and coagulant, include charge neutralization, double layer compression, bridging and sweep (Holt et al., 2002). The process of coagulation separation consists of four steps. The initial step is simple: the chemical is added to wastewater. This is followed by the second step, where the solution is mixed rapidly in order to make certain that the chemicals are evenly and homogeneously distributed throughout the wastewater. In the third step, the solution is mixed again, but this time in a slow fashion, to encourage the formation of insoluble solid precipitates, the process known as "coagulation". The final step is the removal of the coagulated particles by way of filtration or decantation (Yılmaz et al., 2007).

### **1.1.2 Electrocoagulation**

In the electrocoagulation process, the coagulant is generated in-situ by electrooxidation of an anode. The suitable anode materials are iron, aluminum and other metals (e.g. stainless steel, titanium). In the literature, different electrodes were reported like carbon (Alvarez-Gallegos and Pletcher, 1999), mild steel (Golder et al., 2005), stainless steel (Ölmez, 2009). The process occurs in steps during electrocoagulation; (i) anode dissolution, (ii) formation of  $\text{OH}^-$  ions and  $\text{H}_2$  at the cathode, (iii) electrolytic reactions at electrode surfaces, (iv) adsorption of coagulant on colloidal pollutants, and (v) removal by sedimentation or flotation (Can et al., 2006).

A metallic element employed in the anode is oxidized to yield its ions. The metal ions hydrolyze to some extent in water. When aluminum is used,  $\text{Al}^{3+}$  ions are produced in water, which forms soluble monomeric and polymeric hydroxo-metal complexes. The main reactions occurring at electrodes during electrolysis are as follows:

At the anode, aluminum oxidation occurs,



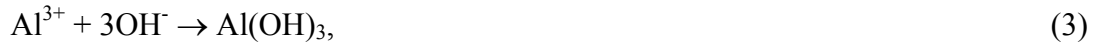
(Standard electrode potential of aluminum is  $\text{Al}^{3+}_{(aq)} + 3e^- \rightarrow \text{Al}_{(s)}$   $E_1^0 = -1.662 \text{ V}$ )

At the cathode, water reduction occurs,



(Standard electrode potential of water is  $E_2^0 = -0.828 \text{ V}$  (Szynkarczuk et al., 1994))

At alkaline conditions,



At acidic conditions,



The standard potential of aluminum dissolution is lower (-1.662 V), than the standard potential of hydrogen evolution, -0.828 V. The dissolution of aluminum is thermodynamically favored ( $E_2^0 \gg E_1^0$ ) and it should proceed spontaneously (Szynkarczuk et al., 1994).

Aluminum ions ( $\text{Al}^{3+}$ ) are produced by electrolytic dissolution of the anode which generates various monomeric and polymeric species.  $\text{Al}^{3+}_{(aq)}$  and  $\text{OH}^-$  ions generated by electrode reactions (1) and (2) react to form various monomeric species such as  $\text{Al}(\text{OH})^{2+}$ ,  $\text{Al}(\text{OH})_2^+$ ,  $\text{Al}(\text{OH})_4^-$ , and polymeric species such as  $\text{Al}_6(\text{OH})_{15}^{3+}$ ,  $\text{Al}_7(\text{OH})_{17}^{4+}$ ,  $\text{Al}_8(\text{OH})_{20}^{4+}$ ,  $\text{Al}_{13}\text{O}_4(\text{OH})_{24}^{7+}$ ,  $\text{Al}_{13}(\text{OH})_{34}^{5+}$  (Can et al., 2006, Gürses et al., 2002).

The adsorption of monomeric and polymeric hydrolysis species on particle surfaces leads to electrical double layer compression and surface charge neutralization. In addition, another coagulation mechanism, i.e. sweep flocculation, is observed at sufficiently high electrolyte dosage (Lu et al., 2005). During the removal of hydroxide precipitate, impurity particles are enmeshed, and they are effectively removed from the suspension. In sweep flocculation, particles are swept out of the medium by an amorphous hydroxide precipitate (Duan and Gregory, 2003). Also, interactions between the colloidal particles and the precipitated polymeric hydroxides become significant.

Many hydrolysis products are cationic and they can interact strongly with negative colloids, giving destabilization, under the correct conditions of coagulant dosage and pH. Excess dosage can give charge reversal and restabilization of colloids. Positively charged precipitate particles may deposit on impurity particles, again giving the possibility of charge neutralization and destabilization. Aluminum additives remove the colloidal particles either by charge neutralization to give insoluble forms, or by adsorption on precipitated metal hydroxide (Duan and Gregory, 2003).

The electrocoagulation is a simple and efficient method for the treatment of many types of water and wastewaters. It is still not widely accepted owing to higher initial capital costs as compared to other treatment technologies. In recent years, many investigations have been particularly focused on the use of electrocoagulation due to the increase in environmental restrictions on effluent wastewater (Koby et al., 2003). According to Abuzaid et al. (2002), it is expected to be economically more feasible than conventional coagulation which stems from cost of purchasing, transportation, storage and handling of chemical coagulants.

The advantages of electrocoagulation method include; high particulate removal efficiency, possibility of complete automation, production of less sludge, large and stable flocs, less total dissolved solid (TDS) and gas bubbles at the cathode (Mollah et al., 2001; Chen, 2004). The amount of chemicals which has to be transported is

lower than conventional coagulation treatment (approx. 1/10 of the amount) as previously reported by Vik et al., (1984). Chemical precipitants mean further cost since they require the purchase and installation of dosing equipment and operating cost for power, disposal of additional sludge, manpower, and of course, the chemicals used (Bektaş et al., 2004). The handling and disposal of the sludge stemming from chemical precipitation is one of the greatest difficulties associated with chemical treatment. Most chemical precipitation operations produce great volumes of sludge. Coagulation plants show that there are considerable operational difficulties involved pH control, chemical mixing and aluminum sulfate dosing (Vik et al., 1984). Besides the obvious advantage that the electrocoagulation process has over these factors in coagulation, electrocoagulation also has some disadvantages; namely expensive electricity, high conductivity of wastewater and the necessity to replace the electrodes.

## **1.2 Aim of the Study**

During the mineral treatment processes, the wastewater containing suspended particles is either re-used in the process or discharged into an aquatic environment. The suspended solids mainly composed of clay minerals and quartz, as in marble wastewater, coal washing wastewater and boron wastewater, must be removed from the effluent prior to re-use or discharge into environment.

Natural dimension stones such as marble, basalt and granite are cut into blocks or plates with rotating blades and are finished by polishing processes. Water is mainly used as a cooling medium in the cutting processes and takes away all the particles produced during cutting and polishing. Suspended solids in the wastewater produced can lead to the development of sludge deposits when untreated wastewater is discharged in the aquatic environment. The wastewater containing fines should be treated in some way. This treatment was carried out through sedimentation by adding flocculants to wastewaters of marble, basalt and granite (Şener, 2007). In another similar study, flocculants was added to wastewater of two marble cutting plants (Seyrankaya et al., 2000).

Clay minerals and quartz in coal are sources of ash and they harmfully affect a number of processes during coal washing, such as flotation, flocculation and dewatering (Hussain et al., 1996). There are numerous studies in the literature related to the flocculation of coal wastewater including various types of minerals (Malayoglu et al., 1998; Foshee et al. 1982; Chandra et al. 1997; Menon et al. 1987 as cited in Sabah et al., 2004). In coal preparation plants, a large amount of water is used for coal cleaning. Since full and half-mechanized coal production methods are recently becoming more common, wastewater produced out of coal processing includes high percentage of ultrafine particles and inorganic impurities. It is significant that these particles be removed from the medium. Sabah et al., 2004 used dual-flocculant systems (anionic–nonionic and nonionic–anionic combinations; nonionic–cationic and cationic–nonionic dual flocculation combinations; anionic–cationic and cationic–nonionic dual flocculant combination) for dewatering of fine coal tailings (30% clay minerals (kaolinite and illite), 23% muscovite, 26% quartz and 20% coal with little amount of carbonate minerals).

In boron mining and processing operations, large amounts of clay-containing tailings are to be discarded. In addition, being rich in boron, the tailings do not only lead to economical loss but also pose serious environmental problems. Large areas have to be allocated for waste disposal. In order to deal with this problem or to remove suspended solids, in a study done by Yılmaz et al., (2006) flocculant or coagulant was added to wastewater drained from the production of boric acid and sodium perborates. The coagulant and flocculant used were  $\text{Al}_2(\text{SO}_4)_3$ ,  $\text{FeCl}_3$ , and polyethylene oxide.

To solve the problem caused by fine clay mineral and quartz particles in many industrial wastewaters (natural dimension stone wastewater, coal washing wastewater and boron wastewater) adding coagulant through conventional method or electrocoagulation method should be used. Coagulation is the most commonly used and practical method of removing suspended particles from suspension such as wastewater.



Within this context, objectives of this thesis are the investigation of the effects of operating parameters (initial pH, applied voltage, current density, time and coagulant dosage) on the removal efficiency of kaolinite or quartz from suspensions by electrocoagulation and conventional coagulation. The study also aims to compare electrocoagulation and coagulation. The study has been carried out in order to compare electrocoagulation and coagulation regarding the pH ranges under investigation and aluminum dosages applied. Furthermore, studies on pure kaolinite and quartz have been involved to comprehend the fundamental processes in electrocoagulation and coagulation.

The key parameters in the coagulation with aluminum by chemical and electrochemical dosing were studied by the speciation of aluminum concentration as function of initial pH, applied voltage, current density and time, and coagulant dosage. The results obtained from the treatments by both coagulation methods in prepared kaolinite and quartz suspension in water were interpreted. In this study, efficiency of turbidity removal from ultrafine kaolinite and quartz suspensions of electrocoagulation and coagulation were examined. Moreover, the optimum operational conditions obtained by changing several key parameters and dominant coagulation mechanisms were determined.

Kaolinite and quartz, being the most common components present in soils and clays leading to water pollution appeared as turbidity, was the selected turbidity causing materials in water for the investigation of the electrocoagulation and coagulation. Kaolinite and quartz particles have negative surface charge in water in wide pH ranges (Gan and Liu, 2008; Hussain et al., 1996 and Hunter, 1981). In addition, as an electrode material, aluminum was chosen owing to its low cost, availability and effectiveness. Furthermore, it has been found that the effluent with aluminum electrodes is very clear and stable (Chen et al., 2000).

The presentation of the thesis consists of five chapters.

This first chapter covered a brief introduction of electrocoagulation and coagulation. Reaction mechanisms accompanied with coagulations and the objective of the thesis were also included in this chapter.

Chapter 2 deals with colloidal background of colloidal systems and potentials related with their properties, mechanism of electrocoagulation and coagulation, as well as previous studies related with electrocoagulation.

Chapter 3 is devoted to the materials and methods used in this thesis study.

Chapter 4 presents the results of the material characterization analyses and electrocoagulation-coagulation experiments.

Finally, Chapter 5 is dedicated to the conclusions drawn from the study.

## **CHAPTER 2**

### **PHYSICO-CHEMICAL PROPERTIES OF COLLOIDAL SYSTEMS**

#### **2.1 Particles in Aquatic Environment**

Natural waters hold a wide range of impurities, most of which stem from weathering of rocks and soils. The effects that human activities have on domestic and industrial wastewaters are also an important contributing factor. Aquatic life is also a key source of numerous constituents of natural waters (Gregory, 2006).

The partition between dissolved and particulate forms is the main point regarding impurities in the aquatic environment. This being a simple concept in principle, distinguishing between these forms is not always straightforward. Water, for many substances including inorganic salt, is a good solvent, and such dissolved impurities constitute the majority of natural waters. Total dissolved solid (TDS) values range from 50 to 1000 mg/L for most fresh waters. Substances relatively insoluble in water might exist as small particles, remaining suspended for long periods. The total concentration of these impurities is known as Total Suspended Solid (TSS). TSS is usually of the order of 10-20 mg/L in a large proportion of natural waters (Gregory, 2006).

It is possible to make the following distinctions between the particles according to the particle size; particles larger than about 50  $\mu\text{m}$  are usually visible as discrete

objects by the naked eye. Particles between 50 to 1  $\mu\text{m}$  can be viewed with an ordinary light microscope, though when particle sizes are reduced below 1  $\mu\text{m}$ , due to the fact that particle sizes become comparable in size with the wavelength of light, particles become increasingly difficult to resolve. For particles smaller than 1  $\mu\text{m}$ , down to a few nm, the electron microscope provides good resolution mainly due to the shorter effective wavelength of electrons. Very small particles (around 20 nm or less) are of similar size to dissolved macromolecules, resulting in an imprecise distinction between particles and soluble matter.

Another very important distinction is the one between *colloidal* and *suspended* (sometimes called *dispersed*) material. Conventionally the upper limit of the colloidal domain is set at 1  $\mu\text{m}$ , and particles having at least one dimension in the size range 1  $\mu\text{m}$  to 0.001  $\mu\text{m}$  are known as colloids (Gregory, 2006).

- For particles smaller than about 1  $\mu\text{m}$ , diffusion becomes an important transport mechanism and this feature tends to prevent particles from settling. Larger particles are able to settle more rapidly since the importance of diffusion is diminished, so such particles tend to be removed by sedimentation over time.
- At around 1  $\mu\text{m}$ , the significance of the surface area of particles relative to their volume begins to increase, as a large surface area provides more opportunity for adsorption of dissolved impurities.
- As particles become smaller, inter-particle interactions have greater significance in relativity to "external" forces such as gravity and fluid drag. These *colloid interactions* are key aspects for aggregation and deposition of particles that are within the colloidal size range.

In consideration of the interaction between dispersed particles and the dispersed medium, colloidal (dispersed) systems can be divided into two groups; lyophilic and lyophobic. In lyophobic (disliking a liquid) systems, there is little or no affinity

between the particles and the solvent. The stability of such systems mainly relies on the charges of the particles. If water is the dispersing medium the name hydrophobic (disliking water) is used. The hydrophobic or lyophobic systems are not very stable. In lyophilic (liking a liquid) systems, there is interaction between particles and solvent in which, the latter combines with the former. In comparison to the lyophobic system in terms of stability, lyophilic systems are more stable. Again if the water is the dispersing medium the term hydrophilic is used. Most inorganic colloids are hydrophobic; whereas most organic colloids are hydrophilic (Jirgensons and Straumanis, 1962). An example of an inorganic colloid is the clay particles that cause turbidity in natural water, and an example of an organic colloid is the colloidal particles in domestic sewage (Sincero and Sincero, 2003).

Another example of a hydrophilic colloidal system is the macromolecules in water, such as proteins, gums, starch, and many synthetic polymers. Much of the natural organic matter in water, such as humic substances, can be regarded as hydrophilic colloids (Gregory, 2006).

The most important difference between hydrophobic and hydrophilic colloids is that the former are not thermodynamically stable. The interface between a particle and water has a characteristic *interfacial energy*. Decrease particle size results in an increase in the total surface area, resulting in a rise in the interfacial energy. This means that small particles have a greater interfacial energy per unit mass in comparison to larger particles, and thus achieve a more stable (lower energy) state by aggregating with other particles to reduce the area in contact with water. Hydrophobic colloids can remain suspended as individual particles for very long periods. Particles in water collide with each other and thus create opportunities to form aggregates. The forces of repulsion between such particles, however, are the cause of why such creation of aggregates does not occur in most cases, since the particles are denied true contact. The most usual reason is that aquatic particles nearly always have a *surface charge*, giving electrical repulsion between particles (Gregory, 2006).

Keeping in mind that the weathering of rocks and soil are the main sources of impurities in natural waters, it can easily be said that most of the suspended matter in natural waters should consist of silica or similar materials, particularly clays, which have a specific gravity of 2.65. Particles with sizes in the order of  $0.01\ \mu\text{m}$  are the main cause of turbidity and give color to the water, making the water objectionable (Sincero and Sincero, 2003). Particles in water may either be undesirable impurities that have to be removed, as in the case of water and effluent treatment, or they may be valuable materials that need to be recovered, as in the cases of mineral processing or biotechnology (Gregory, 2006).

Removal of particles from water may be done by the following methods:

- Sedimentation (including centrifugal methods)
- Flotation (including dispersed air and dissolved air methods)
- Filtration (including deep bed and membrane filtration)

All of the above-mentioned processes depend to a great extent on the size of the particles to be removed, and as such, it is often necessary to increase the particle size by use of processes of coagulation/flocculation. Colloidal interactions are truly important – in particle aggregation and by their effect on the adhesion of particles to other surfaces (such as filter grains and air bubbles) (Gregory, 2006).

## **2.2 Light Scattering and Turbidity**

In the case of a beam of light being directed at a colloidal solution or dispersion, some of the light is absorbed, some is scattered, while the remainder is transmitted undisturbed through the sample. All particles within the water lead to the occurrence of light scattering and this involves no net loss of energy from the beam. Displacement of electrons is induced by electromagnetic radiation and thus results in fluctuating dipoles within particles, leading to a radiation of energy in all directions at the same frequency as the incident radiation. The observed scattering behavior is a result of interference of the radiated and incident light. The intensity

of the induced dipoles depends on the polarizability of the material, and hence on the refractive index. The only requirement for light scattering is that the particle has a refractive index different from that of medium like water. As long as there is a difference in their refractive indexes, particles that are completely transparent to the incident radiation (i.e. with no absorption) are effective in scattering. The turbidity is a direct outcome of light scattering and can be measured either as a reduction in the intensity of transmitted light or an increase in light intensity at a chosen angle (often 90 degrees) to the beam (Gregory, 2006). In physics, as well as in the treatment of solutions, turbidity is defined as the natural logarithm of the fractional decrease in the transmitted intensity of the light, or

$$\frac{I}{I_0} = e^{-\tau \ell}, \quad (5)$$

where  $I_0$  shows the intensity of the entering beam,  $I$  the intensity of the light after it has passed through the length  $\ell$  of the scattering medium and  $\tau$  the turbidity (Jirgensons and Straumanis, 1962).

Turbidity is the most commonly visible verification of particles in water. Even at low concentrations, particles can give a noticeable cloudiness (turbidity) to water. The following particle properties determine light scattering or turbidity:

- The size of the particles relative to light wavelength
- The shape of the particles
- The refractive index of the particles relative to that of the suspension medium (Gregory, 2006).

Light-scattering measurements are of great value for estimating particle size, shape and interactions, and have found particular application in the study of dissolved macromolecular materials (Shaw, 1966).

The intensity of the light scattered by colloidal solutions or suspensions of low

turbidity is measured directly by an instrument called nephelometer and turbidity is reported as nephelometric turbidity unit or NTU.

## **2.3 Origin of Charge on Particles**

Many solid surfaces contain ionizable functional groups; -OH, -COOH. This ionizing group provides the particle electrically charged. The particles may become charged by adsorption of ions from the solutions, for example, a silver bromide sol contains positively charged bromide particles (if an excess of silver nitrate is present) because of adsorption of silver ions on the surface of particles (Jirgensons and Straumanis, 1962). Other charge origination comes from isomorphous substitution or crystal lattice defects in the internal structure of the mineral, e.g., the charge production of clay minerals;  $\text{Al}^{3+}$  substituting for tetrahedral  $\text{Si}^{4+}$  causes to deficiency of positive charge on the crystal lattice. The resulting charge is generally negative on the clay structure (Van Olphen, 1977).

### **2.3.1 Electrical Double Layer**

Whatever the origin of surface charge is, a charged surface in contact with a solution of ions will result in a characteristic distribution of ions in a solution. If the surface is charged, then there must be a corresponding excess of oppositely charged ions (counter-ions) in the solution near the particle to maintain electrical neutrality. The combined system of surface charge and the excess charge in solution is known as the electrical double layer. It is initially convenient to consider a flat charged surface, such as clay surface, in contact with an aqueous solution. The counter-ions are subject to two opposing tendencies; electrostatic attraction to the charged surface and the randomizing effect of thermal motion. The balance between these effects is the determining factor in the distribution of charge and electric potential in solution (Gregory 2006). The concentration of counter-ions near the particle surface is high and it decreases with the increasing distance from the surface. This diffuse character of the counter-ion was recognized by Gouy (1910) and by Chapman (1913), the first to suggest a theoretical treatment of the counter-ion distribution.



The counter-ion atmosphere is often referred to as the diffuse or Gouy layer. The diffuse layer does not merely consist of an excess of ions of opposite charge; simultaneously, there is a deficiency of ions of the same charge (co-ion) in the neighborhood of the surface since these ions are electrostatically repelled by the particle (Van Olphen, 1977).

The Gouy and Chapman model is based on a number of simplified assumptions given below:

- There is an infinite, flat, impenetrable surface.
- Ions in solution are point charges able to approach right up to the charged surface.
- The solvent (water) is a uniform medium with properties that do not dependent on distance from the surface.

These approaches result in a prediction of the manner in which the electrical potential in solution varied with distance from the charged surface. For fairly low values of surface potential, the potential in solution falls exponentially with distance from the surface. The main difficulty with the Gouy-Chapman model is the assumption of ions as point charges because in actuality, ions have a significant size, particularly when hydrated, and this limits the effective distance of closest approach to a charged surface. Allowing for the finite size of ions gives a region close to the surface that is inaccessible to counter-ion charge. This has become known as the *Stern layer*, after Otto Stern, who was the first to introduce the ion size correction into double layer theory in 1924. The Stern layer involves a certain proportion of the counter-ion charge, and the remaining counter-ions are distributed within the diffuse part of the double layer or simply the *diffuse layer* (Gregory, 2006).

A conceptual picture of the Stern-Gouy-Chapman model of the electrical double layer at a flat interface is given in Figure 2.1. This shows the variation of electric potential from the surface, where its value is  $\psi_0$ , to a distance far into the solution,

where the potential is taken as zero. Across the Stern layer, the potential falls rather rapidly, to a value  $\psi_\delta$  (the *Stern potential*) at a distance  $\delta$  from the surface (this is at the boundary of the Stern layer, known as the *Stern plane*). Usually,  $\delta$  is of the order of the radius of a hydrated ion or around 0.3 nm. Although this distance is very small, the Stern layer can have a great influence on double layer properties. From the Stern plane into the solution, through the diffuse layer, the potential varies in an approximately exponential manner, according to the following equation:

$$\psi = \psi_\delta \exp(-\kappa x) \quad (6)$$

where  $x$  is the distance from the Stern plane and  $\kappa$  is a parameter that depends on the concentration of salts in the suspension (or in the medium) (Gregory, 2006).

### **2.3.2 Effect of Electrolyte on the Electrical Double Layer**

The key question for the stability problem is, “What happens to the electrical double layer when a flocculating electrolyte is added to the stable colloidal system”.

The computation of the ion distribution in the diffuse double layer as a function of electrolyte content of the bulk solution demonstrates that the diffuse counter-ion atmosphere is compressed toward the surface when the bulk electrolyte concentration is increased (Figure 2.2). The degree of compression of the double layer is governed by the concentration and valence of the ions of opposite sign from that of the surface charge, while the effect of similar ions is comparatively small. The higher the concentration and the higher the valence of the counter-ions the more the double layer is compressed (Schulze-Hardy rule).

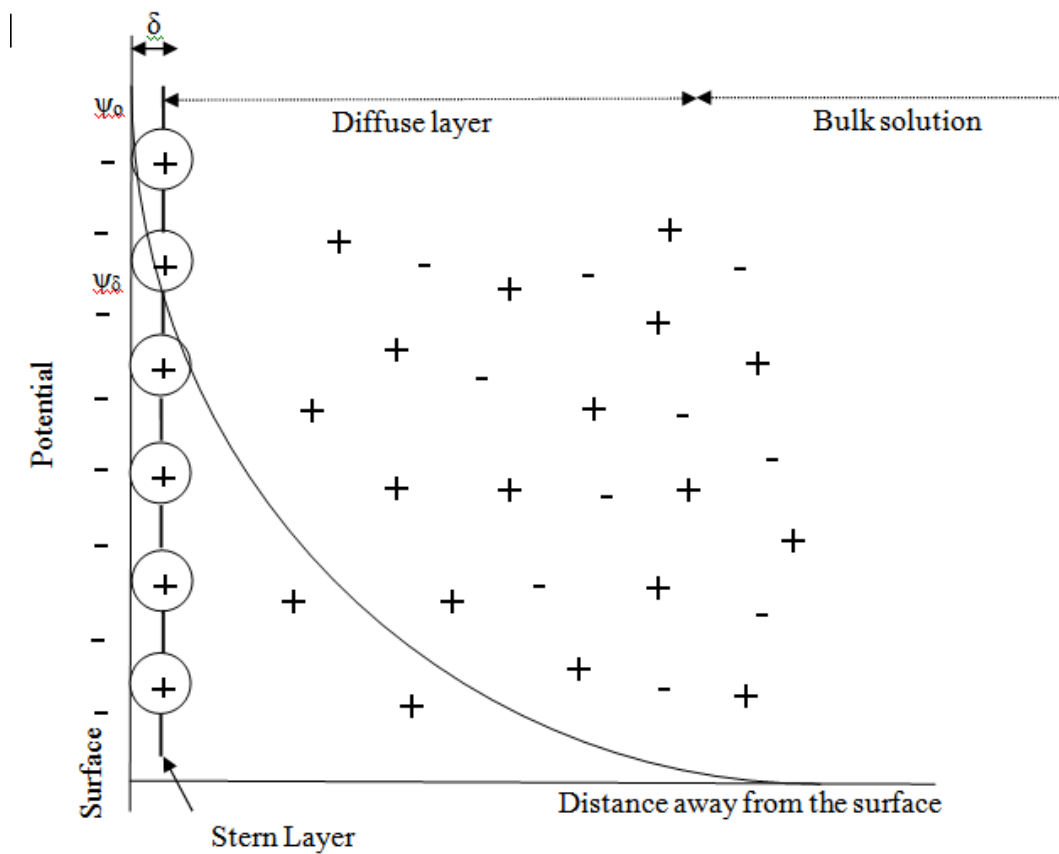


Figure 2.1 Diffuse electrical double layer model according to Stern-Gouy-Chapman.

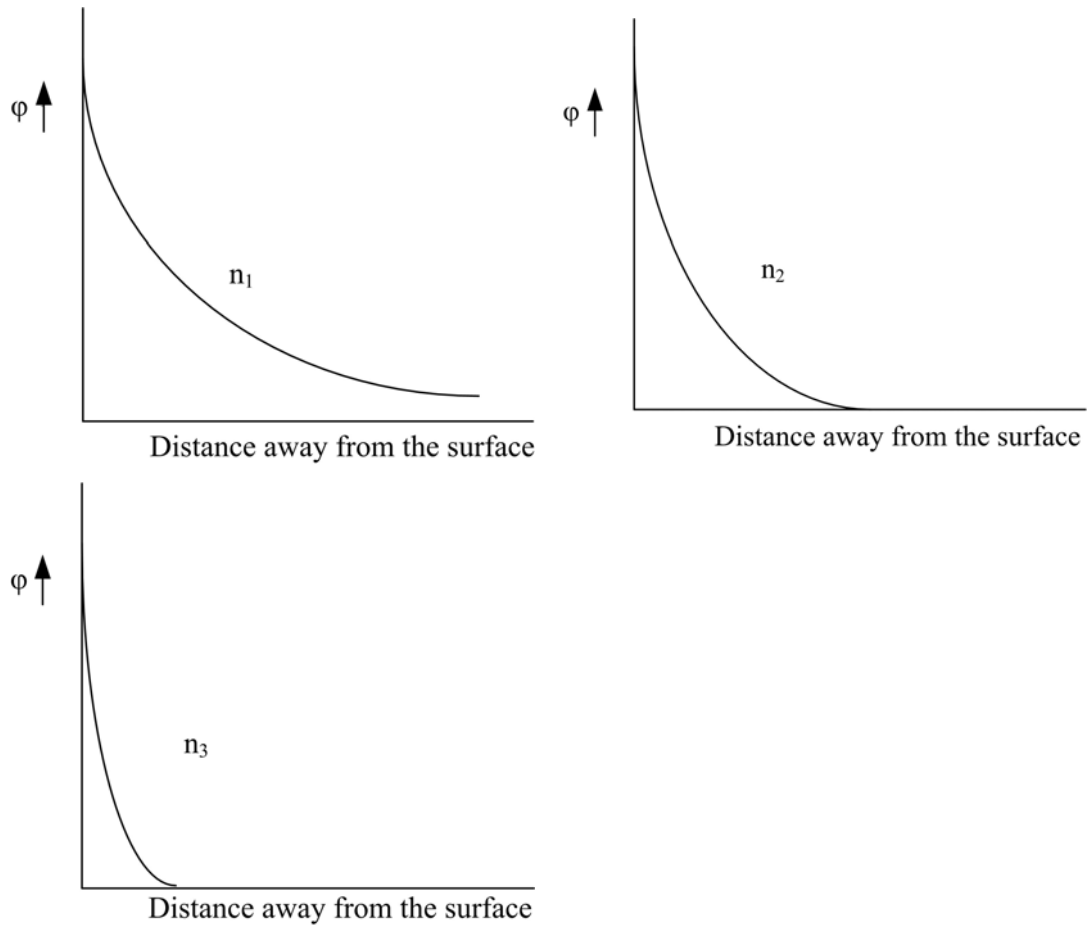


Figure 2.2 Compression of double layer under the effect of electrolyte.  $n_1 < n_2 < n_3$ .  $n_1$ ,  $n_2$ ,  $n_3$  – electrolyte concentration.

## 2.4 Interaction between Particles

There are different kinds of interaction between particles in suspension, depending on the properties, especially on the surface properties of particles. These interactions can give forces of either attraction or repulsion. If attractive forces dominate, then the particles stick together on contact and form aggregates. Particles that repel each other with dominant repulsive forces prevent the process of aggregation. The particles are stable in the latter case, whereas when aggregation forms, the resulting particles are unstable or become destabilized.

### **2.4.1 Repulsion**

When two particles approach each other in suspension owing to their Brownian motion, their diffuse counter-ion atmospheres begin to interfere. It can be shown that this interference results in changes in the distribution of the ions in the double layer of both particles, which involves a rise in the free energy of the system. This results in a need for work to bring about those changes; in other words, there will be repulsion between the particles. The amount of work required to bring the particles from infinite separation to a given distance can be calculated. This amount of work is the repulsive energy or the repulsive potential at the given distance. When the repulsive potential,  $V_R$ , is plotted as a function of distance, a so-called "potential curve" is acquired. The repulsive potential decreases roughly exponentially with increasing particle separation. In Figure 2.3, three potential curves for three different electrolyte concentrations for the same particles are shown, indicated by "low", "intermediate", and "high", as an indicator of the electrolyte concentrations. Since the double layer is increasingly compressed at increasing electrolyte concentrations, the range of the repulsion is considerably reduced (Van Olphen, 1977).

### **2.4.2 The van der Waals Attraction**

Between all atoms and molecules there are attractive forces of various kinds, which J.D. van der Waals postulated in 1873 to account for the nonideal behavior of real gases. If the molecules are polar (i.e., with an uneven distribution of charge), then the attraction between dipoles becomes important. If only one of the interacting molecules has a permanent dipole, then this molecule can induce an opposite dipole in a nearby molecule, thus giving an attraction. Even when the atoms or molecules are nonpolar, the movement of electrons around nuclei give off "fluctuating dipoles," which induce dipoles in other molecules, and hence an attractive force. From the standpoint of colloid stability, this is the most significant of the intermolecular interactions. It is a quantum-mechanical effect, which was first recognized by Fritz London in 1930. This is why the resulting forces are sometimes

known as *London-van der Waals forces*. Nonetheless, they are also known as *dispersion forces* since the fundamental electron oscillations involved are also responsible for the dispersion of light (Gregory, 2006).

The phenomenon of flocculation reveals the existence of interparticle attractive forces. Obviously, in order to compete successfully with the double-layer repulsion which is still operative under flocculating conditions, the attraction must be of comparable range and magnitude. The general van der Waals attractive forces appear to satisfy this requirement. At first glance, it does not seem likely that the van der Waals forces would be large enough or far-reaching enough to satisfy the said conditions, for they are small and they decay rapidly with distance for a pair of atoms. Nevertheless, the van der Waals attraction between atom pairs is additive; thus, the total attraction between particles containing a very large number of atoms is equal to the sum of all the attractive forces between all atoms present within both particles. The summation leads not only to a larger total force but also to a less rapid decay with increasing distance. For two atoms, the van der Waals attractive force is inversely proportional to the seventh power of the distance (or to the sixth power for the attractive energy), whereas for two large particles, the force is inversely proportional to the third power of the distance between the surfaces, and the attractive energy therefore to the second power of that distance, approximately. In the lower part of Figure 2.3, the attractive energy  $V_A$  is plotted as a function of particle separation. As pointed out before, the attraction remains practically the same when the electrolyte concentration of the medium is varied (Van Olphen, 1977).

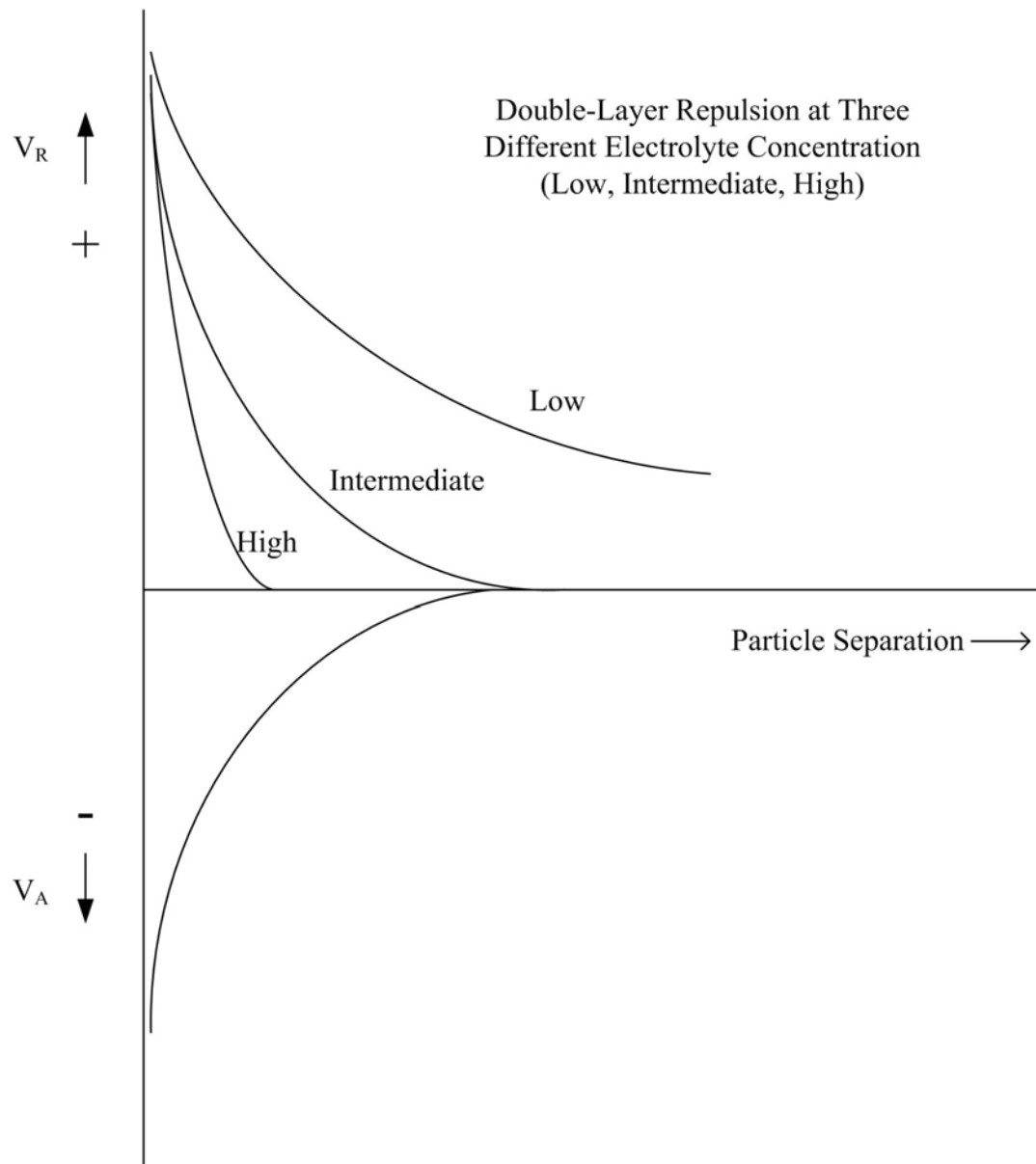
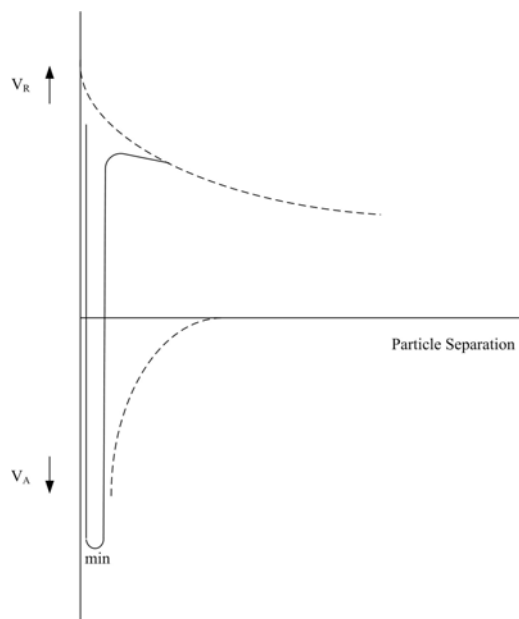


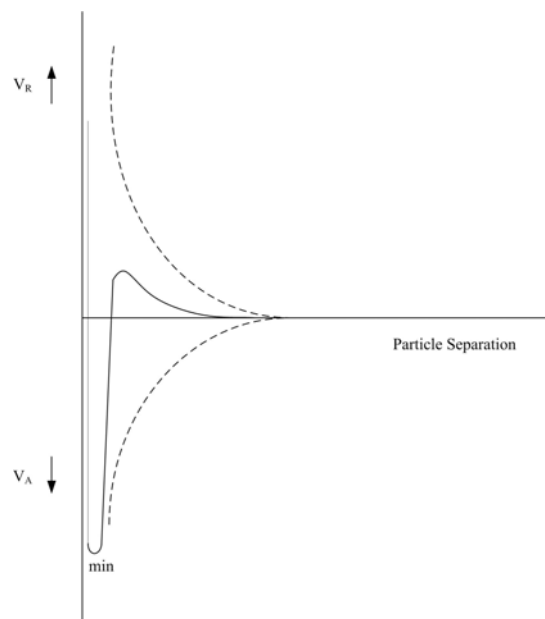
Figure 2.3 Repulsive and attractive energy as a function of particle separation at three electrolyte concentrations.

The net potential curve of particle interaction is constructed simply by adding attractive and repulsive potential at each particle separation, considering the attractive potential as negative and the repulsive potential as positive. Figure 2.4 a, b, c, shows the results of these additions for three electrolyte concentrations indicated as low, intermediate and high. In constructing these three net potential curves, an additional force between the particles must be taken into account. This interaction is a repulsion of a very short range to which there are two possible contributions. The first of these contributions can be the Born repulsion, which becomes effective as soon as extruding lattice points or regions come into contact; resisting the interpenetration of the crystal lattice. A second short range repulsion is the result of specific adsorption forces between the crystal surface and the molecules of the liquid medium (like water). Due to such adsorption forces usually one or two monomolecular layer of water are held rather tightly by the particle surface. For the surface between the two particles to become less than the thickness of the adsorbed water layer on both particles, the adsorbed water must be desorbed. The work required for this desorption appears to be short range repulsion between the particles which become appreciable at particle separations of the order of 1 nm or less. The short range repulsion for the net interaction is represented by the steep rise of the potential curves at very small values for particle separations (Van Olphen, 1977).

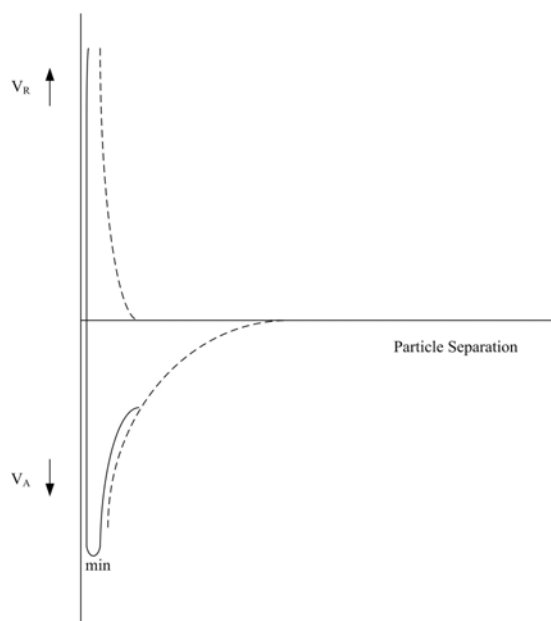




(a) Low electrolyte concentration



(b) Intermediate electrolyte concentration



(c) High electrolyte concentration

Figure 2.4 Net interaction energy as a function of particle separation.

### 2.4.3 The Net Interaction Curve and Stability of Dispersed System

The net interaction curves for a low and a medium salt concentration show a minimum with predominant attraction at close approach and a maximum with predominant repulsion at greater distances. No such maximum is displayed by the curve for a high electrolyte concentration.

The interpretation of stability and flocculation in terms of the net potential curves of particle interaction is based on the following considerations:

At a high electrolyte concentration, the potential curve shows a deep minimum only at close separation, and attraction predominates at any particle distance except at very close approach (Figure 2.4 c). If two particles approach each other due to their Brownian motion, they will agglomerate at the point they reach the position at which the deep attraction minimum occurs. The particle agglomeration occurs at a maximum rate and the process is called rapid coagulation.

If repulsion dominates part of the way during the mutual approach of the particles (curves for medium and low electrolyte concentration), the diffusion will be counteracted by the extraneous repulsive force field, and the rate of agglomeration will decrease. At intermediate electrolyte concentrations (Figure 2.4 b) the coagulation process is retarded by the long-range repulsion. Under these conditions, slow coagulation takes place. At very low electrolyte concentrations (Figure 2.4 a), the coagulation process is retarded to such an extent by the appreciable long-range repulsion that it may take weeks or months for coagulation to become perceptible. For all practical purposes, the system is called "stable" under these conditions.

### 2.4.4 Zeta Potential

Up till now we have discussed surface potential ( $\psi_o$ ), stern potential ( $\psi_\delta$ ) and potential at any point  $\psi$ . There is another potential related with electrokinetic property of the particles which is called zeta potential ( $\xi$ ). The zeta potential is the

electric potential in the double layer at the interface between a particle which moves in an electric field and the surrounding liquid. The zeta potential is calculated from the electrophoretic mobility of the dispersed particles. Its magnitude is considered a measure of the particle repulsion. Upon the addition of the electrolyte zeta potential usually decreases. At the flocculation value of the electrolyte (where rapid coagulation occurs) it is considered to have reached to critical value, below which the particle repulsion will no longer be strong enough to prevent coagulation. It has been realized that the seat of the zeta potential is the shearing plane or slipping plane between the bulk liquid and an envelope of water which moves with the particle. In fact zeta potential is not equal to the surface potential but, to some extent, comparable with the Stern potential, though not necessarily identical with that potential. Figure 2.5 shows the structure and the potential profile in a double layer of flat surface.

The efficiency and control of coagulation or flocculation steps in large scale solid-liquid separation (thickening or clarification) operations can be accomplished by routine measurement of zeta potentials and so-called “zeta potential control” (Riddick, 1968 as cited in Hunter, 1981). Zeta potential measurements were used to follow the turbidity removal of wastewater.

The concentration of potential determining ions at which the zeta potential is zero is called the isoelectric point (iep). The isoelectric point is determined by electrokinetic measurements. The surface charge is zero at the point of zero potential. The zeta potential refers to the hydrodynamic interface while the surface charge is defined for the solid-liquid interface (Butt et al., 2003).

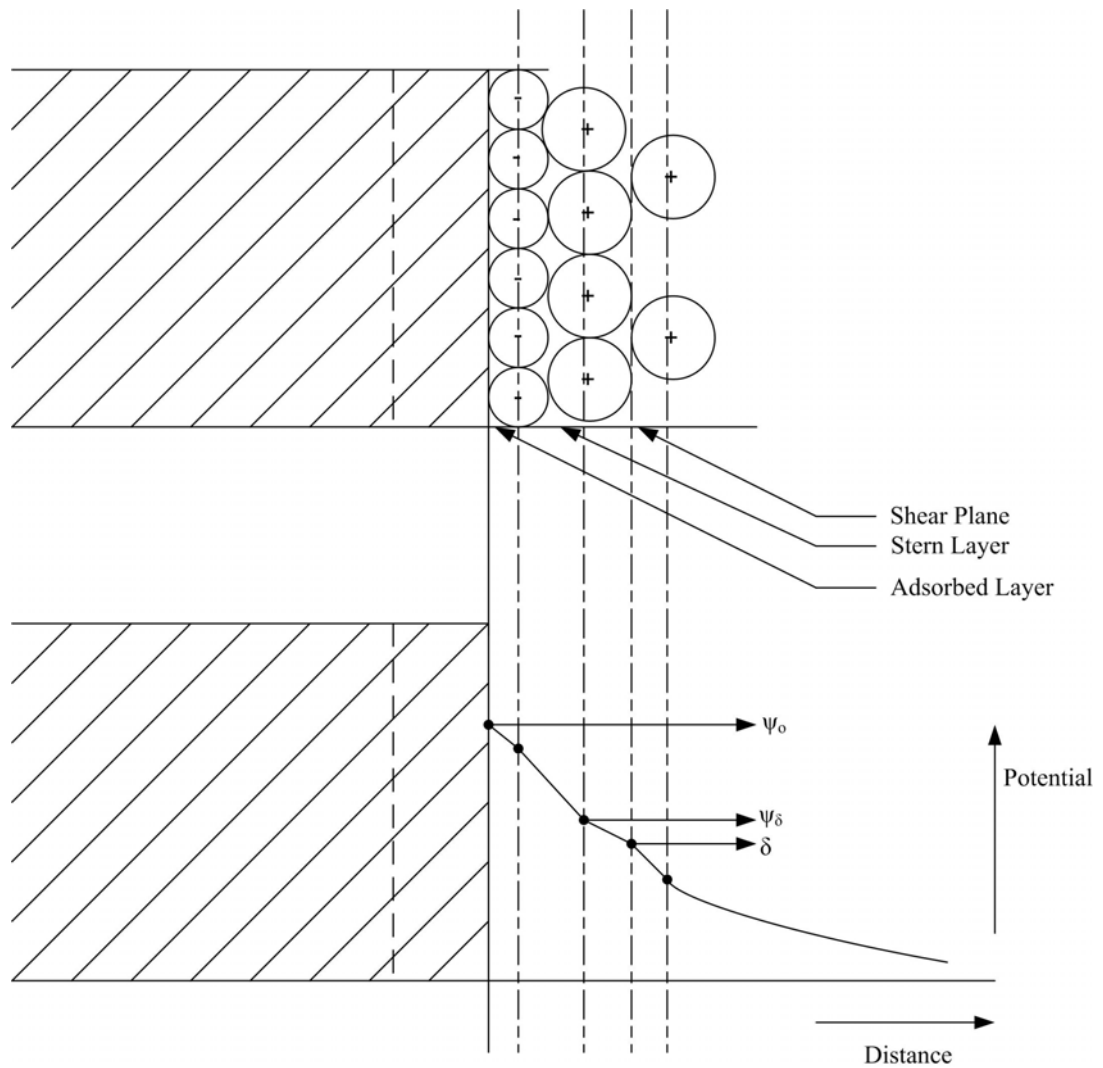


Figure 2.5 The structure and the potential profile in a double layer of flat surface (modified from Figure 1 in Demirçi, 1973).

### 2.4.5 Coagulation

Coagulation is an essential process in water and wastewater treatment. In the area of potable water treatment, clarification of water with coagulating agents has been practiced since ancient times, using a variety of substances – the most notable among them being crushed seeds. The Egyptians, as early as 2000 BC, used

almonds smeared around a vessel to clarify river water. The early Romans were also familiar with alum, though it may not have been for water treatment (Bratby, 2006). Nevertheless, its use as a coagulant by the Romans was mentioned in ca. 77 AD. By 1757, alum was used as coagulant in water treatment in England, and more formally for the treatment of public water supplies in 1881 (Faust and Ally, 1998 as cited in Bratby, 2006). In modern water treatment, coagulation and flocculation are still essential steps in the treatment processes.

The need for a profound understanding of coagulation-flocculation processes is as important today as it has been in the past-even more so since today's waters used for public supplies have an increased number of particulates and organics, further necessitating the effective removal of such substances. The committed goal of many water utilities is to consistently produce treated water turbidities of less than 0.1 NTU. For example, since 1989, the regulatory limit in the United States for treated water turbidity has progressively reduced from 1.0 NTU in 1989 to 0.3 NTU today (Bratby, 2006).

Coagulation is the process of destabilizing colloids, aggregating them, and binding them together for ease of sedimentation. This is achieved by adding simple salts or by charge neutralization, resulting in a tendency in the aggregates (coagula) to be small and dense. Flocculation is limited to the cases where polymer bridging is the dominant mechanism and aggregates (flocs) tend to be larger and more open in structure. It is natural that larger structure tends to be more open and less dense. The distinction between small, compact coagula and larger, less dense flocs is an inevitable result of the stronger interparticle binding in the case of polymers, causing to larger aggregates. In the area of water and wastewater treatment, coagulation refers to destabilization, by the dosing of appropriate additives, and flocculation refers the formation of aggregates, usually by some form of fluid motion. This corresponds to the two stages shown in Figure 2.6 and could be considered chemical and physical aspects of the aggregation process (Gregory, 2006).

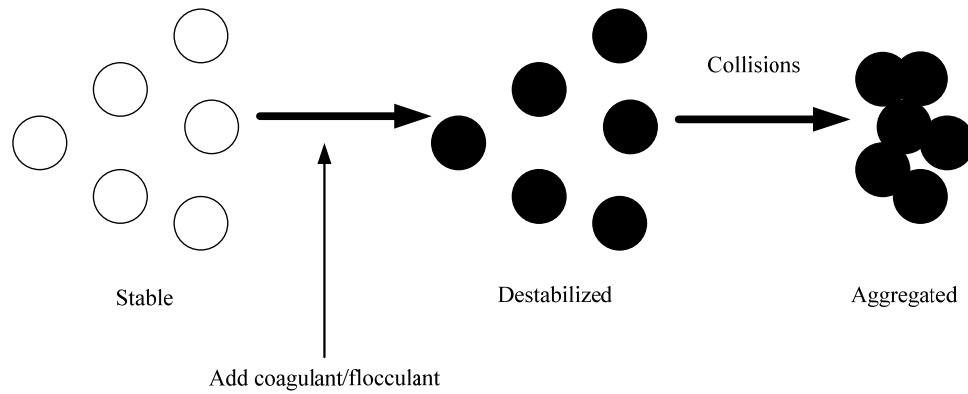


Figure 2.6 Destabilization and aggregation of particles.

The additives used to cause destabilization of colloids may be called coagulants or flocculants, depending on their mode of action. Coagulants would be inorganic salts, including those containing specifically adsorbing counter-ions, and flocculants would be long-chain polymers, which give bridging interactions.

Although there are potentially many different kinds of destabilizing agents the vast majority of those used in practice can be divided into two categories:

- Hydrolyzing metal coagulants
- Polymeric flocculants

Hydrolyzing metal coagulants are the main point of interest in the study.

#### **2.4.5.1 Hydrolyzing metal coagulants**

The most widely used coagulants are based on aluminum and ferric salts. Originally their action was thought to be a result of the trivalent nature of the metals, giving  $\text{Al}^{3+}$  and  $\text{Fe}^{3+}$  ions in solution, which are expected to be very effective in

destabilizing negatively charged colloids. They are effective in removing a broad range of impurities from water including colloidal particles and dissolved organic substances. Their mode of action is generally explained in terms of two distinct mechanisms:

- Charge neutralization of negatively charged colloids by cationic hydrolysis products
- Incorporation of impurities in an amorphous hydroxide precipitate (sweep flocculation) (Duan and Gregory, 2003).

The relative importance of these mechanisms depends on factors such as pH and coagulant dosage.

Hydrolyzing coagulants have been applied routinely since early 20<sup>th</sup> century and they play a vital role in the removal of many impurities from polluted waters. These impurities include such inorganic particles as clays, pathogenic microbes and dissolved organic natural matters. Aluminum sulfate, ferric chloride and ferric sulfate are the most common additives (Duan and Gregory, 2003).

Nearly all colloidal impurities in water are negatively charged and, hence, may be stable as a result of electrostatic repulsion. Destabilization can be achieved by either adding relatively large amount of salts, or by adding smaller quantities of cations that interact with negative colloids, thus neutralizing their charge. Highly charged cations such as  $\text{Al}^{3+}$  and  $\text{Fe}^{3+}$  should be more effective in this respect. Nevertheless, over the normal range of pH values in natural waters (5-8), these simple cations are not found in significant concentrations, due to hydrolysis, which can give a range of products (Duan and Gregory, 2003). Figure 2.7 shows the hydrolysis of  $\text{Al}^{3+}$ .

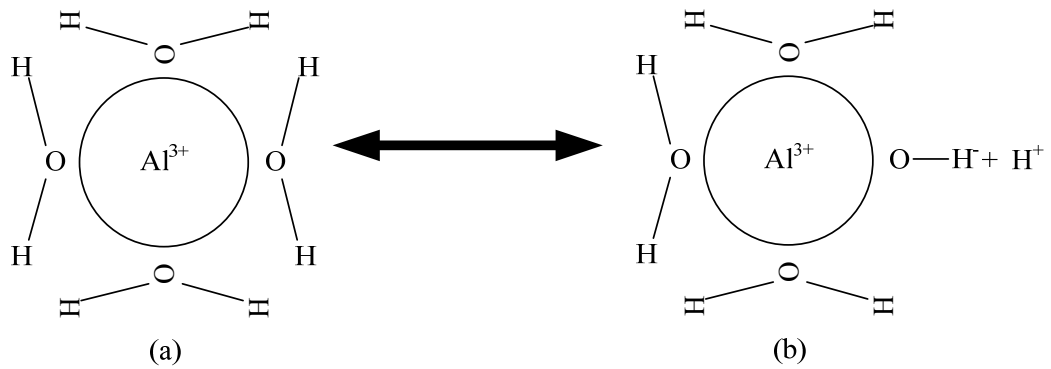
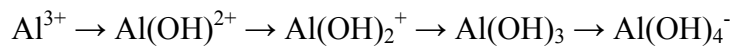


Figure 2.7 Hydrolysis of  $\text{Al}^{3+}$ . (a) Hydrated aluminum cation. (Note: only 4 of 6 water molecules shown) (b) After loss of  $\text{H}^+$  to give  $\text{Al}(\text{OH})^{2+}$  (Gregory, 2006).

If, for simplicity, water molecules in the hydration shell are omitted, different products of hydrolysis reactions can be given as follows:

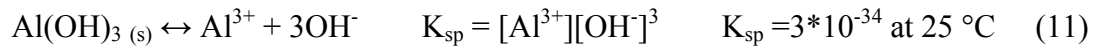


Each of the stages in the hydrolysis process has an appropriate equilibrium constant as given below:



The uncharged hydroxide  $\text{Al}(\text{OH})_3$ , has very low solubility in water and is likely to form a precipitate over a certain range of pH. This precipitation is important in the action of hydrolyzing metal coagulants. The solubility product constant of metal hydroxide is also required:





In fact, regarding coagulation processes, it is much more relevant to consider the solubility constant of amorphous precipitate forming initially. Unfortunately these values are subject to uncertainties, and can only be given as estimated values. They are usually at least hundred times greater than the values of the corresponding crystalline solid. This means that amorphous materials have higher solubility (Gregory, 2006).

For the case of aluminum hydroxide,  $K_{\text{sp}}$  of amorphous form is given as  $3.16 \times 10^{-32}$  (Gregory, 2006).

By using pK values, it is possible to calculate, as a function of pH, the concentration of the various dissolved hydrolysis products in equilibrium with the amorphous hydroxide precipitate. Because of uncertainties over the solubility constants for the amorphous precipitate, the result may not be completely reliable, but they do give a useful indication of the relative importance of different species over the range of pH values. Figure 2.8 is a speciation diagram showing the result of such calculations of aluminum. These calculations are shown in Appendix B. It is evident from the figure that minimum solubility occurs around neutral pH values. The anionic form  $\text{Al(OH)}_4^-$  (aluminate) is the dominant dissolved species above neutral pH.

As it seen from the speciation diagram, the predominant species are the trivalent ion  $\text{Al}^{3+}$  at low pH (up to about 4.5), whereas the aluminate ion,  $\text{Al(OH)}_4^-$ , becomes the predominant species at pH values higher than 8. The intermediate species make only minor contributions at pH values in the region of 4-6.5. The reason that the aluminum species are 'squeezed' into a much narrower pH range is believed to be the result of a transition from octahedral coordination in  $\text{Al}^{3+} \cdot 6\text{H}_2\text{O}$  to the tetrahedral  $\text{Al(OH)}_4^-$  (Gregory, 2006).

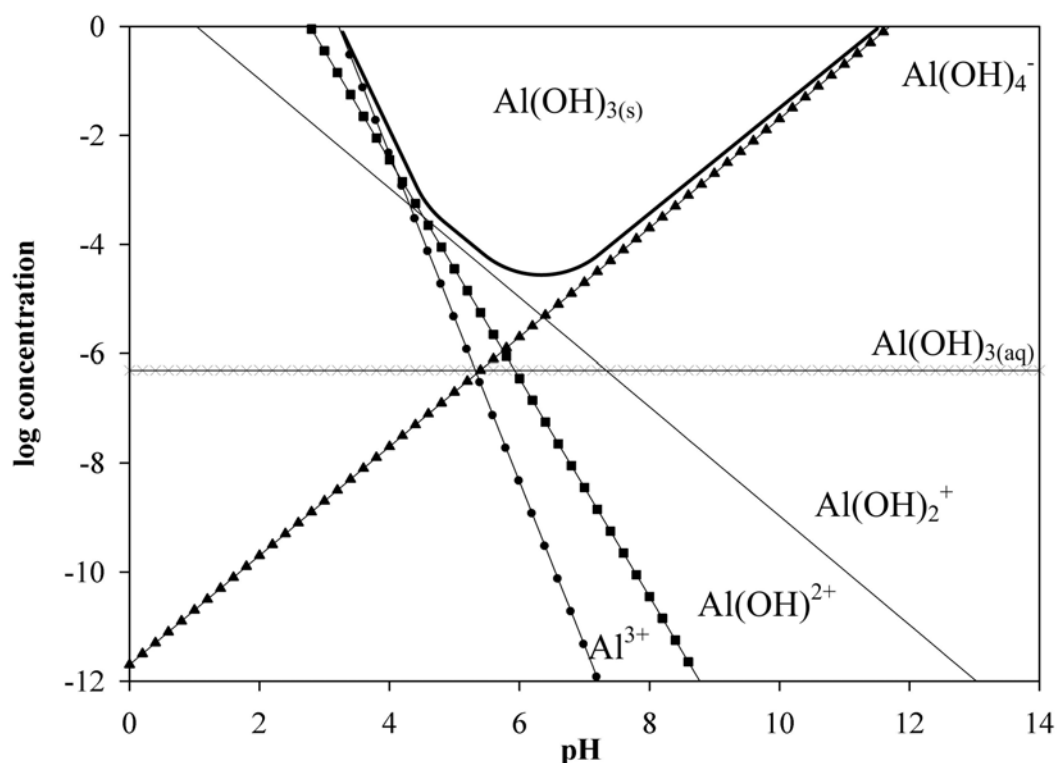


Figure 2.8 Solubility diagram of aluminum hydroxide  $\text{Al(OH)}_{3(s)}$  considering only monomeric aluminum species.

Up to now only monomeric hydrolysis products have been considered. Alternatively, in some conditions polymeric species can also be important. These polymeric species include  $\text{Al}_2(\text{OH})_2^{4+}$  and  $\text{Al}_3(\text{OH})_4^{5+}$ . Nonetheless, these are not likely to be significant at low concentrations of the metals usually used in coagulation. In practice, only the monomeric forms and the hydroxide precipitate are likely to be important. Polymeric hydrolysis product can be prepared under certain conditions. The most known example is  $\text{Al}_{13}\text{O}_4(\text{OH})_{24}^{7+}$ , which can be formed by several methods including controlled neutralization of aluminum salt solutions. Other polymeric species like the octamer  $\text{Al}_8(\text{OH})_{20}^{4+}$  have been

proposed, based on coagulation data. Still, there is no direct evidence for the octamer and it is unlikely to be significant in practice (Duan and Gregory, 2003).

All these hydrolysis metal species can interact with different types of pollutants achieving their removal from the medium of interest. These interaction processes are strongly related to the metal speciation, and they can be summarized into three main types:

- The metallic ionic monomeric species can neutralize the charge of the pollutants by adsorption on their surfaces (or by binding to their ionized groups).
- The metallic ionic polymeric species can bind to several particles (or molecules) of pollutant at a time.
- The pollutants can be enmeshed into growing metallic hydroxide precipitates, or can be adsorbed onto their surfaces (Canizares et al., 2009).

The mechanism of coagulation of suspensions by hydrolyzing metal salts is closely related to the adsorption of dissolved hydrolysis products at low coagulant concentration, as well as the precipitation of the metal hydroxide at high concentrations. Coagulation depends on the charge of these dissolved species or the colloidal properties of the precipitate. It has been found that at low concentrations, and at pH values in the region of 6-7, adsorption of highly charged hydrolyzed species has a strong effect on the particle charge (Ching et al., 1994; Duan 1997 as cited in Gregory and Duan, 1998). At high coagulant concentration, flocculation of colloids will depend on aggregation of primary hydroxide precipitates which is dependent on the pH and coagulant concentration (Duan, 1997 as cited in Gregory and Duan, 1998).

The action of hydrolyzing coagulants is often discussed in terms of four concentration regions (Stumm and Morgan, 1996):

- Very low coagulant dosage; particles are negatively charged and colloidally stable – no coagulation.
- Coagulant dosage is sufficient to give charge neutralization; particles are destabilized and coagulation occurs.
- Coagulant dosage is higher, giving excess adsorption, charge reversal and restabilization.
- Coagulant dosage is still higher; hydroxide precipitation – “sweep flocculation” (see 1.1.2).

#### **2.4.6 Electrocoagulation**

Coagulants are either directly added as a salt like aluminum sulfate or produced by electrochemical reactions at the anodes. The former is called conventional coagulation and the coagulant added is called the chemical dosage. The latter is called electrocoagulation, and coagulant produced is called electrochemical dosage.

Electrochemical processes have been used in water and wastewater treatment since 1887, beginning in England, and then followed by other countries. In the processes in those times both aluminum and iron were used together as anodes which corroded during electrolysis. Foyt (1963) (as cited in Vik et al., 1984) described electrolytic treatment of wastewater using magnesium salt and alkalization in order to remove phosphorus at high pH. The chloride ions in seawater were oxidized to chlorine gas at the anode while hydrogen gas was formed at the cathode. The particles and colloids in water were adsorbed on the  $\text{Mg}(\text{OH})_2(\text{s})$  and flotation occurred due to hydrogen gas formation. After a relatively short operational time,  $\text{CaCO}_3(\text{s})$  deposited at the cathodes and rendered ineffective the flotation process. The process was very effective regarding phosphorus, nitrogen and organics removal, but was found to be expensive compared with biological treatment. Electrocoagulation was studied for treatment of wastewater from food industry (Beck et al., 1974 as cited in Vik et al., 1984). In 1956, Holden (as cited in Matteson et al., 1995) treated river water in Britain using iron electrodes. Two water

treatment plants were run in parallel, the only difference being the chemical dosing system (Vik et al., 1984). Both the investigations in 1946 and 1956 showed promising results, e.g. high water quality as measured by turbidity and color removal, but neither methods was widely accepted due to high initial capital costs as compared to chemical dosing (Matteson et al., 1995). In recent years, however, smaller scale electrocoagulation processes have found a niche in the water treatment industry, proving to be reliable and effective technologies, though they require greater technical understanding for their potential to be fully exploited (Holt et al., 2002).

Electrocoagulation is a complicated process involving many chemical and physical phenomena that make use of consumable electrodes to supply ions into the pollutant system. In an electrocoagulation process the coagulating ions are produced “in situ” and it involves three successive stages:

- i- Formation of coagulants by electrolytic oxidation of the “sacrificial electrode”, such as aluminum and iron,
- ii- Destabilization of the contaminants, particulate suspension, and breaking of emulsion,
- iii- Aggregation of the destabilized phases to form flocs.

The destabilization mechanism of the contaminants, particulate suspension, and breaking of emulsions consists of many steps, and may be summarized as follows:

- Compression of the diffuse double-layer around the charged species by the interactions of ions generated by dissolution of the sacrificial anode.
- Charge neutralization of the ionic species present in polluted medium by the counter ions, produced during the electrochemical dissolution of the sacrificial anode. These counter ions reduce the electrostatic interparticle repulsion to the extent that the van der Waals attraction predominates, thus leading coagulation.

- Floc formation; coagulation results in the formation of the floc, thus creating a sludge blanket that entraps and bridges colloidal particles still remaining in the aqueous medium (Mollah et al., 2004).

The solid oxides, hydroxides and oxyhydroxides provide active surfaces for the adsorption of the polluting species (Mollah et al., 2004).

Electrocoagulation has been successfully employed in removing metals, suspended particles, clay minerals, organic dyes, oil and greases from a variety of industrial effluents. In this process, a potential is applied to the metal anodes, typically fabricated from either iron or aluminum, which causes two separate reactions:

1. Fe/Al is dissolved from the anode generating corresponding metal ions, which almost immediately hydrolyze to polymeric iron or aluminum hydroxide. These polymeric hydroxides are excellent coagulating agents. The consumable (sacrificial) metal anodes are used to continuously produce polymeric hydroxides in the vicinity of the anode. Coagulation takes place when these metal cations combine with the negative particles carried toward the anode by electrophoretic motion. Then they are removed by electroflotation, or sedimentation and filtration. Hence, instead of adding coagulating chemicals as in conventional coagulation process, these coagulating agents are generated in situ.
2. Water is also electrolyzed in a parallel reaction, producing small bubbles of oxygen at the anode and hydrogen at the cathode. These bubbles attract the flocculated particles and, through natural buoyancy, float the flocculated pollutants to the surface (Mollah et al., 2004).

In addition, the following physiochemical reactions may also take place in the electrocoagulation cell (Paul, 1996 as cited in Mollah, et al., 2004):

- Cathodic reduction of impurities present in the medium.
- Discharge and coagulation of colloidal particles.

- Electrophoretic migration of the ions in solution.
- Electroflotation of the coagulated particles by O<sub>2</sub> and H<sub>2</sub> bubbles produced at the electrodes.
- Reduction of metal ions at the cathode.
- Other electrochemical and chemical processes (Mollah et al., 2004).

In an electrocoagulation experiment the electrode or electrode assembly is usually connected to an external DC source. The amount of metal dissolved is dependent on the quantity of electricity passed through the electrolytic solution.

Faraday's law can be written simply between current density (A/cm<sup>2</sup>) and the amount of substance dissolved.

$$w = \frac{itM}{nF} \quad (12)$$

where, w = aluminum dissolved (g Al/cm<sup>2</sup>); i = current density (A/cm<sup>2</sup>); t = time (s); M = molecular weight of Al (M = 27); n = number of electrons involved in the oxidation reaction (n = 3); F = Faraday's constant, 96 500 C/mol.

An agreement is expected to be seen between the calculated amounts of substance dissolved as a consequence of definite quantity of electricity and experimental value. Usually a good agreement is obtained. However, significant error may be introduced, if sufficient attention is not given to the geometry of the electrode as well as the optimum operating conditions of the electrocoagulation cell (Vik et al., 1984).

The measured potential necessary to get the desired current density (i) is defined as a sum of three components:

$$\eta_{AP} = \eta_k + \eta_{Mt} + \eta_{IR} \quad (13)$$

where  $\eta_{AP}$  is the applied overpotential (V),  $\eta_k$  the kinetic overpotential (V),  $\eta_{Mt}$  the concentration overpotential (V),  $\eta_{IR}$  the overpotential caused by solution resistance of IR drop.

IR drop can be easily minimized by means of decreasing the distance between the electrodes and by increasing the surface of the anodes and the specific conductivity of the water.

$$\eta_{IR} = I \left( \frac{d}{A\kappa} \right) \quad (14)$$

where  $I$  is the current (A),  $d$  is distance between the electrodes (m),  $A$  active anode surface ( $m^2$ ),  $\kappa$  specific conductivity ( $10^3$  mS/m) (Vik et al, 1984).

The mass transfer overvoltage  $\eta_{Mt}$  can be diminished by increasing the transport of aluminum ions from the anode surface to the bulk solution, i.e. by increased mixing between the electrodes (Vik et al, 1984).

Kinetic overpotential  $\eta_k$  (also called activation potential) has its origin in the activation energy barrier to electron transfer reactions. The activation overpotential is especially high for evolution of gases on certain electrodes. Both kinetic and concentration overpotentials rise as the current rises. Nonetheless, the effects of these changes need investigating for specific types of physical and chemical species in aqueous solutions (Mollah et al., 2004).

#### **2.4.6.1 Description of the Technology**

An electrolytic cell with an anode and a cathode is basically what an electrocoagulation reactor consists of. Oxidation will cause the anode material to undergo electrochemical corrosion, whereas the cathode will be subjected to passivation, when the cell is connected to an external power source (Mollah et al., 2001; Mollah et al., 2004). But, since electrodes with large surface area are required



for a workable rate of metal dissolution, the afore-mentioned arrangement is generally not suitable for the treatment of pollutant liquid medium. This requirement was satisfied by use of monopolar electrodes either in parallel or series connections. Figure 2.9 shows a simple arrangement in which a pair of anodes and cathodes is connected in parallel mode, forming an electrocoagulation cell. In this set-up, a resistance box is necessary to regulate the current density, as well as requiring a multimeter to read the current values. The conductive metal plates are commonly known as ‘sacrificial electrodes’. The sacrificial electrodes may be made up of the same or of different materials as anode (Mollah et al., 2001).

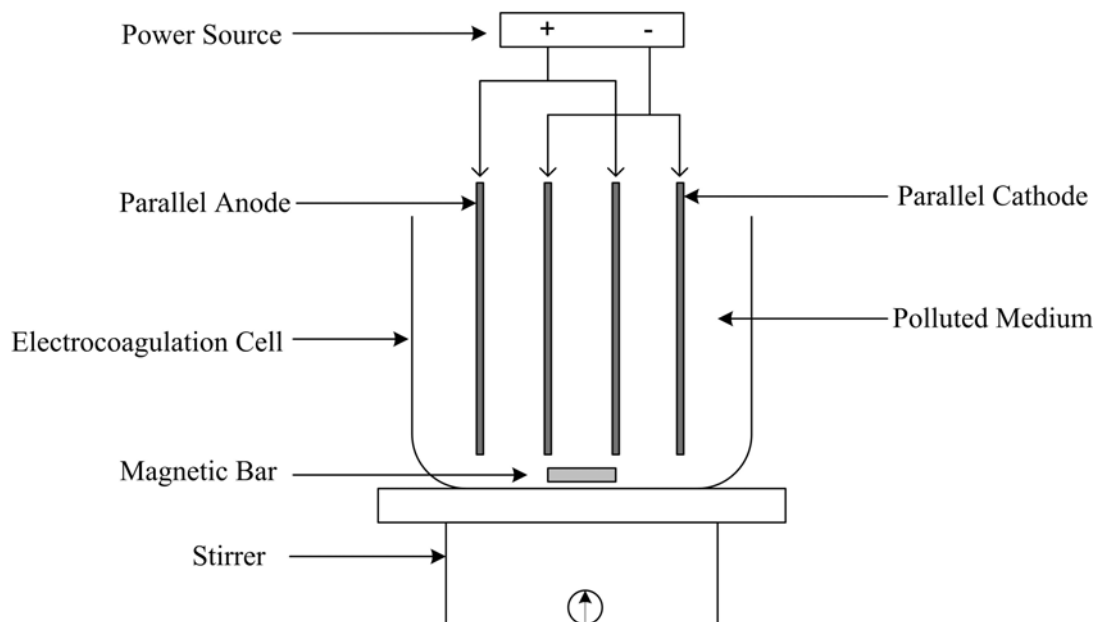


Figure 2.9 Bench-scale electrocoagulation reactor with monopolar electrodes in parallel connection.

An arrangement of an electrocoagulation cell with monopolar electrodes in series is shown in Figure 2.10. As depicted in the figure, the ‘sacrificial electrodes’ while having internal connection within each other, do not have any inter-connections with the outer electrodes (Mollah et al., 2001).

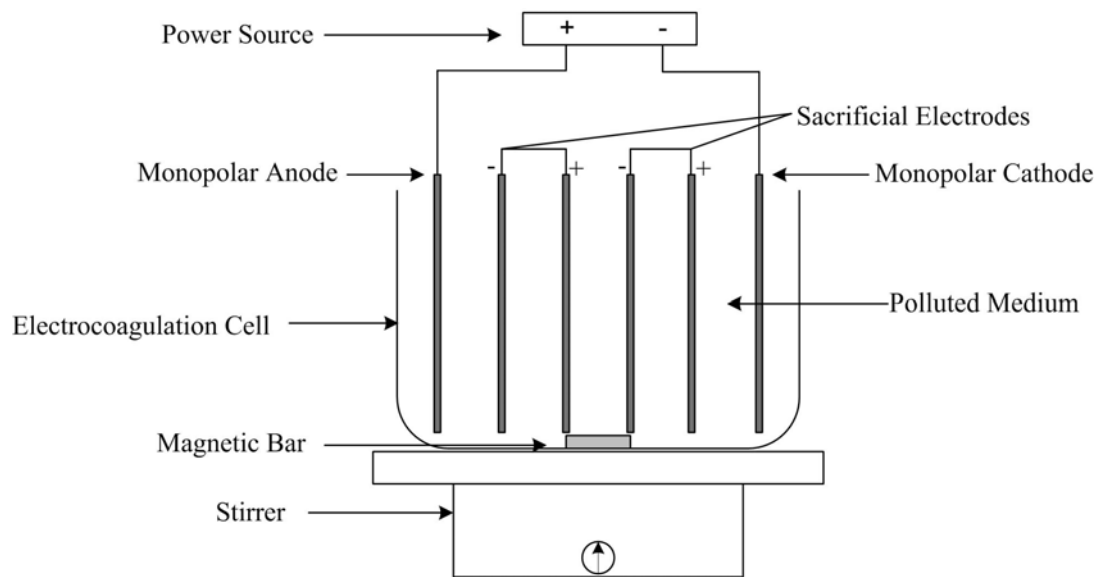


Figure 2.10 Bench-scale electrocoagulation reactor with monopolar electrodes in series connection.

Since cells that are connected in a series mode have higher resistance, a higher potential is necessary for a given current flow, although the same current would, however, flow through the electrodes. On the other hand, cells connected in a parallel mode have their electric current divided between all the electrodes in relation to the individual resistance of the cell.

The use of bipolar electrodes in a parallel connected cell is also possible. In such case as shown in Figure 2.11, two parallel electrodes that are connected to the electric power source are situated on either side of the sacrificial electrode, with no

electrical connection to the sacrificial electrode. This way, conducting maintenance during use becomes easier in comparison due to the simple set-up. If an electric current is passed through the electrodes, the neutral sides of the connected plate will be transformed to charged sides, which have opposite charged compared to the parallel side beside it. In this setup, the sacrificial electrodes are referred to as bipolar electrodes (Mollah et al., 2001). Thus, during electrolysis, the positive side undergoes an anodic reaction, whereas a cathodic reaction takes place on the negative side.

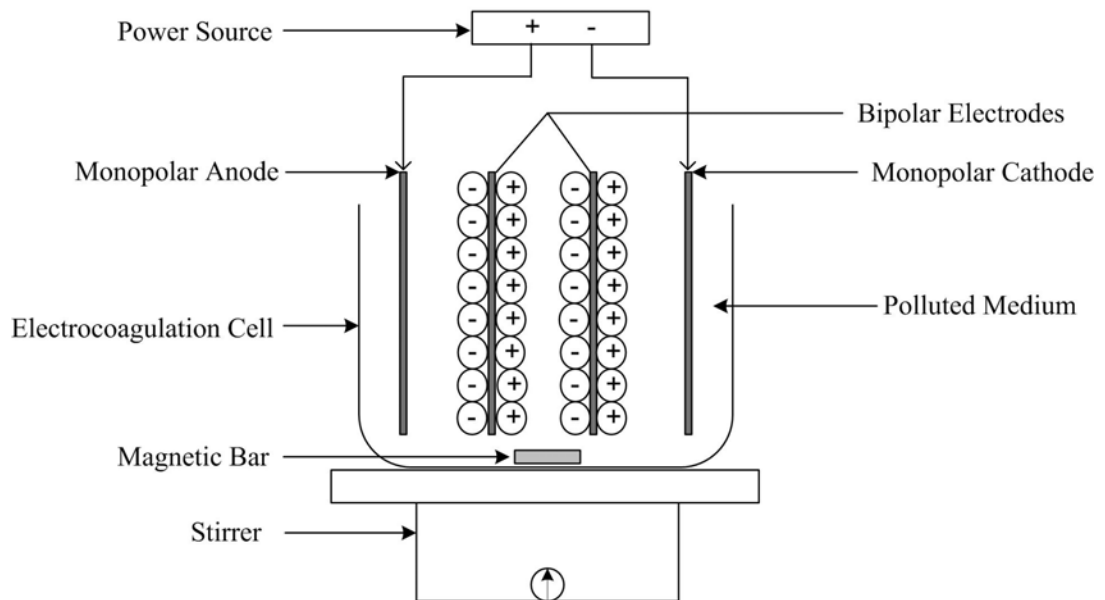


Figure 2.11 Bench-scale electrocoagulation reactor with bipolar electrodes in parallel connection.

*Reaction types in the electrocoagulation process involved in the study:*

The mechanism of electrocoagulation depends to a great extent on the chemistry of the aqueous medium, particularly its conductivity. Moreover, other characteristics such as pH, particle size and chemical constituent concentrations will also influence

the electrocoagulation process. In this study, electrocoagulation of the polluted medium was accomplished by using an aluminum electrode. The electrolytic dissolution of the aluminum anode produces the cationic monomeric species such as  $\text{Al}^{3+}$  and  $\text{Al}(\text{OH})_2^+$  at low pH. At appropriate pH values (Figure 2.8), they are transformed into  $\text{Al}(\text{OH})_3$  and finally polymerized to  $\text{Al}_n(\text{OH})_{3n}$  according to the following reactions:



Nevertheless, depending on the pH of the medium, other ionic species such as  $\text{Al}(\text{OH})_2^{2+}$ ,  $\text{Al}_2(\text{OH})_2^{4+}$ , and  $\text{Al}(\text{OH})_4^-$  may also be present in the system. The gelatinous charged hydroxo cationic complexes can effectively remove pollutants by adsorption to produce charge neutralization, and by enmeshment in a precipitate (Mollah et al., 2001).

#### 2.4.6.2 Previous Studies

The summary of some important previous studies related with electrocoagulation is given below:

Vik et al., (1984) studied electrocoagulation with aluminum electrodes for humus removal from potable water. The study presented results showing the correlation between the current density and the aluminum dosing. A comparison of electrocoagulation with conventional coagulation showed that the aquatic humus is removed equally well with both methods. Conventionally coagulated water (using alum) holds higher concentrations of sulphate, and thus has a higher specific conductivity than the electrochemically treated water. The electrochemically treated water holds higher residual aluminum concentrations than the conventionally treated water owing to the higher pH values as expected.

Szynkarczuk et al., (1994) studied electrochemical coagulation of clay suspensions. In their studies, suspension of kaolinite and bentonite was coagulated by electrochemical treatment where aluminum anodes dissolve and aluminum ions interact with clay particles, forming flocs which precipitate. In the research, effect of several factors such as NaCl concentration, applied voltage, flow conditions within the cell were examined. It was concluded that aluminum concentration has a key role in decreasing the turbidity of the supernatant and the clarity of the supernatant depended on applied current, applied voltage, flow conditions and the presence of NaCl.

Chen et al., (2000) separated pollutants from restaurant wastewater by electrocoagulation. The characteristics of restaurant wastewater were investigated and high oil and grease contents were detected. Different electrode materials and operational conditions were examined. Aluminum was found to be better than iron. Charge loading was found to be the only factor affecting the treatment efficiency significantly. The optimum charge loading and current density were 1.67–9.95 F/m<sup>3</sup> wastewater and 30–80 A/m<sup>2</sup> depending on the wastewater tested. The removal efficiency of oil and grease exceeded 94% for all wastewaters tested. The experimental results also pointed out that in the electrocoagulation wastewater can be neutralized.

Abuzaid et al., (2002) investigated ground water coagulation of the Eastern Province of Saudi Arabia using stainless steel electrodes. The ground water was found to have a conductivity of 4400  $\mu$ S/cm and chloride and sulfate concentrations of 834 and 550 mg/L respectively. The turbidity of ground water was increased to 76 nephelometric turbidity unit (NTU) by the addition of bentonite. Turbidity of ground water was measured as 0.6 NTU. The efficiency of stainless steel electrodes for the in-situ formation of ferric hydroxide was investigated. The electrical current input was found to be inversely proportional to the residual turbidity in the test water. At a contact time of 5 min and a natural chloride content, the highest turbidity removal efficiency of 95% was achieved at a current of 1 A. When the current was reduced to 0.5 A and the contact time was increased to 10 min, the

residual turbidity was reduced from 4.0 to 1.6 NTU. Furthermore, similar turbidity removals were achieved at a much shorter contact time (2 min) when 1 g/L sodium chloride was added to the test water. Due to the significance of pH variation with regard to coagulation, the phenomenon of voltage-induced hydrogen evolution was investigated as well. While the solutions final pH increased with the increase in current and contact time, it decreased with the increase in sodium chloride concentration. This trend was attributed to two reasons; first, the increase in NaCl concentration increased the conductivity of the solution which reduces the voltage needed to have a certain current. Voltage reduction would reduce the hydrogen evolution, which is responsible for the increase in pH. Second, the increase in NaCl concentration increased the amount of chloride ions, which could be electrically converted to chlorine gas. The increase in chlorine gas production increased the concentration of hypochloric acid in the test water. This tended to reduce the solution final pH.

Holt et al., (2002) studied on quantitative comparison between coagulation and electrocoagulation based on turbidity removal associated with a clay pollutant. It was found that coagulation was more effective than electrocoagulation under acidic conditions ( $\text{pH} \sim 4$ ) and low coagulant levels (4 mg-Al/L). Highly effective coagulation was observed at intermediate alum dosage levels (4-20 mg-Al/L), where the isoelectric point occurred at  $\text{pH} \sim 7.8$ . Three operating stages (lag, reactive and stable) were identified in a batch electrocoagulation reactor. Little or no turbidity change was observed in the lag stage with the majority ( $\sim 95\%$ ) of the turbidity removal occurring during the reactive stage. At the isoelectric point, occurring during the reactive stage, the greatest turbidity reduction occurs, indicating aggregation by a sorption mechanism (compared to the charge neutralization as in the case of chemical coagulation). During the stable stage, continued precipitation of aluminum hydroxide and a decrease in turbidity indicated a sweep coagulation mechanism. The highest current (2 A) reduced the pollutant level in the shortest time, 1% residual turbidity after 30 min, though the highest efficiency (in terms of pollutant removed per unit of aluminum added) was achieved at the lowest current (0.25 A).

Kobyas et al., (2003) investigated the textile wastewater (Gebze, Turkey) by electrocoagulation using iron and aluminum electrodes. The effects of relevant wastewater characteristics such as conductivity and pH, and important process variables such as current density and operating time on the chemical oxygen demand (COD) and turbidity removal efficiencies were explored. Moreover, the electrode and energy consumptions for each electrode were calculated. The results show that iron is superior to aluminum as sacrificial electrode material, from COD removal efficiency and energy consumption points.

Yılmaz et al., (2005) investigated parameters affecting boron removal from wastewaters by electrocoagulation using aluminum electrode. Several working parameters, such as pH, current density, boron concentration and type and concentration of supporting electrolyte were studied in an attempt to attain a higher removal capacity. The experiments were carried out by keeping the pH of solution constant and optimum at the value of 8. Even though energy consumption increased with decreasing boron concentration, boron removal efficiency was higher at 100 mg/L than that of 1000 mg/L. Current density was an essential parameter affecting removal efficiency. Boron removal efficiency and energy consumption rose with increasing current density from 1.2 to 6.0 mA/cm<sup>2</sup>. The types of different supporting electrolyte were examined and it was found that the highest boron removal efficiency, 97%, was obtained with CaCl<sub>2</sub>.

Can et al., (2006) studied the textile wastewater by combined coagulation and electrocoagulation. They investigated the effects of initial addition of a coagulant such as polyaluminum chloride (PAC) or alum on the COD removal efficiency of electrocoagulation treatment of textile wastewaters. The two salts exhibited the same performance in chemical coagulation, yet in the combined electrocoagulation (CEC), PAC was found to significantly enhance the COD removal rate and efficiency, depending on the amount of the total aluminum supplied, by initial addition and electrochemical generation. A comparative operating cost analysis was also given and it was found that with the same operating cost per mass of COD

removed, CEC performance was 80%, in contrast to 23% with electrocoagulation, in 5 min of operation.

The work of Canizares et al., (2007) intended to compare both continuous and batch processes, and the efficiencies of the coagulation and the electrocoagulation processes with hydrolyzing aluminum salts, and to determine the similarities or differences that exist between both coagulation processes. The charge neutralization by the adsorption of monomeric hydroxocations onto the kaolin surface was found to be the primary coagulation-mechanism for low concentration of aluminum and acidic pHs (below 4). In the range of pH 4–7, two primary mechanisms explained the experimental behavior of the system: sweep flocculation for high concentration of aluminum, and a combination of precipitation-charge-neutralization and charge neutralization by adsorption of monomeric or polymeric aluminum, for low concentration of aluminum. In the continuously-operated processes, the efficiency in the turbidity removal seemed to be much related to the aluminum species present in the treated waste, and not to the way of adding aluminum to the reaction system. For the same steady-state pH and aluminum concentration, the same turbidity removal was achieved in both, the coagulation and the electrocoagulation processes. For high aluminum/kaolin ratios, kaolin suspensions which contain sulfate as electrolyte, achieved better removals of turbidity than those containing chloride ions. The operation mode (continuous or discontinuous) had great influence on the efficiency of the electrocoagulation processes. Similar efficiencies were attained for low (below 5 mg/L) and high doses of aluminum (above 20 mg/L). Nevertheless, at intermediate doses a strong difference was observed, with a more marked decrease in the efficiency in the discontinuous process. This observation was explained regarding that the addition of aluminum in the continuous process was instantaneous (and not progressive as in the discontinuous one), and thus, the sweep coagulation mechanism was more favored.



## CHAPTER 3

### MATERIALS AND METHODS

In this chapter, the materials used in electrocoagulation and coagulation, and the methods applied will be given in two sub-sections; materials and methods.

#### 3.1 Materials and Characterization

Electrocoagulation and coagulation tests were conducted with suspensions of ultrafine kaolinite ( $\text{Al}_4(\text{Si}_4\text{O}_{10})(\text{OH})_8$ ) and ultrafine quartz ( $\text{SiO}_2$ ) in water. The kaolinite and quartz samples were obtained from Eczacıbaşı Esan, Turkey.

Specific gravities of samples were measured with Beckman Model 930 Air Comparison Pycnometer which measures volume of powdery, granular, porous and irregularly shaped solids. Measurements were repeated at least three times, by getting different amounts of solid sample and then results of the measurements were averaged. Average specific gravities of kaolinite and quartz samples were found 2.60 and 2.65, respectively.

All samples were prepared to minus 10  $\mu\text{m}$  by wet sedimentation method. Stokes law was used to determine the settling time for particles using equations 18 and 19.

$$V_s = \frac{g(\rho_p - \rho_w)D^2}{18\eta} \quad (18)$$

$$\text{where } V_s = \frac{h}{t} \quad (19)$$

In the equations,  $g$  is the gravitational acceleration ( $981 \text{ cm/sec}^2$ ),  $\rho_p$  is the density of the particles ( $\text{g/cm}^3$ ),  $\rho_w$  is the density of water ( $\text{g/cm}^3$ ),  $D$  is the particle diameter ( $\text{cm}$ ) and  $\eta$  is viscosity of water ( $0.01 \text{ g/cm.sec}$ ),  $t$  is the time required for a  $10 \text{ }\mu\text{m}$  particle to settle from the water level to the bottom of the graduated cylinder, distance  $h$ . For example,  $10 \text{ }\mu\text{m}$  kaolinite particles settle  $15 \text{ cm}$  in  $29$  minutes.

Cation exchange capacity of kaolinite and quartz was determined by using methylene blue method (ASTM C 837-81 standard test method (see Appendix C)). Methylene blue is a dye and has the formula  $\text{C}_{16}\text{H}_{18}\text{N}_3\text{S}(\text{Cl}) \cdot 3\text{H}_2\text{O}$  with the formula weight  $373.9$ . The reagent solution of methylene blue was prepared by dissolving  $3.73 \text{ g}$  in  $1$  liter of distilled water. After preparation  $1 \text{ mL}$  of stock solution corresponded to  $0.01 \text{ meq}$  (equivalent weight and formula weight are identical). Then,  $2 \text{ g}$  dried clay (or quartz) was placed in a  $600\text{-mL}$  beaker,  $300 \text{ mL}$  distilled water was added and stirred. pH was adjusted to about  $3$  by adding appropriate amount of  $0.1 \text{ M}$  sulfuric acid. Methylene blue solutions present in a burette was added as  $5 \text{ mL}$  portions into the suspension with continuous stirring. A drop of the suspension was taken out using a dropper (or a glass stirring rod), and placed on the filter paper. The appearance of the drop on the filter paper was observed. The end point was indicated by the formation of a light blue halo around the drop.

The calculation of cation exchange capacity (in other words methylene blue index, MBI) was done by using the following equation (ASTM C 837-81);

$$\text{MBI} = \frac{E \times V}{W} \times 100 \quad (20)$$

where MBI is the methylene blue index for clay in  $\text{meq}/100\text{g}$  clay,  $E$  is milliequivalents of methylene blue per milliliter ( $1\text{mL} = 0.01 \text{ meq}$ ),  $V$  is milliliters

of methylene blue solution required for the end point in the titration, and W is grams of dry material.

Experiments were carried out using 2 g kaolinite and 2 g quartz samples. In kaolinite case, 15 mL methylene blue solution was used. In quartz, MBI was not identified because no blue halo was observed by addition of first 5 mL methylene blue.

For the adsorption characteristics of the materials, particle size distribution and BET surface area analysis were done.

Elemental composition and mineral characteristics of the kaolinite and quartz samples were determined using X-ray fluorescence (XRF), X-ray powder diffraction (XRD), and infrared spectrometry (FTIR) methods.

Scanning electron microscope (SEM) analyses were done to determine the morphology of the samples.

In addition, zeta potential of the suspended particles was measured. The results of particle size distribution, XRD analysis, and zeta potential measurements are presented in Appendix D.

Particle size distribution of kaolinite and quartz suspensions was determined by a Malvern Mastersizer 2000, which uses light scattering technique to get intensity patterns. Analysis was done in Central Laboratory of METU. Particle diameter and volume were calculated by the Mastersizer using Mie theories. The Mie theory (Thiele and French, 1998) includes both diffraction and diffusion of the light around the particle in its medium. It measures particles from 0.02  $\mu\text{m}$  to 2000  $\mu\text{m}$ , depending on the material properties.

Surface area measurements were done at İnönü University Mining Engineering Department. A Tri Star 3000 (Micromeritics, USA) surface analyzer was used to

measure nitrogen adsorption isotherm at 77 °K. Before measurement, the sample was degassed at 400 °C for 2 hours. The BET surface area ( $S_{\text{BET}}$ ), external surface area ( $S_{\text{ext}}$ ), micropore area ( $S_{\text{mic}}$ ), mesopore area ( $S_{\text{meso}}$ ), total pore volume ( $V_t$ ), average pore diameter ( $D_p$ ) were obtained from the adsorption isotherms. Mesopore volume ( $V_{\text{meso}}$ ) was determined by subtracting the micropore volume ( $V_{\text{mic}}$ ) from total pore volume.

Elemental composition of the samples was determined by Benchtop X-ray Florescence Spectrometer in METU Mining Engineering Department and Spectro X-Lab 2000 PED-XRF spectrometer in Ankara University Geological Engineering Department.

In the measurements, samples were prepared from 6.25 g of powder that was pressed (at 15 tons for 1 min) to form discs (40-mm diameter and 3 mm thick) for the former spectrometer. For the latter spectrometer, sample was prepared from 4 g of powder that was pressed (at 15 tons for 1 min) into thick pellets of 32 mm diameter after mixing them with the wax as binder. The results of elemental composition with both spectrometers were similar and here elemental composition according to second spectrometer was considered.

Mineral composition of the samples was determined by Rigaku Miniflex Diffractometer in METU Chemistry Department using Cu  $K\alpha$  (30 kV, 10 mA,  $\lambda=1.54050$  Å) radiation. Scanning was done between  $5^\circ < 2\theta < 70^\circ$ . The measurements were made with 0.01 and 0.05 degree steps and 1 degree/minute rate. The divergence slit was variable and receiving slit scattering were 0.3 mm and 4.2 degree, respectively.

XRD analysis of quartz was done by using quartz sample directly. However, in the kaolinite sample XRD analysis was done in two ways. One is using air-dried sample directly. The other is using clay fraction of the sample. To get the clay fraction, 10 g kaolinite was suspended in 1000 ml of distilled water until good dispersion was achieved. After 4 hours, the sample from the 5 cm top of the beaker was transferred

to centrifuge tubes and centrifuged at 600 rpm. The solid residue was dried at room temperature and used for XRD measurement.

FTIR analysis of samples was done using VARIAN 1000FTIR Spectrometer in METU Chemistry Department. IR pellets were prepared using spectroscopic grade KBr after heating at 180 °C for several hours. In the pellet, KBr to sample ratio was 100 mg/3mg. The IR spectra of samples were taken in the range of the 400 to 2000  $\text{cm}^{-1}$ .

The morphology of the samples used in the study was investigated with Quanta 400F Field Emission scanning electron microscope in METU Central Laboratory. SEM images were obtained from the materials as powder form. Samples were coated with a very thin layer of a gold-palladium (Au-Pd) alloy.

The zeta potential ( $\zeta$ ) of kaolinite and quartz particles was measured with Zetasizer Nano-Z meter in the Research Laboratory of Mining Engineering Department of METU. The Zetasizer takes a series of measurements (here 3 measurements) and gives an average potential. For the zeta potential measurements 10 mg sample was put into a 100 mL of distilled water. 0.1 M  $\text{H}_2\text{SO}_4$  and 0.1 M NaOH solutions were used to adjust the pH of the suspension to the desired values and zeta potential was measured.

The particle size distribution, BET surface area analysis, cation exchange capacity, XRF, XRD and FTIR analyses, SEM characterization and zeta potential measurements results for kaolinite and quartz particles were given in Chapter 4.

### **3.2 Experimental Methods**

Kaolinite suspensions used for electrocoagulation and coagulation were prepared by mixing appropriate amounts of powdered material with 250 mL of distilled water so that a solid concentration of 0.20 g/L was obtained. Quartz suspensions were prepared in the same way with the solid concentration of 0.32 g/L. The pH of

suspension was adjusted to the desired values using 0.1 M H<sub>2</sub>SO<sub>4</sub> and 0.1 M NaOH solutions and measuring the pH with a pH meter (Hanna pH 211).

Before and after electrocoagulation and coagulation the turbidity of suspensions was measured with a Lamotte Model 2008 Portable Turbidimeter. The results were expressed in nephelometric turbidity units (NTU). Measurement accuracy was  $\pm 2\%$  of reading or 0.05 NTU. Photodetector was silicon photodiode, centered at 90° to the incident light path.

The batch electrocoagulation cell used in the experimental study was constructed of plexiglass with dimensions of 65 mm  $\times$  65 mm  $\times$  110 mm (Figure 3.1). The electrode arrangement consisted of two stainless steel cathodes which were interspersed with two aluminum anodes, and brass rods were used to connect the parallel plate electrodes in monopolar mode. The aluminum anodes and stainless steel cathodes were made from plates with dimensions of 55 mm  $\times$  45 mm  $\times$  3 mm, and the spacing between the electrodes was 21 mm. The effective electrode area of each electrode was 23 cm<sup>2</sup>. The electrodes were connected to a DC power supply. Suspensions were stirred using a magnetic stirrer (Velp Scientifica) adjusted to an optimal rate (300 rpm) in order to attain the highest efficiency of turbidity removal. A conductivity meter (Lovibond SensoDirect Con2000) and a digital thermometer (Hanna Checktemp 1) were employed to measure electrical conductivity and temperature of the suspensions, respectively. A water jacket was used to keep the suspension at room temperature (nominally 21 °C). The current that flows through the cell and the voltage across the electrodes were measured with an ampermeter and a voltmeter, respectively. Before each electrocoagulation run, the electrodes were washed with acetone to remove surface grease, and impurities on the aluminum and stainless steel electrode surfaces were removed by means of dipping electrodes for 1 min in a special solution. The solution was prepared by mixing 50 cm<sup>3</sup> of 35% HCl and 100 cm<sup>3</sup> of hexamethylenetetramine aqueous solution (2.80%) as described by Kobya et al. (2003).

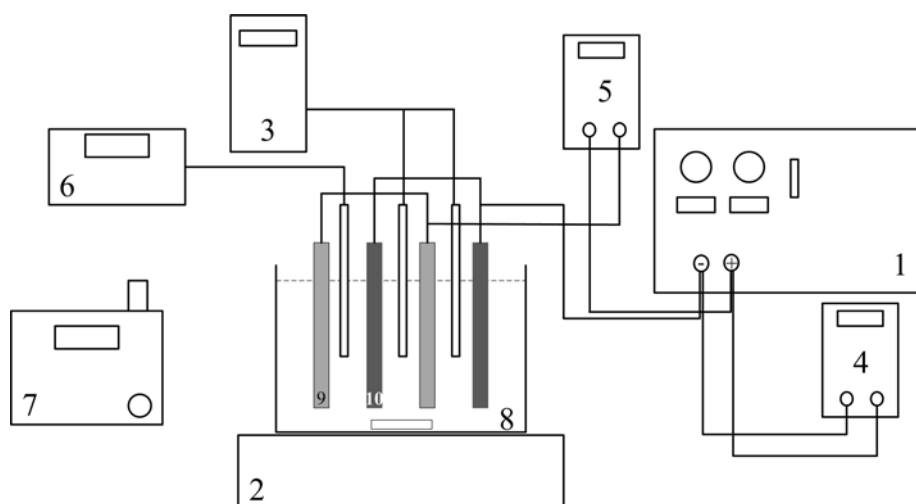


Figure 3.1 Schematic diagram of electrocoagulation experimental setup (1) Power supply, (2) Magnetic stirrer, (3) Conductivity meter, (4) Voltmeter, (5) Ampermeter, (6) pH meter, (7) Turbidimeter, (8) Electrocoagulation cell, (9) Aluminum electrodes, (10) Stainless steel electrodes.

Conventional coagulation tests were conducted using the standard jar testing technique (Figure 3.2) with the addition of aluminum sulfate solutions ( $10^{-2} - 10^{-6}$  mol/L) at room temperature (nominally 21 °C) and a constant stirring speed of 300 rpm. Experimental variables of electrocoagulation and conventional coagulation studies are presented in Table 3.1.

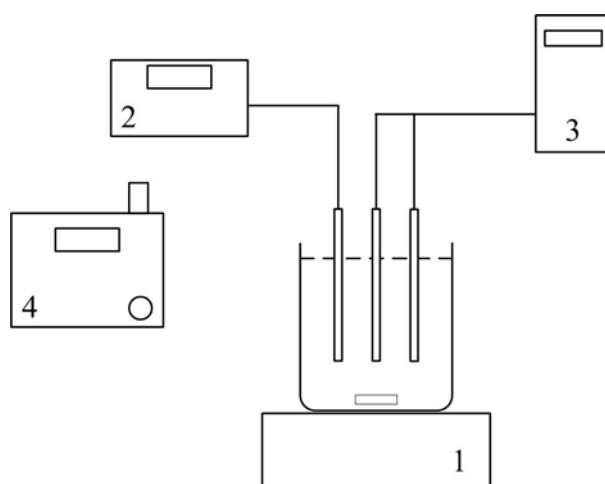


Figure 3.2 Coagulation Unit (1) Magnetic Stirrer, (2) pH meter, (3) Conductivity meter, (4) Turbidimeter.

Table 3.1 Experimental variables for electrocoagulation and coagulation experiments.

<b>Electrocoagulation</b>	
pH	2-11
Voltage	0-60 V
Current density	10-200 A/m <sup>2</sup>
Time	1-60 min
<b>Coagulation</b>	
pH	2-11
Aluminum dosage	0-100 mg Al/L



The amount of aluminum dissolved in an electrocoagulation experiment was theoretically calculated using Faraday's Law, which expresses the relationship between the amount of metal dissolved or deposited and the current density (Eq. 12).

After each electrocoagulation or conventional coagulation run, the coagulated suspension was poured into a 300-ml beaker, and 20-ml sample solution was taken from a fixed depth at a predetermined settling time to measure the turbidity. Settling times of 0, 5, 10, 20, and 30 minutes were separately studied by running replicate electrocoagulation and coagulation tests. Ten minutes of settling time was found to be the most appropriate duration in the experiments. The efficiency of turbidity removal, R (%), was calculated using the formula given below;

$$R (\%) = \frac{T_o - T_t}{T_o} * 100 \quad (21)$$

where,  $T_o$  is the initial turbidity of the suspension just before electrocoagulation or coagulation, and  $T_t$  is the turbidity at the end of a predetermined settling time (t) after the electrocoagulation or coagulation run.

## **CHAPTER 4**

### **RESULTS AND DISCUSSION**

In this chapter, the results of the experiments and the resultant discussions are given under the following titles: (1) materials characteristics, (2) preliminary experimental studies (3) effect of initial pH on electrocoagulation and coagulation (4) effect of voltage on electrocoagulation (5) effect of current density and time on electrocoagulation (6) effect of aluminum dosage on electrocoagulation and coagulation of kaolinite and quartz suspensions.

#### **4.1 Material Characteristics**

Material characterization studies involve particle size distribution, BET surface area, cation exchange capacity (CEC), analysis to get element composition, analysis to get mineral composition and zeta potential measurement. All these studies have been explained separately for kaolinite suspension and quartz suspension.

##### **4.1.1 Kaolinite**

The volume-basis particle size distribution of the kaolinite sample as measured by the Malvern Mastersizer 2000 is shown in Figure 4.1. The  $d_{50}$  (median) size and the  $d_{90}$  (90% finer) size were determined as 1.82  $\mu\text{m}$  and 4.93  $\mu\text{m}$ , respectively.

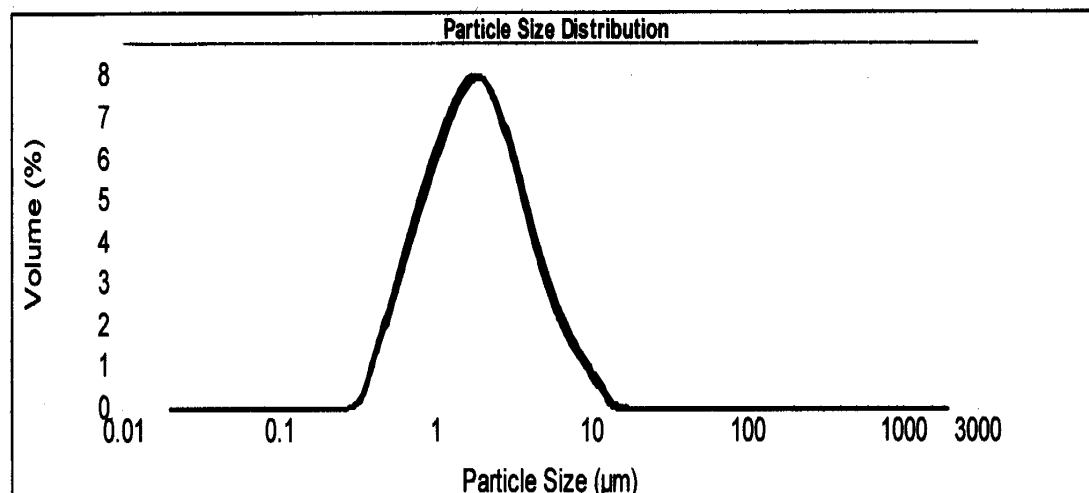


Figure 4.1 Particle size distribution of kaolinite.

When a solid is porous and consists of discrete particles as in this case, it is convenient to describe the outer boundary of the particles as the external surface ( $S_{\text{ext}}$ ) (IUPAC, 1972). Pores can be classified according to their sizes ( $D_p$ ) as:

- (i) pores with widths exceeding 50 nm (500 Å) are called macropores;
- (ii) pores with widths not exceeding 2 nm (20 Å) are called micropores;
- (iii) pores of sizes between 2 and 50 nm are called mesopores (IUPAC, 1972).

The micropore volume ( $V_{\text{mic}}$ ) and mesopore volume ( $V_{\text{meso}}$ ) correspond to the volume of the adsorbed material which completely fills the micropores and mesopores expressed in terms of bulk liquid ( $N_2$ ) at atmospheric pressure and at the temperature of measurement, respectively.

The BET surface area analysis results for kaolinite particles are given in Table 4.1. The total surface area was 16.42 m<sup>2</sup>/g. Kaolinite particles had mesopore structure ( $2 < D_p < 50$  nm).

Cation exchange capacity (MBI) of kaolinite was calculated 7.5 meq/100g clay.

Table 4.1 BET surface analysis of kaolinite.

Material	$S_{\text{BET}}$ ( $\text{m}^2/\text{g}$ )	$S_{\text{ext}}$ ( $\text{m}^2/\text{g}$ )	$S_{\text{mic}}$ ( $\text{m}^2/\text{g}$ )	$S_{\text{meso}}$ ( $\text{m}^2/\text{g}$ )	$V_{\text{t}}$ ( $\text{cm}^3/\text{g}$ )	$V_{\text{mic}}$ ( $\text{cm}^3/\text{g}$ )	$V_{\text{meso}}$ ( $\text{cm}^3/\text{g}$ )	$D_{\text{p}}$ (nm)
Kaolinite	16.42	12.50	3.92	12.50	0.039073	0.001912	0.037161	9.52

$V_{\text{t}}$  – Single point adsorption total pore volume of pores less than 165.5682 nm diameter at  $P/P_0$  0.98817836

Table 4.2 Elemental composition (%) of kaolinite.

Element	%
<b>SiO<sub>2</sub></b>	48.15
<b>Al<sub>2</sub>O<sub>3</sub></b>	38.36
<b>Na<sub>2</sub>O</b>	0.133
<b>MgO</b>	<0.023
<b>P<sub>2</sub>O<sub>5</sub></b>	<0.00069
<b>Cl</b>	0.02427
<b>SO<sub>3</sub></b>	0.1984
<b>K<sub>2</sub>O</b>	0.5033
<b>CaO</b>	0.0856
<b>TiO<sub>2</sub></b>	0.4996
<b>MnO</b>	0.00376
<b>Fe<sub>2</sub>O<sub>3</sub></b>	0.4323
<b>V<sub>2</sub>O<sub>5</sub></b>	0.0172
<b>Cr<sub>2</sub>O<sub>3</sub></b>	0.0632
<b>H<sub>2</sub>O<sup>+</sup></b>	11.50

Elemental composition analysis of kaolinite (Table 4.2) showed that amount of silicon dioxide and aluminum oxide was 48.15% and 38.36%, respectively, which was consistent with the expected kaolinite structure. In addition, Na<sub>2</sub>O (0.133%), K<sub>2</sub>O (0.503%), TiO<sub>2</sub> (0.499%), SO<sub>3</sub> (0.198%), Fe<sub>2</sub>O<sub>3</sub> (0.432%) were present which may be due to the presence of some other silicates. About 11.5% loss on ignition (LOI) corresponds to adsorbed water in kaolinite structure.

Mineral composition of kaolinite was determined by XRD and FTIR analyses. All peaks of the XRD trace were almost consistent with the values expected for the kaolinite ICDD card numbered 75-1593 (Table D.2) thus, kaolinite sample used in the study was almost pure (Figure 4.2). Small amount of impurity came from quartz. As it is seen from Figure 4.2, some quartz peaks were observed. XRD traces of sample after direct drying and after separation of clay fraction and drying were closely the same. In the XRD trace some shifting was observed such that 7.02, 4.40, 4.31, 4.12, 3.81, 3.69, 2.73, 2.54 were present instead of 7.13, 4.46, 4.36, 4.16, 3.84, 3.73, 2.75, and 2.56 respectively (Table D.2 in Appendix D).

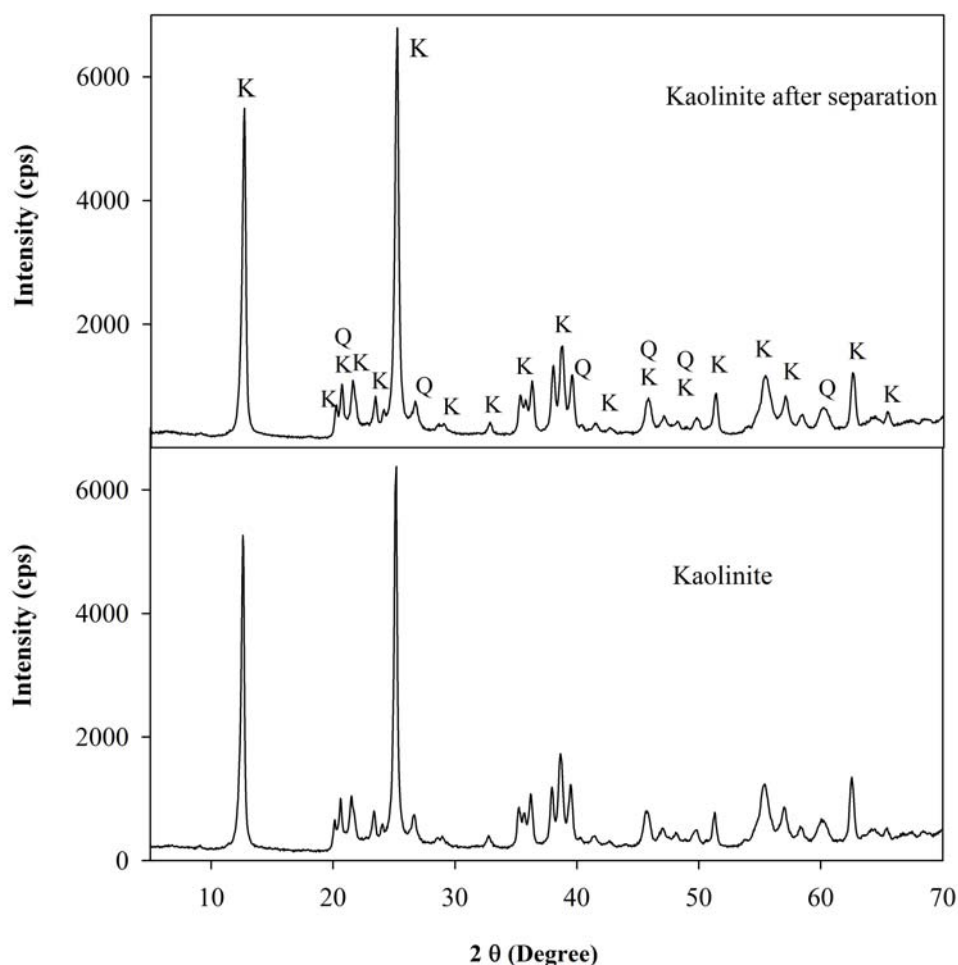


Figure 4.2 XRD pattern of kaolinite sample (air dried). K: kaolinite, Q: quartz.

In the IR studies of clay, the Si-O stretching vibrations were observed at  $790.9\text{ cm}^{-1}$ ,  $693.4\text{ cm}^{-1}$  and  $538.8\text{ cm}^{-1}$  and  $468.9\text{ cm}^{-1}$ . The strong bands at  $3696.7\text{ cm}^{-1}$ ,  $3622.5\text{ cm}^{-1}$ ,  $3450.4\text{ cm}^{-1}$ , indicated the possibility of the hydroxyl linkage (Marel and Beutelspacher 1976 and Nayak and Singh, 2007). However, a broad band at  $3450.4\text{ cm}^{-1}$  and a band at  $1633.4\text{ cm}^{-1}$  in the spectrum of clay suggested the possibility of hydration water in the clay. The interlayer hydrogen bonding in clay was assigned by a characteristic band at  $3622.5\text{ cm}^{-1}$ . Most of the bands such as  $3696.7\text{ cm}^{-1}$ ,  $3622.5\text{ cm}^{-1}$ ,  $3450.4\text{ cm}^{-1}$ ,  $1033.3\text{ cm}^{-1}$ ,  $914.5\text{ cm}^{-1}$ ,  $790.9\text{ cm}^{-1}$ ,  $693.4\text{ cm}^{-1}$ ,  $538.8$

$\text{cm}^{-1}$ ,  $468.9 \text{ cm}^{-1}$  proved the presence of kaolinite (Tuddenham and Lyon, 1960 as cited in Nayak and Singh, 2007).

All the above mentioned bands were observed in the kaolinite sample studied (Figure 4.3). Therefore, it was possible to say that the sample studied was pure kaolinite.

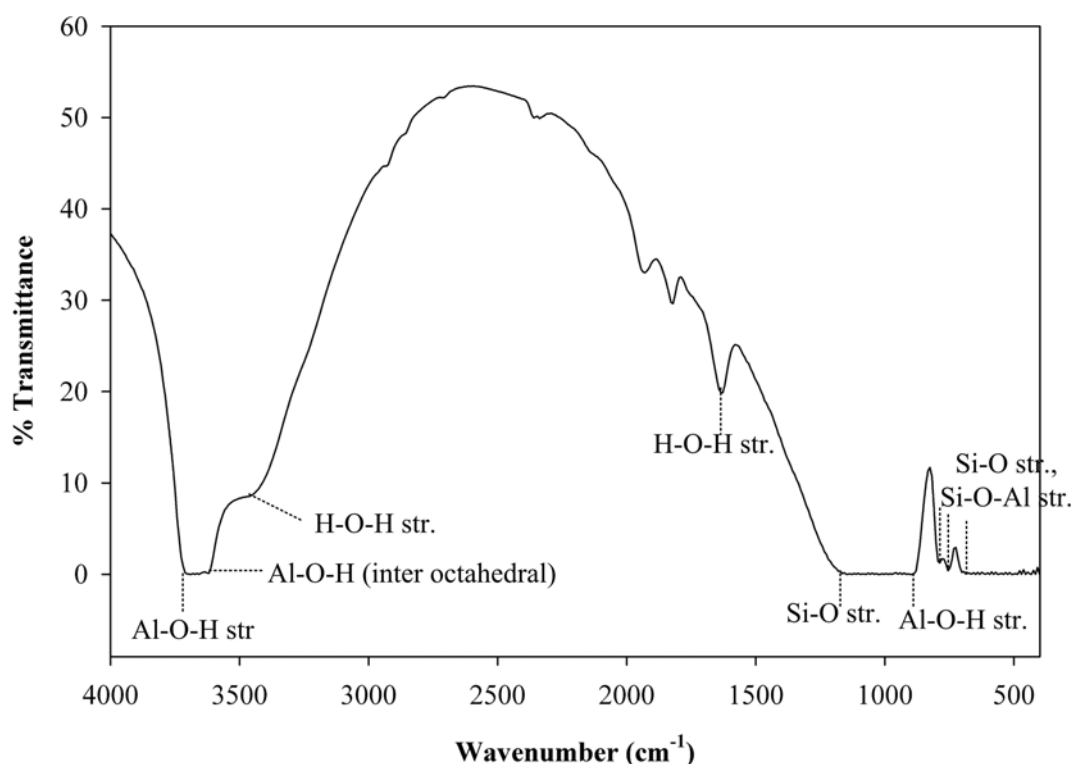


Figure 4.3 Infrared spectrum of the kaolinite.

SEM characterization of the kaolinite particles is illustrated between Figures 4.4 - 4.6. It is seen from the figures, after 10 minutes coagulation no individual particles had been observed easily. This showed the adsorption of coagulant on the surface of the particles and formation the bridges between the particles.

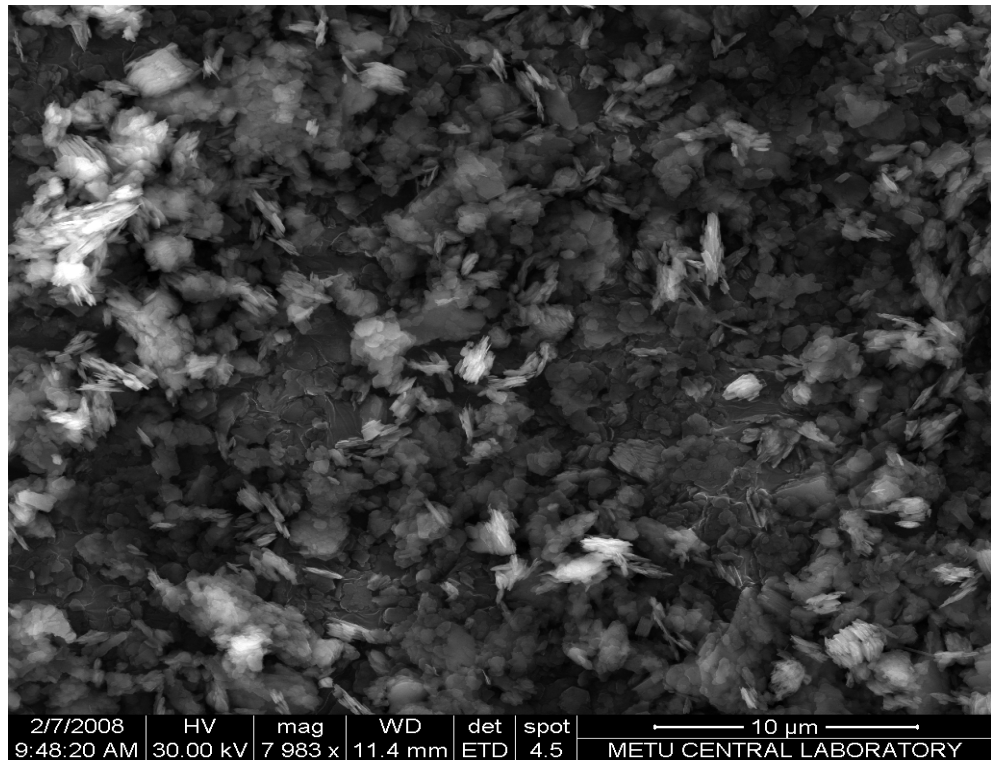


Figure 4.4 The SEM micrograph kaolinite particles before coagulation.

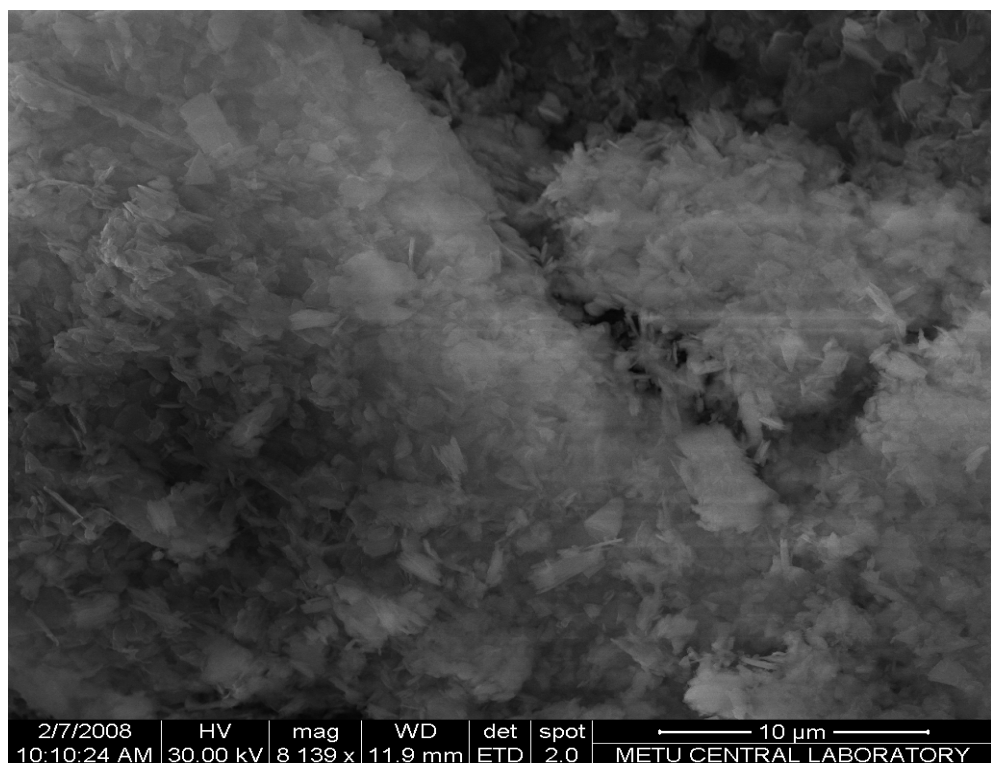


Figure 4.5 The SEM micrograph of kaolinite particles after electrocoagulation.



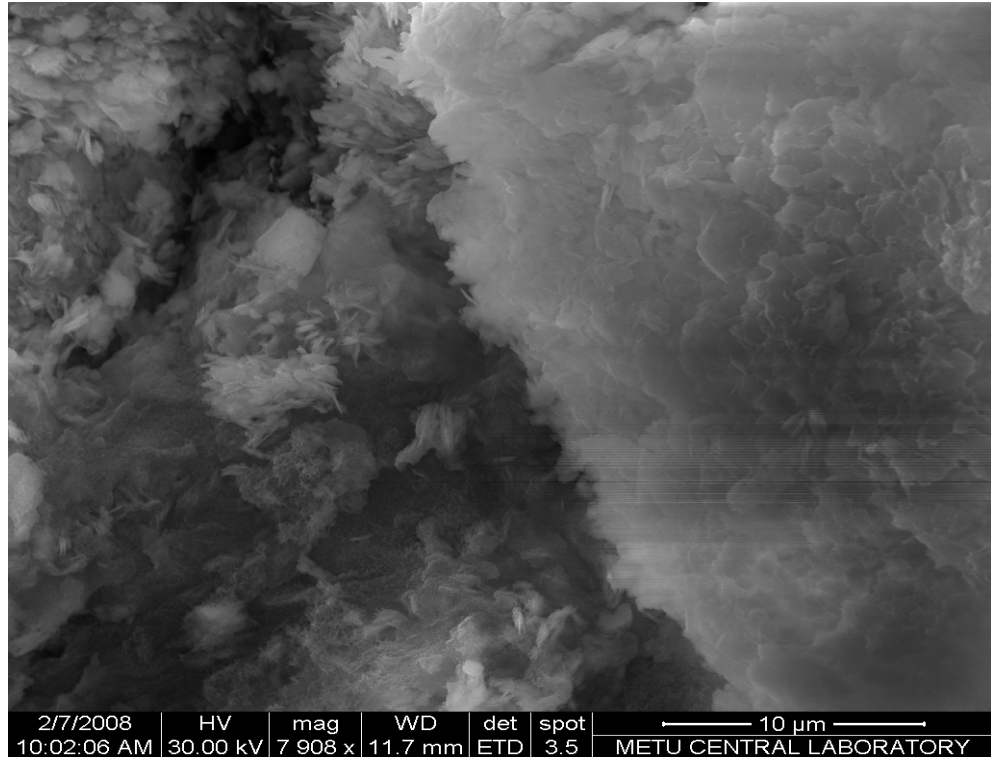


Figure 4.6 The SEM micrograph of kaolinite particles after coagulation.

The zeta potential of particles is a good indicator of their electrical potentials: the higher the zeta potential, the higher the surface potential of charged particles (kaolinite or quartz particles). The results obtained for zeta potential values measured against pH were plotted in Figure 4.7. Kaolinite zeta potentials showed negative surface charge in the pH range under investigation. There was no zero point of charge value for the samples. The negative charge of kaolinite particles may come from the edge charges and layer charges due to slight isomorphous substitution in the kaolinite lattice (Van Olphen, 1977). At the edges of the plate the tetrahedral silica sheets and octahedral alumina sheets are disrupted, and primary bonds are broken. This situation is similar to that on the surface of silica and alumina particles in silica and alumina sols. That part of the edge surface at which the octahedral sheet is broken may be compared with the surface of an alumina particle;



Such a surface carries a positive double layer in acid solution with aluminum ions acting as potential determining ion and a negative double layer in alkaline solution with  $\sim\text{AlO}^-$  acting as potential determining ions. The zero point of charge does not necessarily occur at neutral pH; it is actually known to vary with the crystal structure of the alumina particle. Hence, there is a definite possibility that in a neutral clay suspension a positive double layer is created on the edge surfaces due to the exposed alumina sheet (Van Olphen, 1977). The part of the edge surface at which the broken tetrahedral sheet is exposed may be compared with the surface of a silica particle;



Although silica surfaces normally carry a negative double layer, their charge is known to become positive in the presence of very small amounts of aluminum ions in the suspensions. Since such small concentrations of aluminum ions will occur in the equilibrium liquid of a clay suspension due to the slight solubility of the clay, it is quite possible to have a positive double layer on the broken silica surface on the edge (Van Olphen, 1977). In all pH values, these two charging mechanisms should be considered together. Negative surface charge is predominant this means that charge producing groups is silanol group (eq. 24).

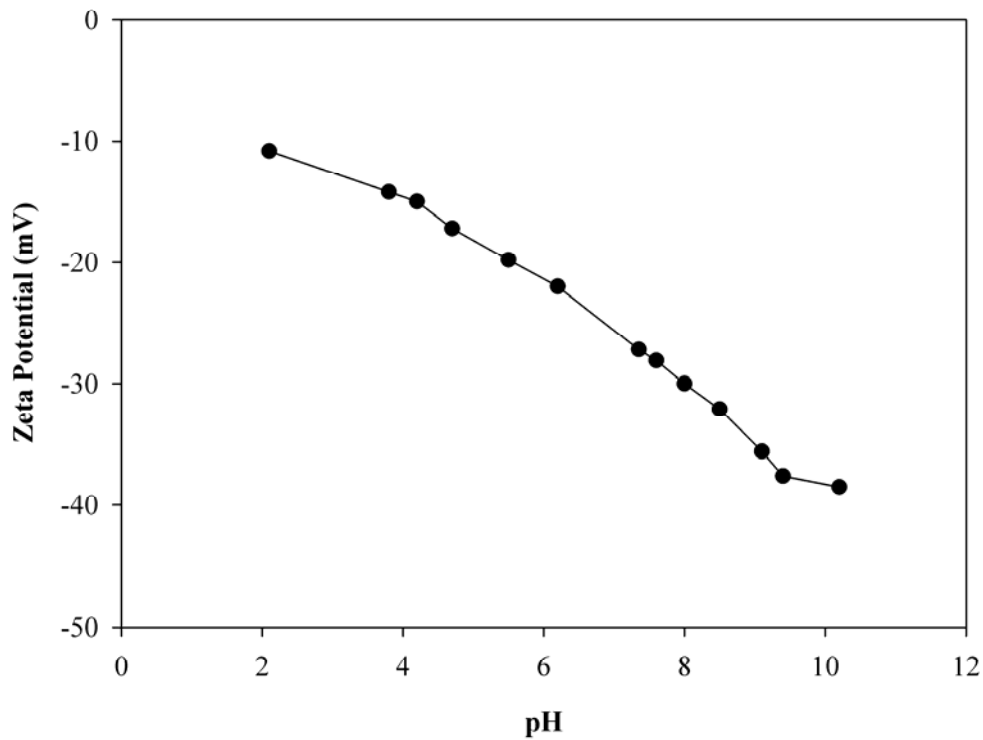


Figure 4.7 Zeta potential measurements of kaolinite sample at different pH.

#### 4.1.2 Quartz

The results of particle size distribution analysis showed that the median and 90%-finer sizes of the quartz sample were 5.13  $\mu\text{m}$  and 11.61  $\mu\text{m}$ , respectively, with the most probable particle size corresponding to 7  $\mu\text{m}$  (Figure 4.8).

The BET surface area of quartz sample was 2.12  $\text{m}^2/\text{g}$ . Table 4.3 summarizes the surface area analysis of quartz. The sample was found to have mesopore structure.

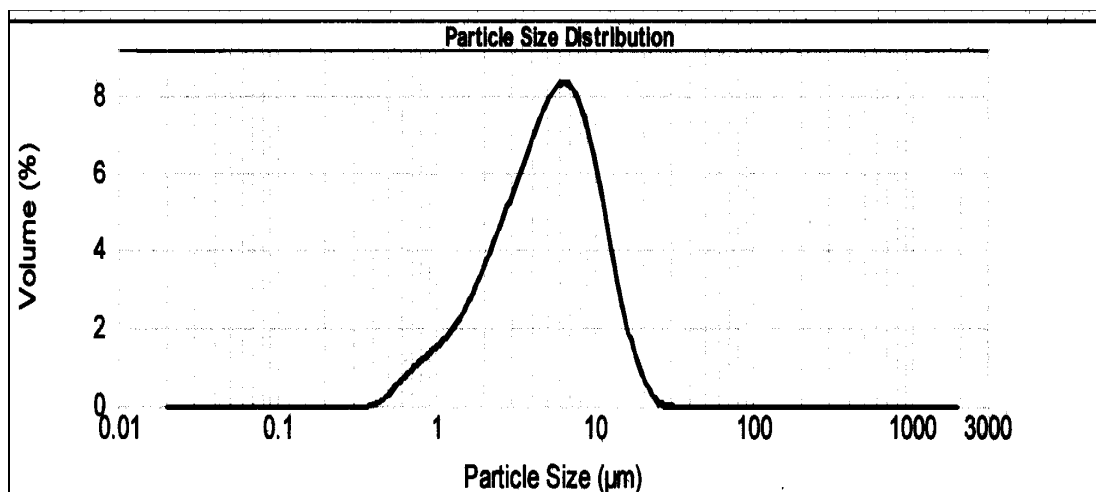


Figure 4.8 Particle size distribution of quartz.

Table 4.3 BET surface analysis of quartz.

Material	$S_{\text{BET}}$	$S_{\text{ext}}$	$S_{\text{mic}}$	$S_{\text{meso}}$	$V_t$	$V_{\text{mic}}$	$V_{\text{meso}}$	$D_p$
	(m <sup>2</sup> /g)	(m <sup>2</sup> /g)	(m <sup>2</sup> /g)	(m <sup>2</sup> /g)	(cm <sup>3</sup> /g)	(cm <sup>3</sup> /g)	(cm <sup>3</sup> /g)	(nm)
Quartz	2.12	1.26	0.86	1.26	0.004045	0.000466	0.003579	7.64

$V_t$  – Single point adsorption total pore volume of pores less than 165.5682 nm diameter at  $P/P_0$  0.98817836

Table 4.4 Elemental composition (as % of oxides) of quartz.

<b>Element</b>	<b>%</b>
<b>SiO<sub>2</sub></b>	99.5
<b>Al<sub>2</sub>O<sub>3</sub></b>	<0.0038
<b>Na<sub>2</sub>O</b>	<0.11
<b>MgO</b>	0.024
<b>P<sub>2</sub>O<sub>5</sub></b>	<0.00069
<b>Cl</b>	<0.0002
<b>SO<sub>3</sub></b>	<0.0001
<b>K<sub>2</sub>O</b>	<0.0012
<b>CaO</b>	<0.0014
<b>TiO<sub>2</sub></b>	0.0434
<b>MnO</b>	0.0358
<b>Fe<sub>2</sub>O<sub>3</sub></b>	0.0709
<b>V<sub>2</sub>O<sub>5</sub></b>	0.00093
<b>Cr<sub>2</sub>O<sub>3</sub></b>	0.0435

Mineral composition of quartz was determined by XRD and FTIR analyses. All peaks of the XRD trace (Figure 4.9) were consistent with the values expected for the quartz in reference to International Centre for Diffraction Data (ICDD) card numbered 46-1045 given in Table D.5 (Appendix D). The main peak of 3.34 Å° was shifted to 3.30 Å° in XRD trace of the sample. Similarly second intensive peak of 4.26 Å° was shifted to 4.19 Å°. The shifting of other peaks was not significant. The reason for shifting may have been due to the change in crystallographic structure of quartz. XRD trace of quartz supported the results of elemental composition. The mineral related with ferric oxide (hematite) was not identified in the XRD pattern because of its very small amount and/or amorphous structure.

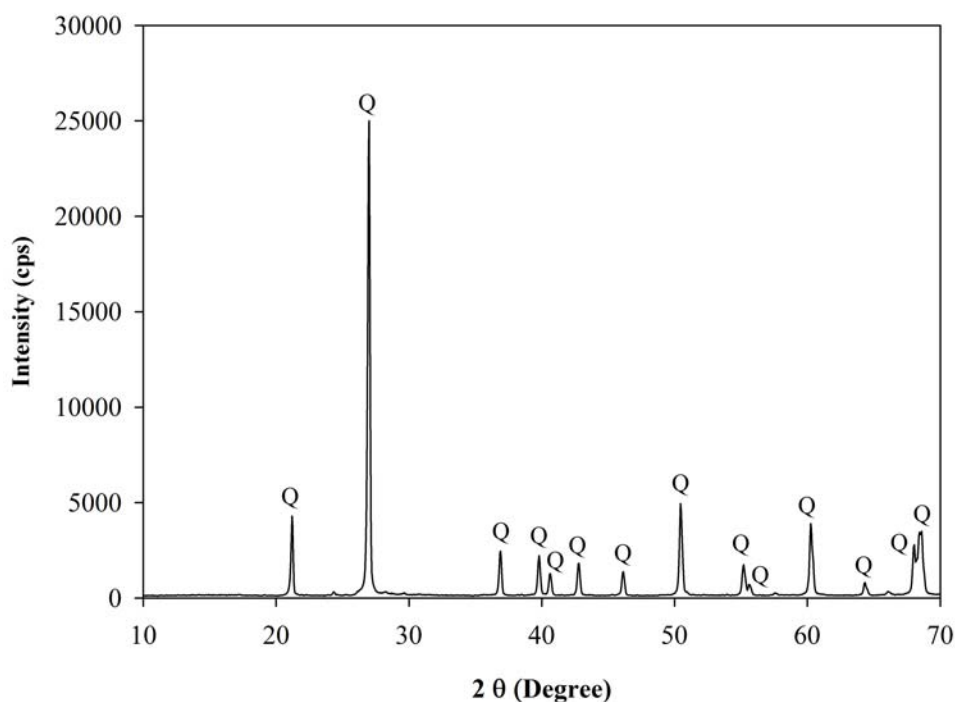


Figure 4.9 XRD pattern of quartz.

FTIR spectrum of quartz (Figure 4.10) also supported the results of XRF and XRD. In the IR studies of quartz, the Si-O stretching and bending vibrations were observed at  $1172\text{ cm}^{-1}$ ,  $1082\text{ cm}^{-1}$ ,  $790\text{ cm}^{-1}$ ,  $693\text{ cm}^{-1}$ ,  $512\text{ cm}^{-1}$ ,  $460\text{ cm}^{-1}$ . These IR bands confirmed the presence of quartz (Marel and Beutelspacher, 1976). The appearance of  $\nu$  (Si-O-Si) and  $\delta$  (Si-O) bands also supported the presence of quartz. A broad band at  $3450.4\text{ cm}^{-1}$  and a band at  $1633.4\text{ cm}^{-1}$  in the spectrum showed the possibility of water of hydration in the sample (Nayak and Singh, 2007). The bands at  $787\text{ cm}^{-1}$ ,  $952\text{ cm}^{-1}$ ,  $1069\text{ cm}^{-1}$ ,  $1170\text{ cm}^{-1}$  corresponded to Si-O stretching vibration. In addition, the band at  $459\text{ cm}^{-1}$  belongs to Si-O-Si bending vibration (Niimi et al., 1999).

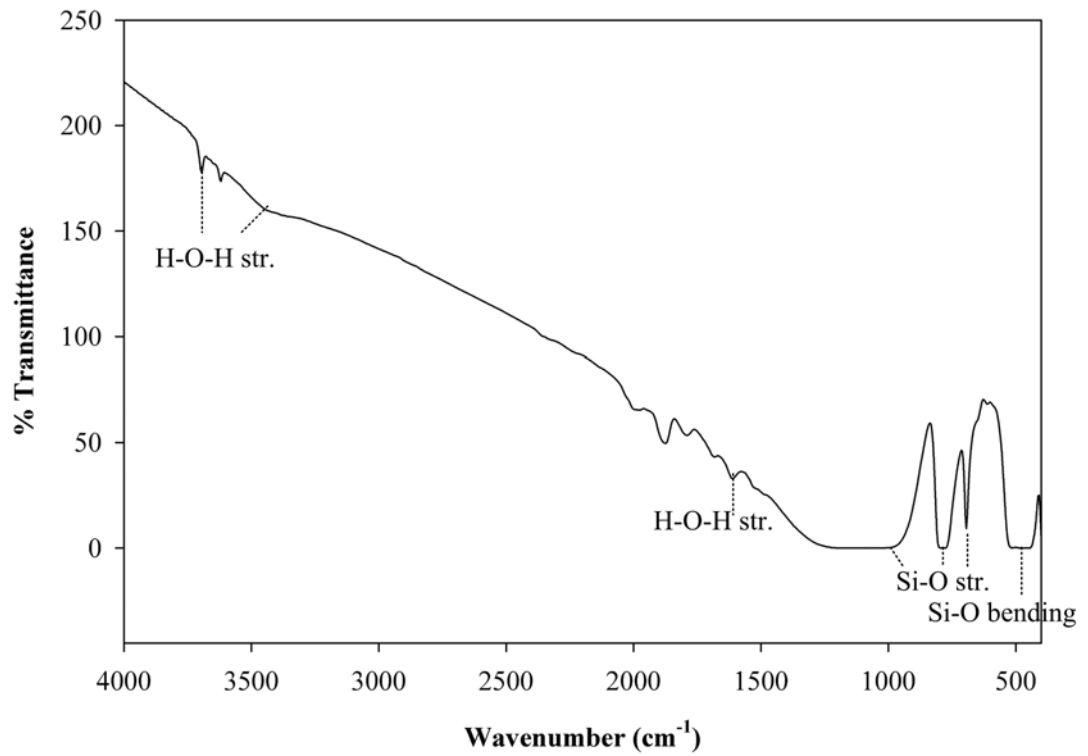


Figure 4.10 Infrared spectrum of quartz.

In order to detect any possible variations in the quartz with electrocoagulation and coagulation, SEM micrographs of the samples were taken (Figures 4.11-4.13). After 10 minutes of coagulation, less number of individual particles was observed. This showed the adsorption of coagulant on the surface of the particles which led to the formation of the bridges between the particles.

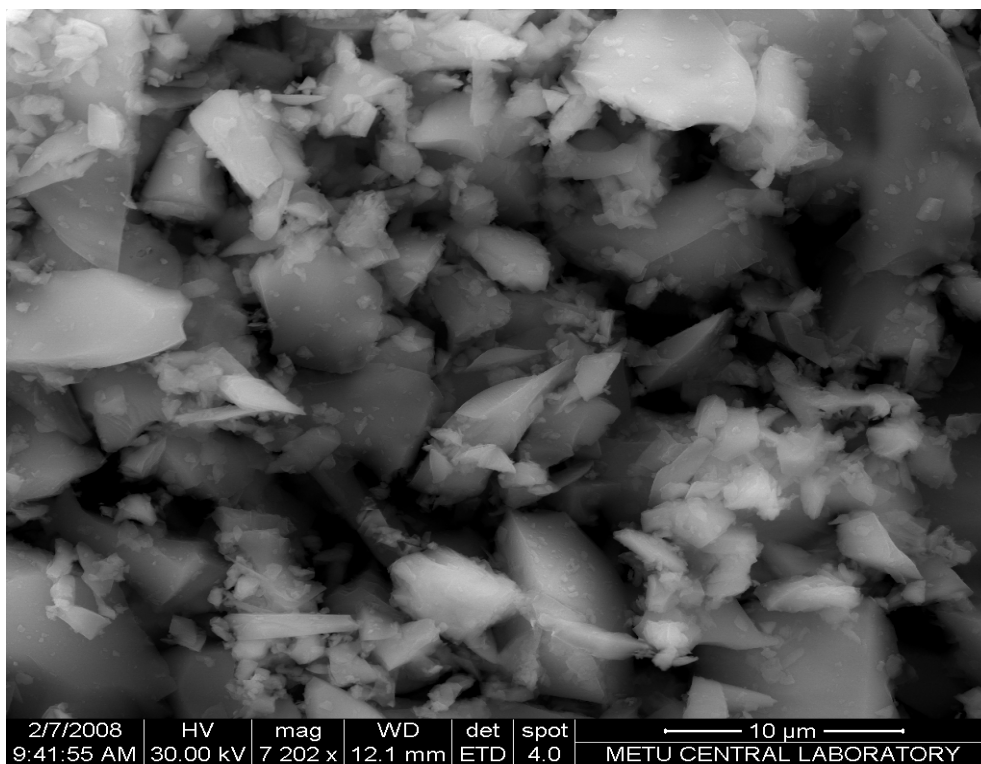


Figure 4.11 The SEM micrograph of quartz particles before coagulation.

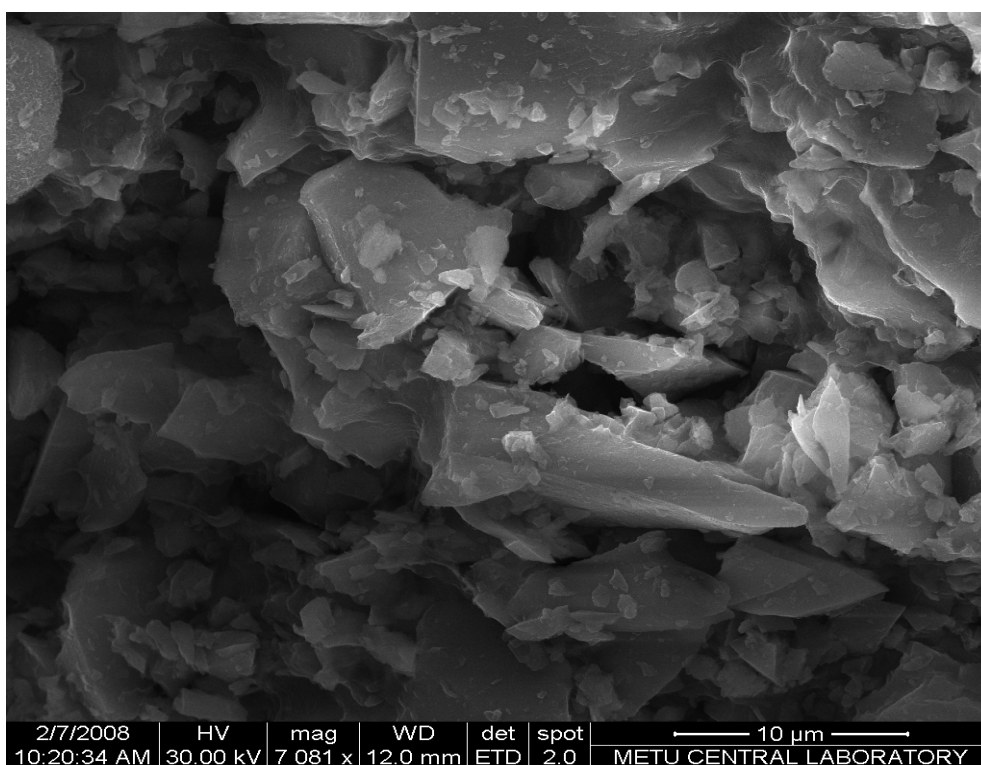


Figure 4.12 The SEM micrograph of quartz particles after electrocoagulation.



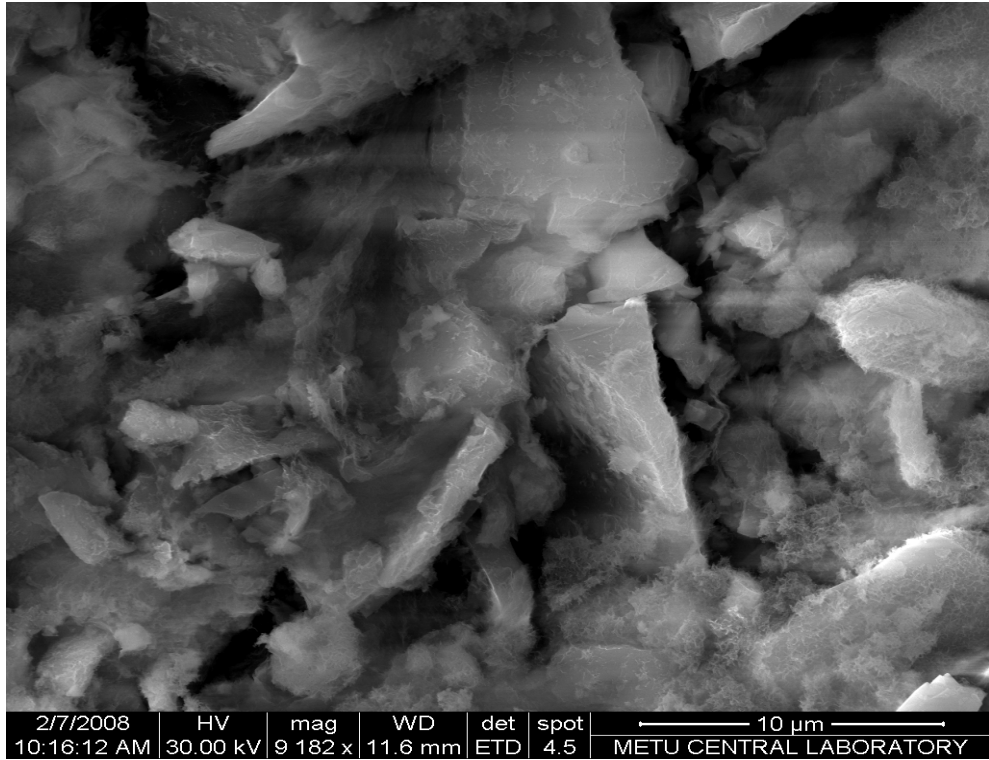


Figure 4.13 The SEM micrograph of quartz particles after coagulation.

Finally, in the case of quartz, no point of zero charge was observed in the pH range 2-10 (Figure 4.14). Zeta potential decreased with increasing pH. The negative surface charge might have arisen from the reaction of silicon ion with water to form silanol group ( $-\text{SiOH}$ ) whose ionization gives  $-\text{SiO}^-$  ion (eq. 24) at any pH values (Van Olphen, 1977).

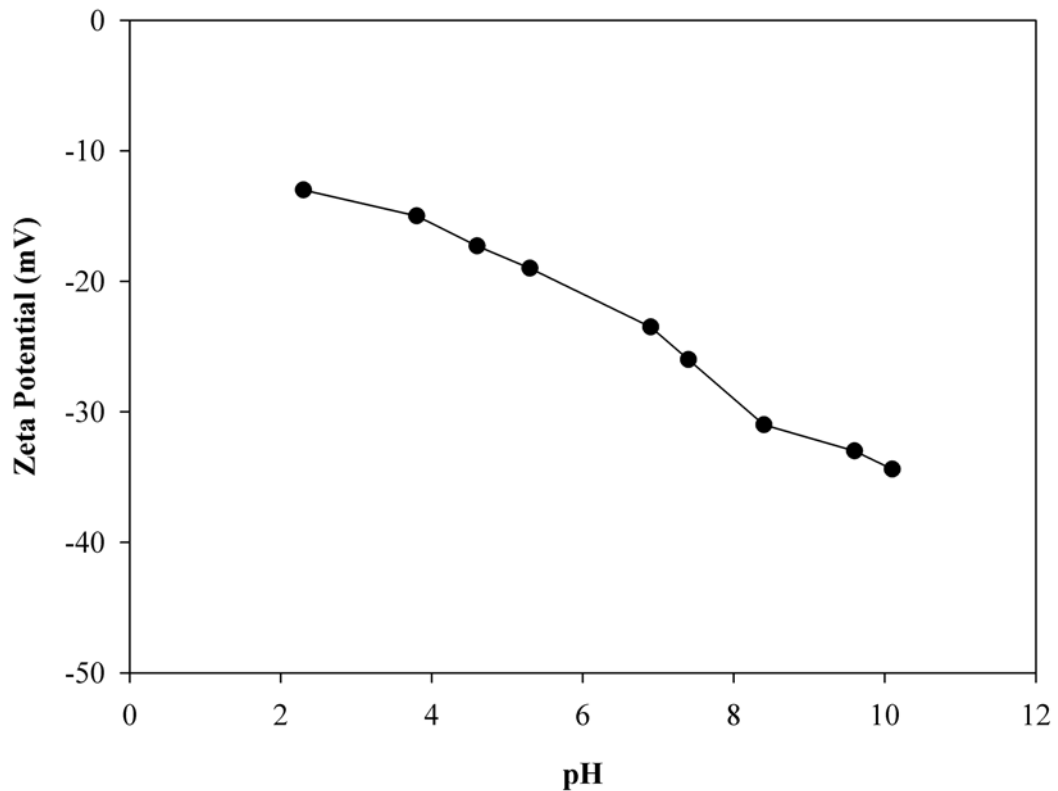


Figure 4.14 Zeta potential measurements of quartz sample at different pH.

## 4.2 Electrocoagulation and Coagulation of Kaolinite and Quartz in Suspensions

In the electrocoagulation, coagulant is produced by electrooxidation of an appropriate anode, aluminum for the case studied. Electrodissolution of the sacrificial anode to the suspension leads to the formation of hydrolysis products that are effective in the destabilization of colloidal particles (Canizares et al., 2006). In the coagulation, aluminum sulfate was used as the coagulant.

In the studied electrocoagulation system, anode was established by monopolar parallel aluminum plate and monopolar parallel stainless steel plate (see Figure 2.9,

Figure 3.1). Electrolysis voltage was varied from 10 V to 60 V (see Table 3.1). The electrode reactions are as follows:

At the anode,



At the cathode,



Overall cell reaction,



At alkaline conditions,



At acidic conditions,



The  $\text{Al}^{3+}$  produced may undergo various reactions in solutions, in other words hydrolyze in solution;



Besides, polymeric species such as  $\text{Al}_2(\text{OH})_2^{4+}$ ,  $\text{Al}_3(\text{OH})_4^{5+}$  and  $\text{Al}_{13}\text{O}_4(\text{OH})_{24}^{7+}$  may also be formed, depending on solution pH.



where  $\text{Al}_x(\text{OH})_y^{(3x-y)+}$  represents positively charged Al-OH polymers, such as  $[\text{Al}_{13}(\text{OH})_{30}]^{9+}$ ,  $[\text{Al}_{24}(\text{OH})_{60}]^{12+}$ ,  $[\text{Al}_{54}(\text{OH})_{144}]^{18+}$  (Sparks, 2002).

All these aluminum species are important in coagulation mechanism of kaolinite and quartz particles in the suspension. The variables that affect electrocoagulation and coagulation as mentioned before are pH of the suspension, amount of aluminum, parameters related with electrolysis (applied voltage, current density), and electrocoagulation time.

The effects of these parameters on electrocoagulation and coagulation are explained in the following subsections (4.3-4.6). However, it is beneficial to initially discuss some preliminary testwork and the study that gives the relationship between conductivity, turbidity removal efficiency and amount of aluminum in the subsection 4.2.1.

#### **4.2.1 Preliminary Testwork**

In order to decide on the range of experimental parameter values, a number of preliminary experiments were carried out which can be summarized as follows:

##### **4.2.1.1 The Effect of Stirring Rate, Electrode Distance and Ultrasonic Treatment on Electrocoagulation**

When the stirring rate was varied between 100 rpm and 500 rpm, the removal efficiency increased from 78.8% to 85.1% for kaolinite suspension and from 77.6% to 83% for quartz suspension (Figure 4.15). Daneshvar et al., 2003 stated that flocks were formed and attached together and precipitation took place easier. With further increase in stirring rate, the flocks were degraded, desorption started and removal efficiency decreased. By doing this experiment, the optimum stirring rate was found to be 300 rpm.

Distance between electrodes was varied from 10 mm to 21 mm which did not have a sound effect on the turbidity removal efficiency (Figure 4.16). It was decided to keep the distance between electrodes at 21 mm which was the convenient distance in the plexiglass cell determined experimentally.

The effect of ultrasonic power (Sonics and Materials Inc. Vibra cell) (100 watt) on the electrocoagulation process was investigated (Figure 4.17). Ultrasonic power did not affect the electrocoagulation of kaolinite and quartz suspensions. This might be due to the uniform distribution of particles in the suspension.

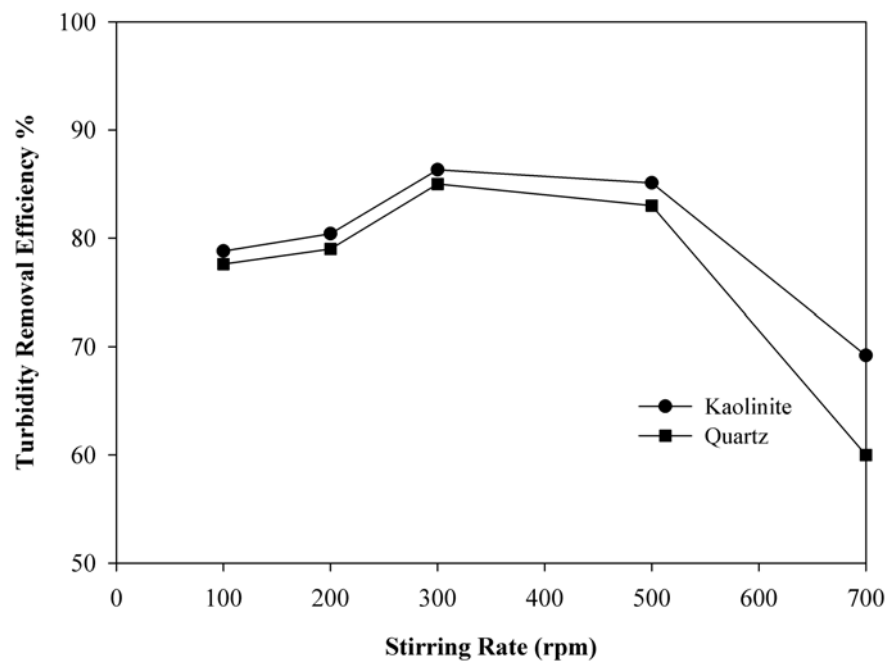


Figure 4.15 The effect of stirring rate (rpm) on turbidity removal efficiency (pH: 9, 40 V; 10 min).

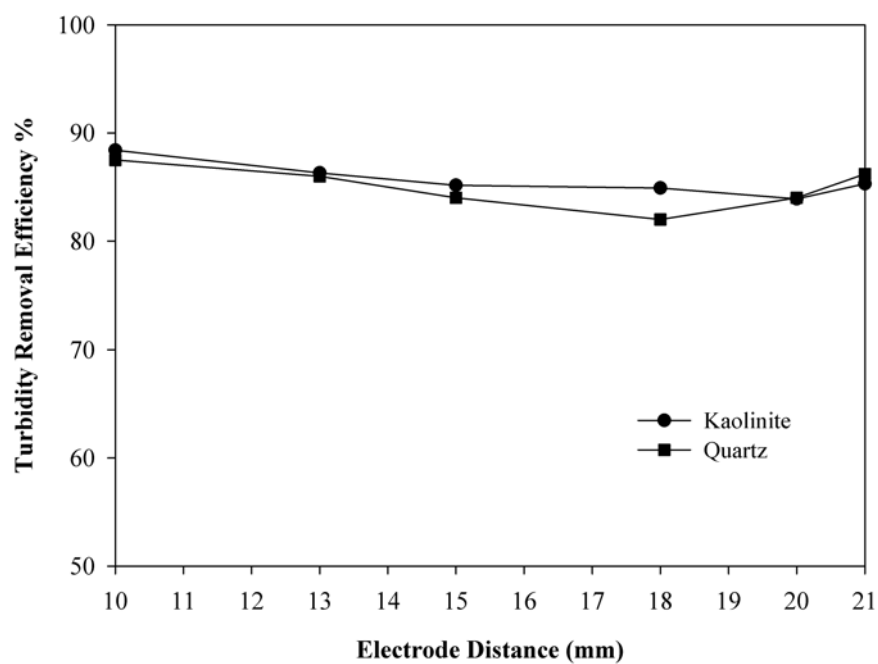


Figure 4.16 The effect of electrode distance (mm) between the electrodes on turbidity removal efficiency (pH: 9, 40 V; 10 min).

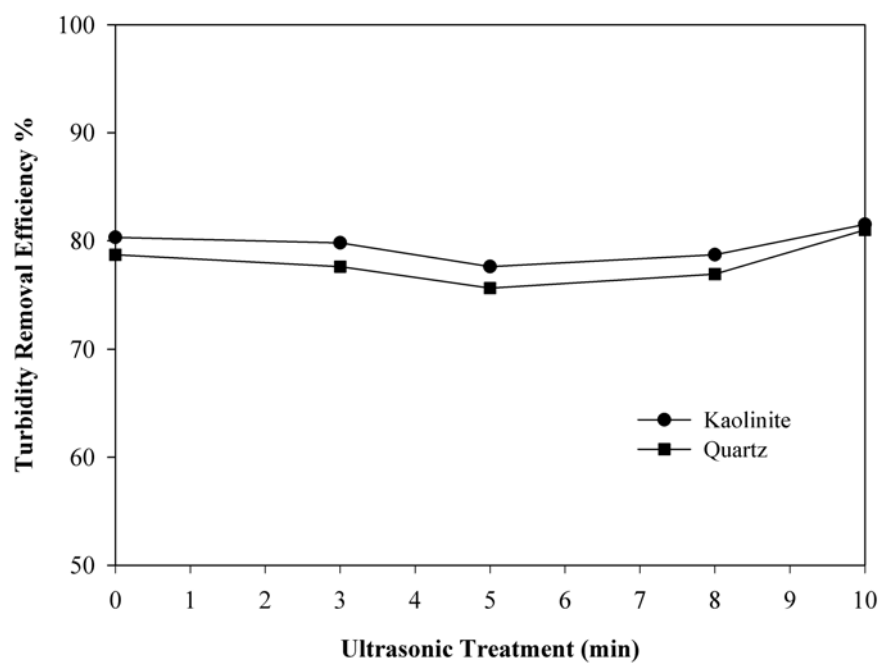


Figure 4.17 The effect of ultrasonic treatment on the electrocoagulation (pH: 9, 40 V; 10 min).

#### 4.2.1.2 The Effect of Time on Coagulation

The effect of coagulation time was studied at constant alum level of 15 mg Al/L at pH 6.5 (Figure 4.18). It was clearly seen from the figure that the coagulation time had no significant improvement on the pollutant removal after 10 minutes. Turbidity removal efficiencies ranging from 82 to 95% were obtained for the coagulation time varied from 1 to 60 minutes. 10 minutes coagulation time was found enough for the removal of colloidal kaolinite and quartz from suspensions with conventional coagulation.

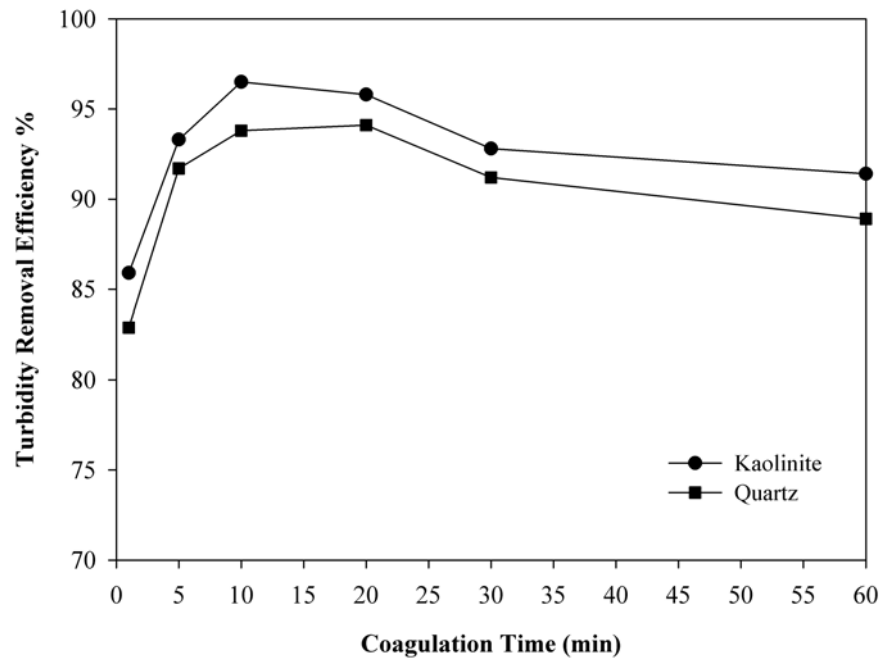


Figure 4.18 The effect of coagulation time on turbidity removal efficiency of kaolinite and quartz from suspension (15 mg Al/L; pH: 6.5).

#### 4.2.1.3 Relationship between Current Density, Conductivity, Energy Consumption, Turbidity Removal Efficiency and Amount of Aluminum

As expected, the conductivity of suspensions increased linearly with increasing NaCl concentration. An increase in conductivity decreased the ohmic drop between electrodes and therefore more aluminum ions could be produced at the same energy input. Also, the formation of  $(\text{AlCl})^{2+}$  ions is expected to promote chemical dissolution ( $\text{Al} + 3\text{H}_2\text{O} \rightarrow \text{Al}(\text{OH})_3 + 3/2\text{H}_2$ ) of electrodes (Szynkarczuk et al., 1994).

In order to examine the effect of conductivity on removal efficiency, turbidity removal efficiency versus conductivity curve was drawn (Figure 4.19).

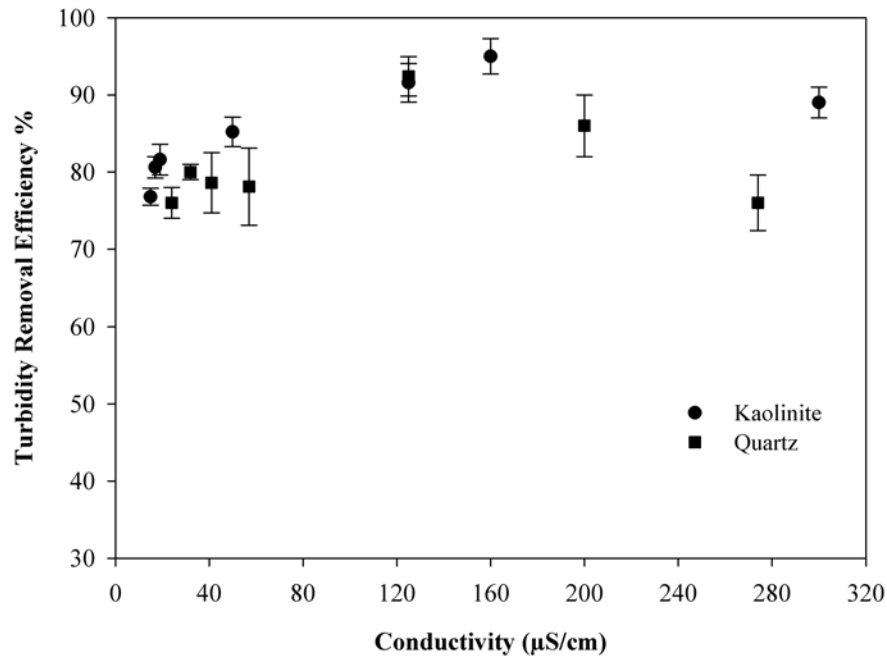


Figure 4.19 The effect of conductivity on turbidity removal efficiency (pH: 9; 40 V; 10 min).



It appears that conductivity had some effect on the removal efficiency of kaolinite and quartz in suspension in the investigated range (15 – 300  $\mu\text{S}/\text{cm}$ ). In the previous studies, Chen et al., (2000) found that conductivity had little effect on the separation of pollutants from restaurant wastewater in the investigated range from 443 to 2850  $\mu\text{S}/\text{cm}$ . Kobya et al., (2003) studied the effect of wastewater conductivity on the performance of the electrocoagulation process using aluminum and iron electrodes. They found that the turbidity removal efficiency remained almost unchanged in the conductivity range of 1000–4000  $\mu\text{S}/\text{cm}$  for both electrode materials. But, it was in contrast to that given by Lin and Peng (1994) for electrocoagulation of textile wastewater using iron electrodes.

The current density also determines the amount of aluminum released from the electrode. When current density was changed from 17 to 174  $\text{A}/\text{m}^2$ , the amount of aluminum was increased from 1  $\text{gAl}/\text{m}^2$  to 10  $\text{g Al}/\text{m}^2$  (Figure 4.20). Current density is related to the ionic strength, greater ionic strength generally causes an increase in current density for the same cell voltage. In this study, ionic strength was adjusted by the addition of NaCl (Table 4.5 and Table 4.6) into the suspension.

The effect of conductivity on theoretical amount of aluminum released from the electrodes and the energy consumption for kaolinite and quartz suspensions are shown graphically in Figure 4.20 and Figure 4.21. Adding NaCl to increase suspension conductivity (voltage was kept constant) increased the energy consumption. As conductivity was increased from 24 to 274  $\mu\text{S}/\text{cm}$ , the energy requirement increased from 1 to 10  $\text{kwh}/\text{m}^3$  at the same voltage (40 V) for quartz suspension. For kaolinite suspension, increasing conductivity from 15 to 300  $\mu\text{S}/\text{cm}$ , increased energy consumption from 0.3 to 11  $\text{kwh}/\text{m}^3$  at the same voltage (40 V).

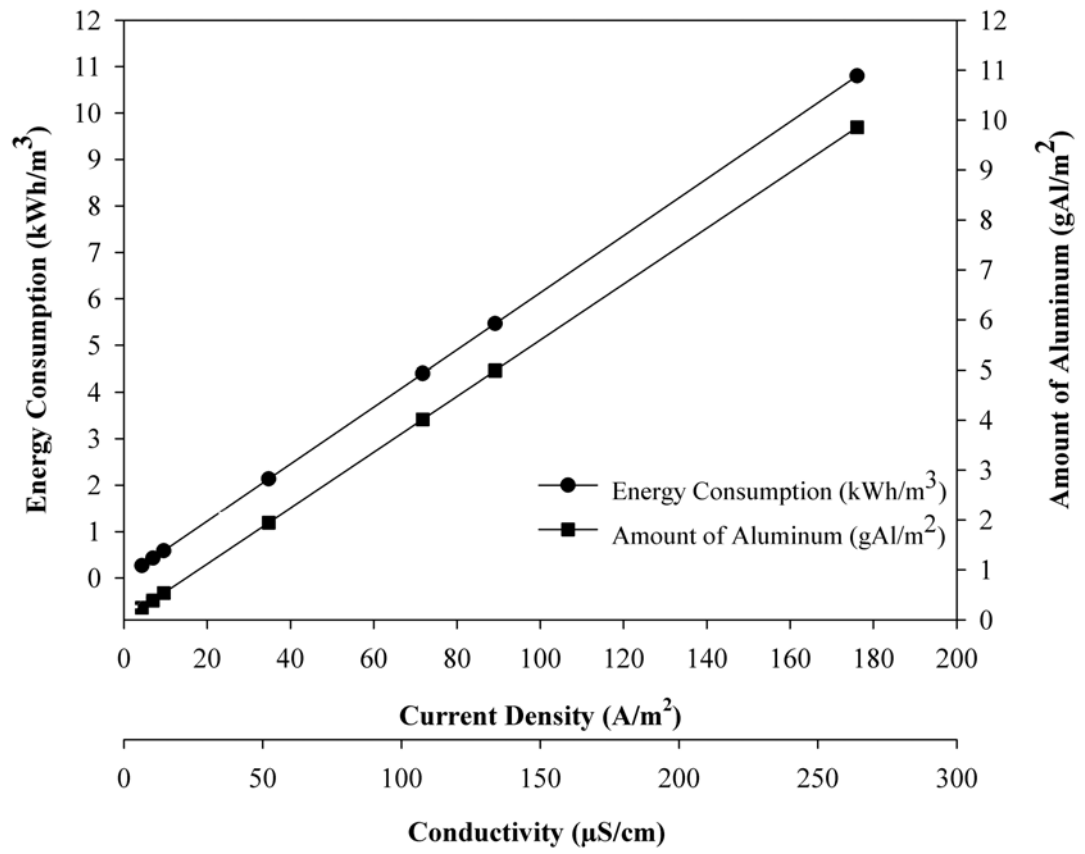


Figure 4.20 The effect of current density ( $A/m^2$ ) and conductivity ( $\mu S/cm$ ) on energy consumption and total dissolved aluminum ( $g Al/m^2$ ) in kaolinite suspension (pH:9; 40 V; 10 min).

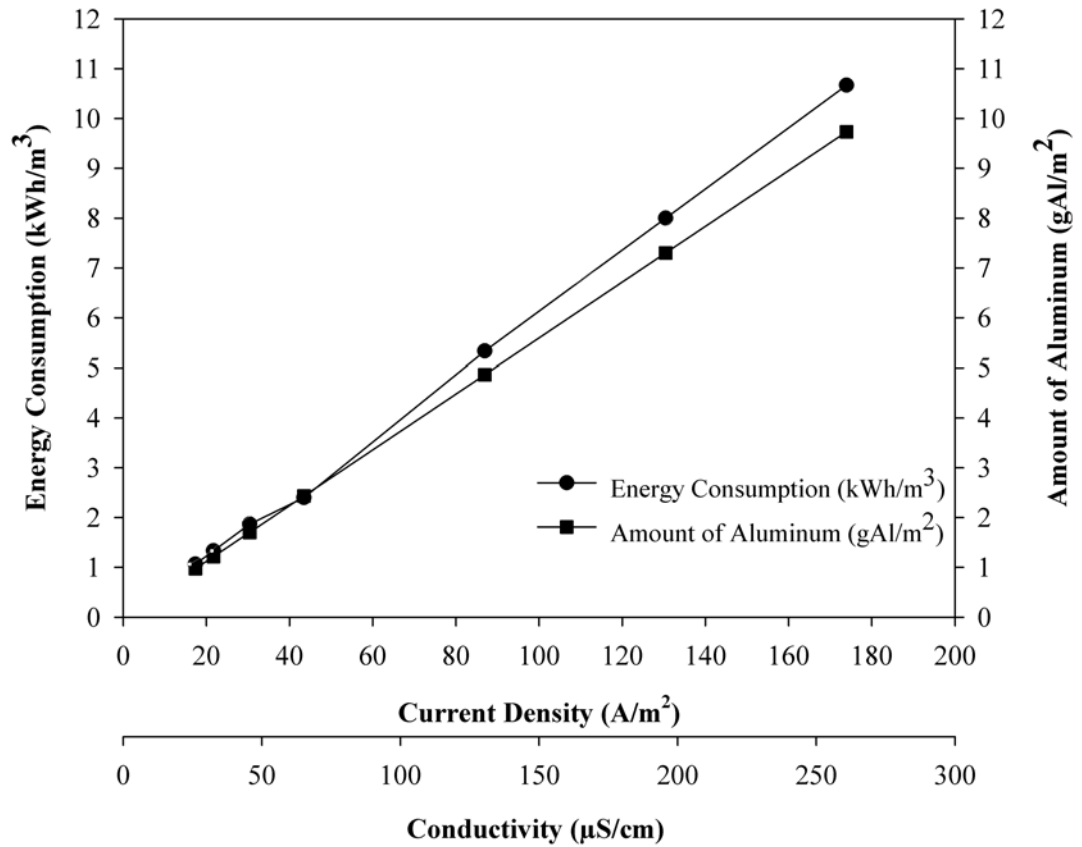


Figure 4.21 The effect of current density (A/m<sup>2</sup>) and conductivity (µS/cm) on energy consumption (kwh/m<sup>3</sup>) and amount of aluminum (g Al/m<sup>2</sup>) in quartz suspension (pH:9; 40 V; 10 min).

In summary, turbidity removal efficiency increased with increasing current density and conductivity, due to formation of higher amount of Al<sup>3+</sup> ion and the resultant increase in formation rate of Al(OH)<sub>3</sub>. All the results obtained were consistent with the previous studies (Koby et al., 2003, Yilmaz et al., 2005).

### 4.3 Effect of Initial pH on Electrocoagulation and Coagulation

pH is an important factor influencing the performance of both electrocoagulation and coagulation processes. To examine its effect in a comparative manner, electrocoagulation and coagulation experiments with different initial pH values were conducted in the pH range of 2 to 11. Figures 4.22 and 4.24 display the effect of initial pH on the turbidity removal efficiencies of kaolinite and quartz particles for electrocoagulation and coagulation cases. Figures 4.23 and 4.25 show zeta potential measurements of kaolinite and quartz suspensions as a function of initial pH, where the zeta potentials refer to those determined after electrocoagulation or coagulation tests.

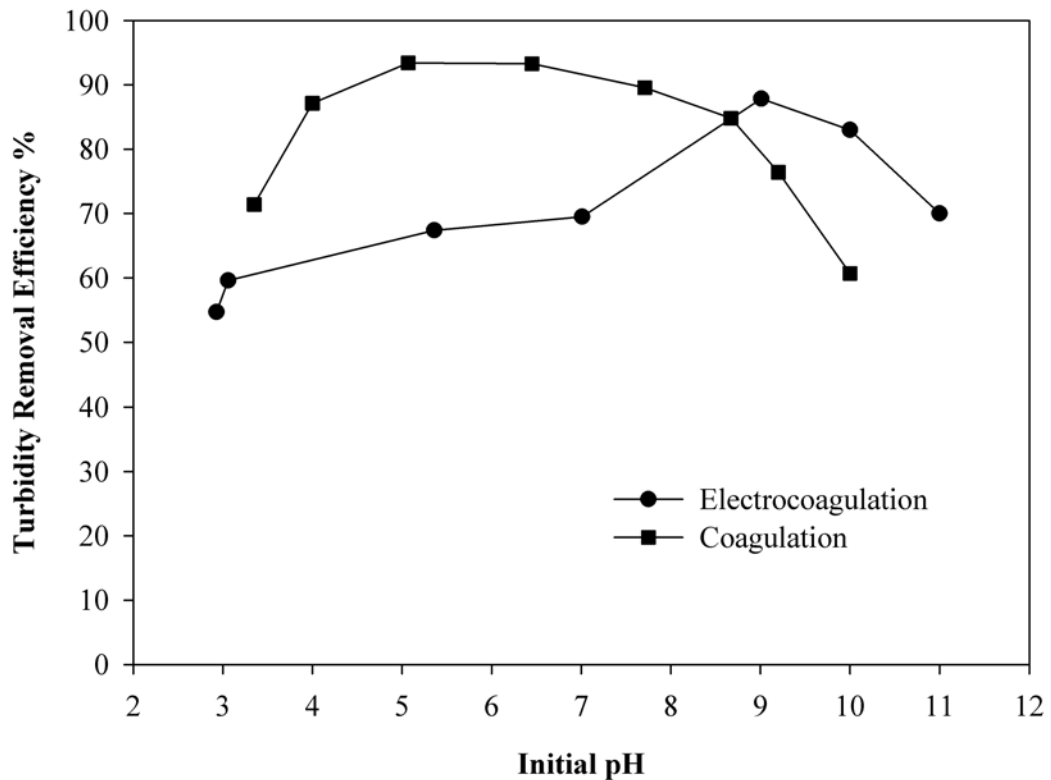


Figure 4.22 The effect of initial pH on the turbidity removal efficiency for kaolinite suspension (electrocoagulation: 40V; 10 min; coagulation 15 mg Al/L; 10 min).

In the electrocoagulation of kaolinite suspension, the highest turbidity removal efficiency (about 90%) (Figure 4.22) occurred near pH 9, where the zeta potential approached the isoelectric point of the kaolinite particles (Figure 4.23). pHs below 9 led to positive values of the zeta potential, whereas higher values of pH caused negative zeta potentials. This behavior could be explained in terms of the charge of the kaolinite particles, which were positive due to the adsorption of cations such as  $\text{Al}^{3+}$ ,  $\text{Al}(\text{OH})_2^+$ , and  $\text{Al}(\text{OH})^{2+}$  and negative due to the adsorption of negatively charged ion ( $\text{Al}(\text{OH})_4^-$ ). In the coagulation case for kaolinite suspensions, the turbidity removal efficiency (%) reached maximum turbidity (about 90 %) within the pH range of 5 to 8 (Figure 4.22). The change in turbidity removal was 71% at pH 3.35 and increased steadily to 93.3% up to pH 6.5 and then gradually decreased. Zeta potential measurements after coagulation of kaolinite suspension are also presented in Figure 4.23. It was seen that the zeta potential of kaolinite suspension after coagulation experiments was positive within the range of pH 3.35-6.5 and negative within the range of pH 6.5-10. This behavior could be indicative of the formation of particles of precipitate that are initially positively charged (due to the adsorption of hydroxo cations) and that later turn their charges to negative (due to the adsorption monomeric hydroxo anions) (Stumm and Morgan, 1996). The zeta potential curve went through two isoelectric points at around pH values of 3.5 and 6.5. This was explained by Hunter, 1981 that the first iep corresponded to the laying down of the hydroxide. The second iep normally occurred at pHs below the iep of the metal hydroxide. It was observed that turbidity removal was effective at about pH 6.5 which is the second the isoelectric point of kaolinite suspension. At this pH, the highly charged  $\text{Al}^{3+}$  cation is the dominant species that binds to the negatively charged particles. Aluminum cations also contribute to the charge neutralization of the particles as the isoelectric point is attained. It is seen from Figure 4.23 that the zeta potential decreased from 0 to a value below -25 mV between pH 6.5 and pH 10. This was probably due to an increase in negatively charged ions, specifically the hydroxyl ion added to increase the pH.

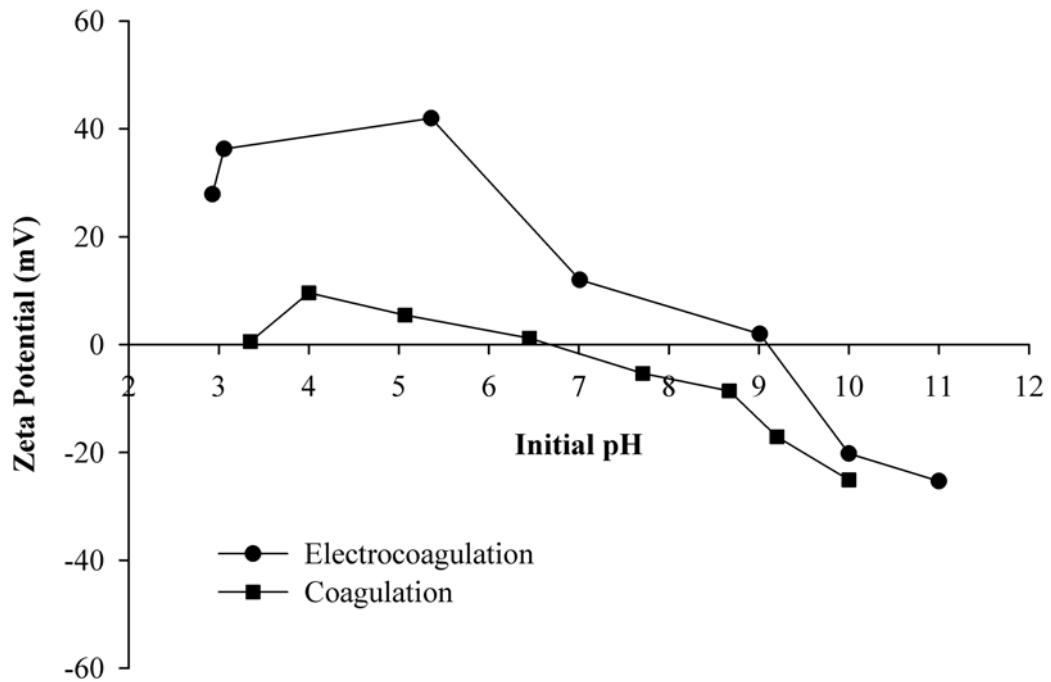


Figure 4.23 Zeta potential measurements after electrocoagulation (40 V; 10 min) and coagulation (15 mg Al/L; 10 min) of kaolinite suspension as a function of initial pH.

In the electrocoagulation of quartz suspension, turbidity removal efficiencies were much higher in the alkaline region than those in acidic or near-neutral pH values (Figure 4.24). The most effective turbidity removal efficiency took place at pH 9 with the value of 89.7%. It is seen from the Figure 4.25 that the zeta potential increased until pH 5 and then decreased with increasing pH, leading to a sign reversal at pH 9, which are all closely related with the adsorption of hydrolyzed aluminum species in solution. In the coagulation of quartz suspension, turbidity removal efficiencies remained at their highest values in the pH range of 6 to 8 where the zeta potential values were close to zero. Turbidity removal efficiency increased drastically from pH 2 to pH 5, and the degree of increment decreased and reached a value of about 95% at pH 6, stayed almost constant up to pH 8, then the

removal efficiency decreased severely (Figure 4.24). The zeta potential curve passed through two isoelectric points at around pH values of 3.2 and 6.5. The isoelectric point at pH 3.2, however, did not lead to good turbidity removal results. The suspension was destabilized and coagulated by a charge neutralization mechanism. However, zeta potential decreased, resulting in a stable solution reflected by a decline in turbidity removal performance. At a highly alkaline pH (>10) turbidity removal efficiency was decreased, due to restabilisation of the particles and the dominance of the aluminate ion in solution (Holt et al., 2002). Thus, at alum concentration of 15 mg-Al/L turbidity removal efficiency is better and occurs over a wider pH range.

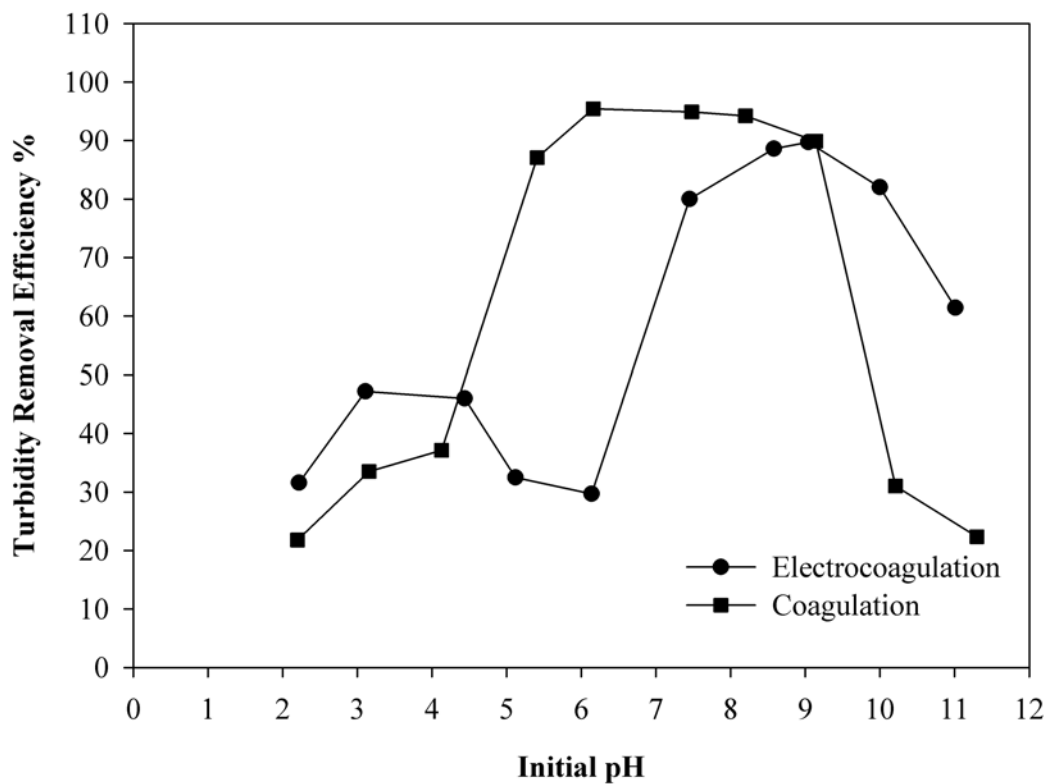


Figure 4.24 Turbidity removal efficiency for electrocoagulation (40 V; 10 min) and coagulation (15 mg Al/L; 10 min) experiments at different initial pHs for quartz suspension.

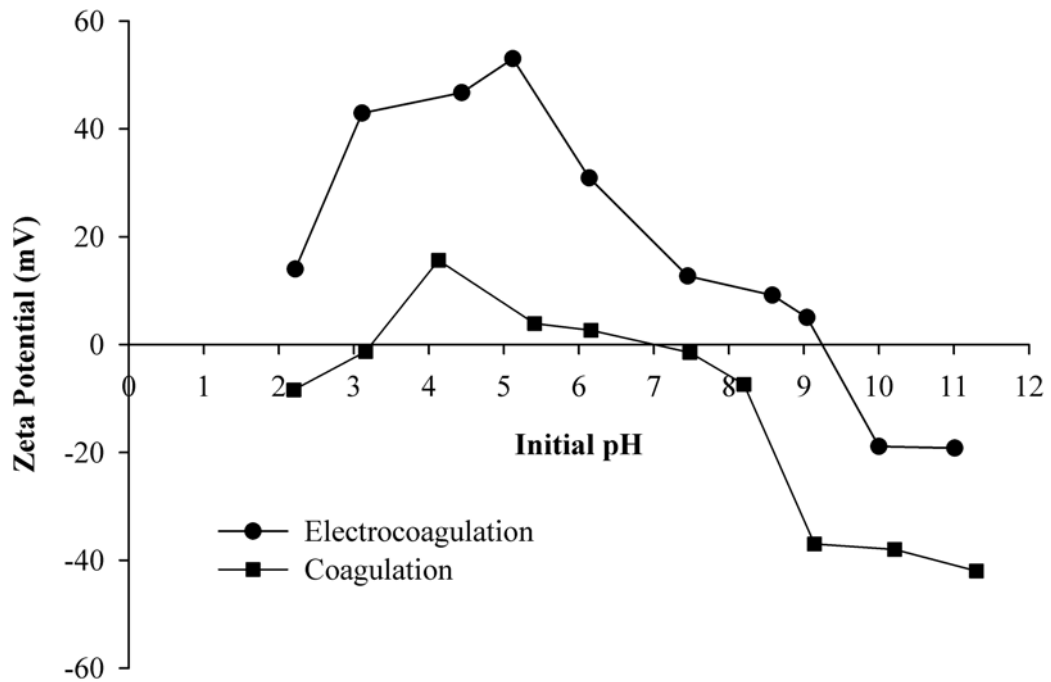


Figure 4.25 Zeta potential measurements after electrocoagulation (40 V; 10 min) and coagulation (15 mg Al/L; 10 min) experiments at different initial pHs for quartz suspension.

Furthermore, the zeta potentials measured in the acidic pH values after coagulation were much lower than those measured in the electrocoagulation case for the same pH values. In the case of coagulation, sulfate anion was also introduced into the solution by the added coagulant, aluminum sulfate. Sulfate can adsorb on positively charged aluminum hydroxide precipitate and reduce its positive charge at pHs below about 8 or 9 (Gregory, 2006). This explains the reason for the low zeta potential values and a sign reversal in the acid region for the conventional coagulation as shown in Figure 4.23 and Figure 4.25.



The hydrolysis of aluminum either released from the electrodes in electrocoagulation or added into solution as aluminum sulfate in conventional coagulation, and the adsorption of the hydrolysis products on the particles are greatly affected by the varying pH of the suspension (Figure 2.8). Nonhydrolyzed  $\text{Al}^{3+}$  and cationic hydrolysis products,  $\text{Al}(\text{OH})^{2+}$  and  $\text{Al}(\text{OH})_2^+$ , are the dominant species in the solution at pH values of less than 5. The cationic hydrolysis products, rather than the nonhydrolyzed  $\text{Al}^{3+}$  (Stumm and Morgan, 1996), are adsorbed strongly on negatively charged particles, which leads to charge neutralization, and also to charge reversal with an excess amount of aluminum ions (Duan and Gregory, 1998). This charge reversal produced positive zeta potential on kaolinite and quartz particles and low turbidity removal efficiencies was observed. Formation of positive surface charge on kaolinite and quartz and decreased turbidity removal efficiency are mainly due to electrical repulsion between the particles at pH values less than 5. In this investigation, the zeta potential curve gave the highest positive value at about pH 5. Then, the zeta potential decreased with increasing pH, leading to a sign reversal at pH 9. These two results were both closely related with the adsorption of hydrolyzed aluminum species on the particle. At pH values 5 to 8.5, especially with an excessive aluminum concentration, amorphous aluminum hydroxide precipitation becomes important. The aluminum hydroxide precipitate is known to have an isoelectric point in the region of pH 8 to 9 (Duan and Gregory, 2003); and hence, it is positively charged at lower pH values.

The adsorption of the positively charged precipitate on the negatively charged kaolinite and quartz particles led to charge neutralization and lower zeta potential values resulting in better coagulation, as are indicated by the increasing turbidity removal efficiencies in Figure 4.22 and Figure 4.24. This precipitation may occur either on the surface of particles and give rise to charge neutralization, or the hydroxide precipitates formed in the bulk may attach to the particles causing sweep flocculation. This change in zeta potential and adsorbed aluminum species change the turbidity removal efficiency of the coagulant. As it is seen from Figure 4.22 and Figure 4.24, turbidity removal efficiencies were much higher in the alkaline region than those in acidic or near-neutral pH values. The highest turbidity removal

efficiency (about 90%) was near pH 9 where the zeta potential curve approaches the isoelectric point of the kaolinite and quartz particles. At pH values higher than 9, the aluminate ion,  $\text{Al}(\text{OH})_4^-$  became the predominant species which cannot be adsorbed on the negatively charged quartz particles. Hence, the turbidity removal efficiencies deteriorated.

The results have been interpreted in terms of the mechanism previously proposed in literature for coagulation. The charge neutralization by the adsorption of monomeric hydroxocations ( $\text{AlOH}_2^+$ ,  $\text{AlOH}^{2+}$ ) onto the kaolinite and quartz surface can be the primary coagulation-mechanism for low concentration of aluminum and acidic pHs ( $< 5$ ). In a previous study (Canizares et al., 2007), the coagulation mechanism for the removal of kaolinite from suspension was determined as charge neutralization at pH below 4. This slight difference may be due to the different structure of kaolinite. In the range of pH 5–8, two primary mechanisms can explain the experimental behavior of the system: sweep flocculation for high concentration of aluminum, and a combination of precipitation-charge-neutralization and charge neutralization by adsorption of monomeric or polymeric aluminum such as  $\text{Al}_2(\text{OH})_2^{4+}$ ,  $\text{Al}_3(\text{OH})_4^{5+}$  and  $\text{Al}_{13}\text{O}_4(\text{OH})_{24}^{7+}$ .

The charge neutralization and/or the enmeshment of the particles into a precipitate are the main coagulation mechanisms in the treatment of kaolinite and quartz particles from suspension. The charge neutralization can be achieved by the adsorption of cationic aluminum species or by the precipitation of charged aluminum hydroxide precipitates onto the surface of particles. The generation of a growing aluminum hydroxide precipitate take place in the system at high concentrations of aluminum and pH values close to neutrality (sweep flocculation) (Canizares et al., 2008).

#### **4.3.1 Change in the Suspension pH during Electrocoagulation**

pH of the suspension changes during the electrocoagulation process (Chen, 2000, Vik et al., 1984, Kobya et al., 2003). This change in pH depends on the type of the

electrode used and initial pH of the medium. The suspension pH increases during electrocoagulation when the initially adjusted pH is less than 8, and decreases if the initial pH is greater than 8 (Koby et al., 2003).

In the present study, similar variation was seen in kaolinite and quartz suspensions (Figure 4.26). When initial pH was 2.2, the final pH was found to be 3.01 and 3.5 for kaolinite and quartz suspensions respectively. When initial pH was 9.3, the final pH was found to be 8.2 and 8.0 for kaolinite and quartz suspensions respectively.

The increase in pH (for pH<8) was attributed to the formation of OH<sup>-</sup> on the cathode by the following reaction:



The formed OH<sup>-</sup> reacted with H<sup>+</sup> in the solution and reduced its effect.

It is formerly stated that when initial pH was greater than 8, basic dissociation of the amphoteric aluminum hydroxide Al(OH)<sub>3</sub> decreased the pH according to the following reaction (Chen et al., 2000, Koby et al., 2003, Vik et al., 1984, Mouedhen et al., 2008):



As reported by previous studies (Chen et al., 2000, Koby et al., 2003), electrocoagulation exhibits some pH buffering action, especially in alkaline medium.

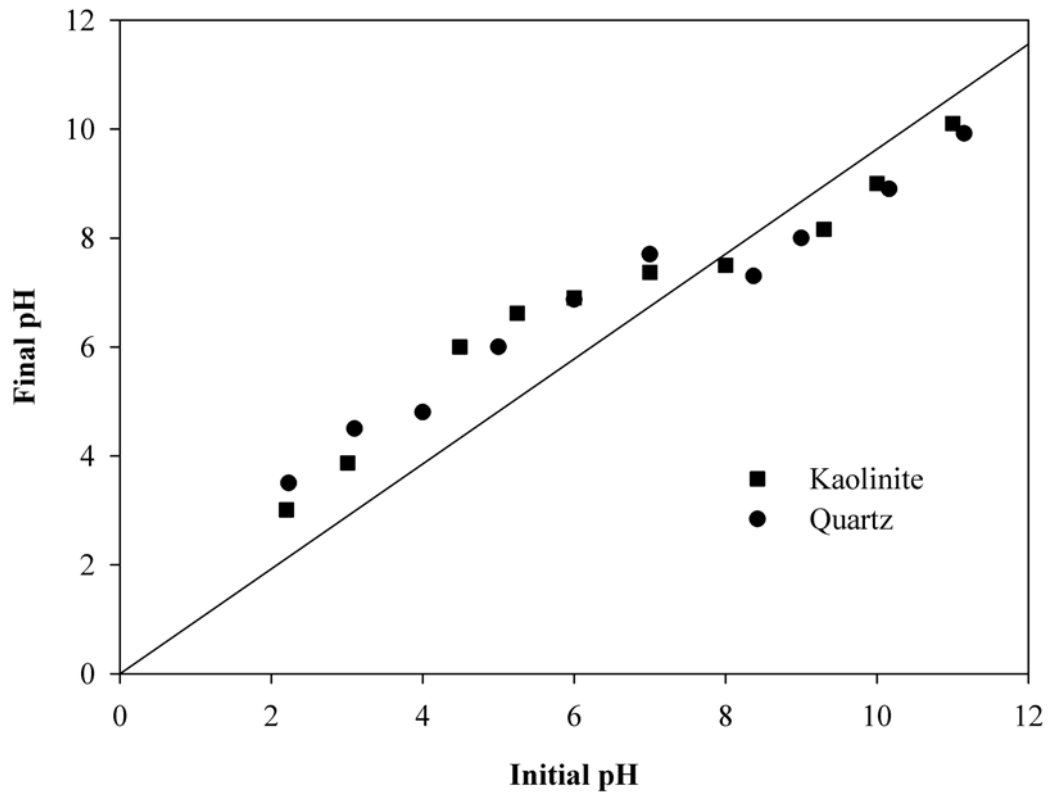


Figure 4.26 pH change after electrocoagulation of kaolinite and quartz suspensions (40 V; 10 min).

#### 4.4 Effect of Voltage on Electrocoagulation

One of the most important parameters that can affect the electrochemical process is the applied voltage. Therefore, the effect of the applied voltage on the turbidity removal efficiency should be known. In order to examine this effect, experiments were carried out with a wide range of applied voltage, from 0 to 60 V, at fixed values of pH (pH 9), suspension concentration (0.20 g kaolinite/L; 0.32 g quartz/L), and electrocoagulation time (10 min) (Figure 4.27 and Figure 4.28). As the applied voltage increased, the removal efficiency and the current passing through the solution increased. The latter caused dissolution of aluminum from the sacrificial

electrode forming aluminum hydroxide species. These species neutralized the electrostatic charges on dispersed particles to reduce the electrostatic interparticle repulsion so that the van der Waals attraction predominates, thus enhancing agglomeration (Wang et al., 2009). At low voltages ( $< 20$  V), amount of aluminum dissolved from anodes stays insufficient. This prevents effective compression of the double layer and destabilization of the suspended particles.

In the kaolinite and quartz suspensions, when the applied voltage was raised to 40 V, the removal efficiency increased to about 90 % because a larger amount of  $\text{Al}^{3+}$  was produced via anodic metal dissolution, causing coagulation. When the voltage was increased to 50 V, no further improvement occurred in the removal efficiency. In electrocoagulation, the optimal applied voltage was determined to be 40 V for both suspensions.

Current density at each applied voltage was calculated using Faraday Law (Eq. 12). The results obtained were plotted in Figure 4.27 and Figure 4.28. As it is seen from the figures, current density increased with increasing applied voltage as expected. The current density at the optimum turbidity removal efficiency of kaolinite was found to be  $21.6 \text{ A/m}^2$  after 10 minutes of electrocoagulation conducted with suspensions having about 28-32  $\mu\text{S/cm}$  conductivity. For quartz case, the current density at the optimum turbidity removal efficiency was found to be  $23.9 \text{ A/m}^2$  after 10 minutes of electrocoagulation conducted with suspensions having about 30  $\mu\text{S/cm}$  conductivity. The conductivity did not significantly change during each experimental run for the range of voltages tested. The low conductivity of our system rooted from the low ionic strength of the solutions. If the ionic strength of the medium had been high, it would have caused an increase in current density at the same applied voltage or a decrease in cell voltage at the constant current density. This was the case in some previous studies such as “separation of pollutants from restaurant wastewater by electrocoagulation” held by Chen et al., 2000. In this study, conductivity was in the range of (443 - 2850  $\mu\text{S/cm}$ ) which was very high relative to our case (being 30  $\mu\text{S/cm}$ ).

It was also observed during the experiments that, with long electrocoagulation times and high voltages, floating particles attached to hydrogen gas bubbles released from the cathode became an important turbidity removal mechanism; as it has been previously reported by Holt et al. (2004).

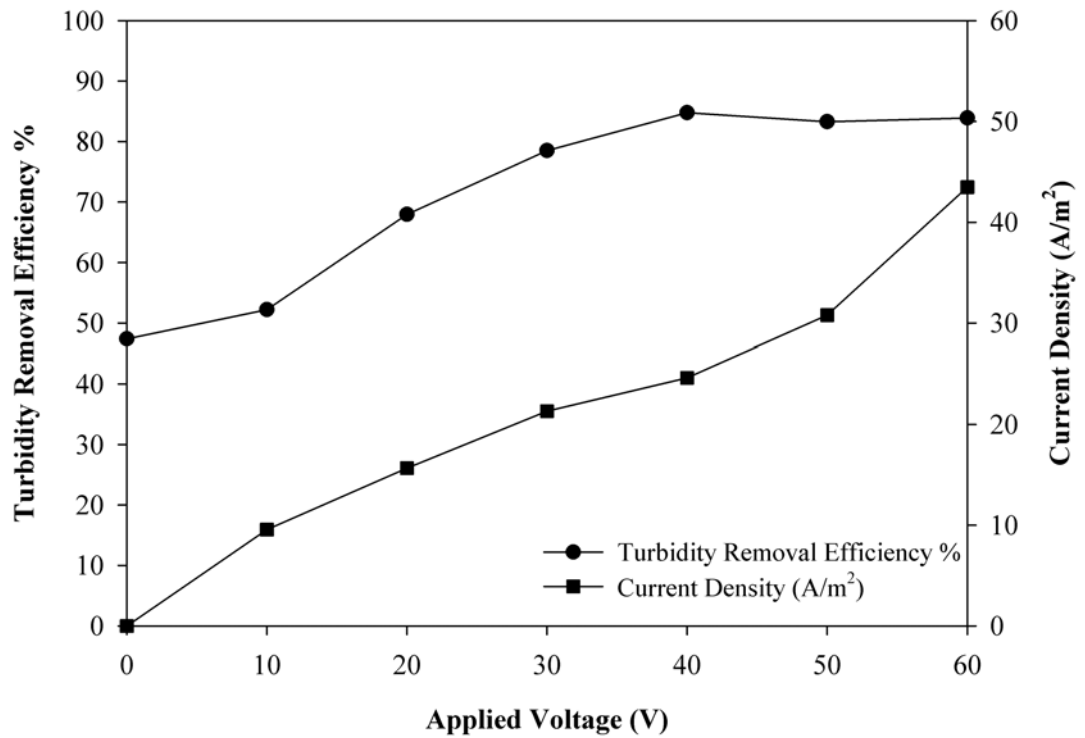


Figure 4.27 The effect of applied voltage on current density and turbidity removal efficiency in the kaolinite suspension.

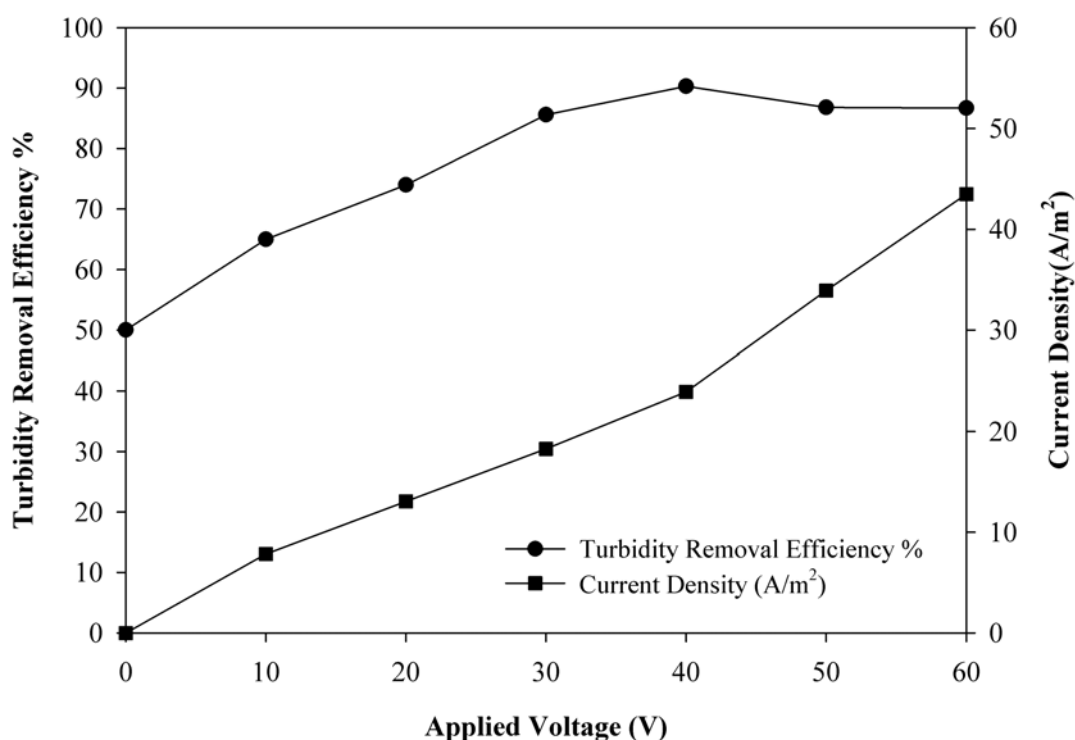


Figure 4.28 The effect of applied voltage on current density and turbidity removal efficiency in quartz suspension.

## 4.5 Effect of Current Density and Time on Electrocoagulation

### 4.5.1 Effect of Current Density on Electrocoagulation

Waste mineral suspensions may have a range of dissolved ionic species that change the ionic strength and hence the conductivity of the suspensions. This, in turn, changes the current density at constant applied voltage. Therefore, the effect of increasing current density on turbidity removal efficiency was studied at constant voltage by adding appropriate amounts of NaCl to kaolinite and quartz suspensions. Table 4.5 and Table 4.6 show the amounts of NaCl added and the resulting current densities and conductivities in 40-V electrocoagulation experiments.

Table 4.5 Concentration of NaCl added (g/L) and the resultant changes in current density and conductivity in kaolinite suspension.

<b>NaCl addition (g/L)</b>	<b>Current Density (A/m<sup>2</sup>)</b>	<b>Conductivity (μS/cm)</b>
0.0005	4.348	15
0.0015	6.957	17
0.0025	9.565	19
0.0180	34.783	50
0.0555	71.739	125
0.0730	87.130	160
0.1430	176.087	300

Table 4.6 The concentration of NaCl added (g/L) and the resultant changes in current density and conductivity in quartz suspension.

<b>NaCl addition (g/L)</b>	<b>Current Density (A/m<sup>2</sup>)</b>	<b>Conductivity (μS/cm)</b>
0.005	17.39	24
0.009	21.74	32
0.014	30.44	41
0.021	43.48	57
0.056	87.96	125
0.093	130.44	200
0.130	173.91	274



Previously, it was shown that current density can influence the treatment efficiency of the electrocoagulation process (Bektaş et al., 2004; Holt et al., 2005; Yılmaz et al., 2005; Merzouk et al., 2009a). Figure 4.29 depicts the effect of current density on the removal efficiency of kaolinite suspension. Current density in the kaolinite suspension started with the value of  $4.3 \text{ A/m}^2$  which corresponds to the turbidity removal efficiency of 76.8%. It increased to  $17 \text{ A/m}^2$  with the turbidity removal efficiency of 83.5%. On the other hand, in the case of quartz suspension, turbidity removal efficiency was observed as 76% at a value of  $17 \text{ A/m}^2$  current density. This means that removal efficiency of kaolinite at the same current density ( $17 \text{ A/m}^2$ ) was greater than that of quartz suspension. However, the optimum turbidity efficiency for both suspensions was about 90% which was accompanied with the same current density of about  $87 \text{ A/m}^2$  (Figure 4.29). These results might show that the charging mechanism of kaolinite and quartz was the same; due to the broken bond surfaces. With increasing current density, removal efficiency was not changed much in kaolinite whereas it was greatly changed in quartz. 89% efficiency was observed in case of kaolinite at  $173\text{-}176 \text{ A/m}^2$  while efficiency in case of quartz was 76% at the same current density (Figure 4.29). The significant change in removal efficiency of kaolinite relative to quartz particles might be related with the higher surface area of kaolinite than quartz.

The effects of current density on turbidity removal efficiency of quartz suspensions are also plotted in Figure 4.29. The turbidity removal efficiency appeared to increase up to 92% at  $87 \text{ A/m}^2$  current density and decreased at higher current densities. The increase in turbidity removal efficiency could be explained by greater percentage of destabilized particles, which was due to charge neutralization with more aluminum ions released from the electrodes with increasing current density. Decrease in turbidity removal efficiency at higher current density ( $>130 \text{ A/m}^2$ ) is most likely explained by the formation of slow-settling, low density flocs with the more aluminum hydroxide precipitates (Szynkarczuk et al., 1994). In the experiment the current was varied between  $0.004 \text{ A} - 0.42 \text{ A}$  which correspond to  $17 \text{ A/m}^2 - 174 \text{ A/m}^2$  current densities. The current not only determines the coagulant dosage rate but also the bubble production rate. Hence, the collision

between particles, floc growth and the potential for material removal is determined by the current (Holt et al., 2002).

There are two effects of NaCl addition that should be considered. Firstly, it may increase the conductivity of the suspension, which results in higher current passing through the system at the same applied voltage. Secondly, it may intensify the ionic strength of the suspension hence compresses the electrical double layer. The first effect was quite dominant and it increased turbidity removal efficiency due to increased amount of aluminum entering the suspension. However, the second effect was considered negligible due to significantly low concentration of NaCl ( $<2.4 \times 10^{-3}$  M).

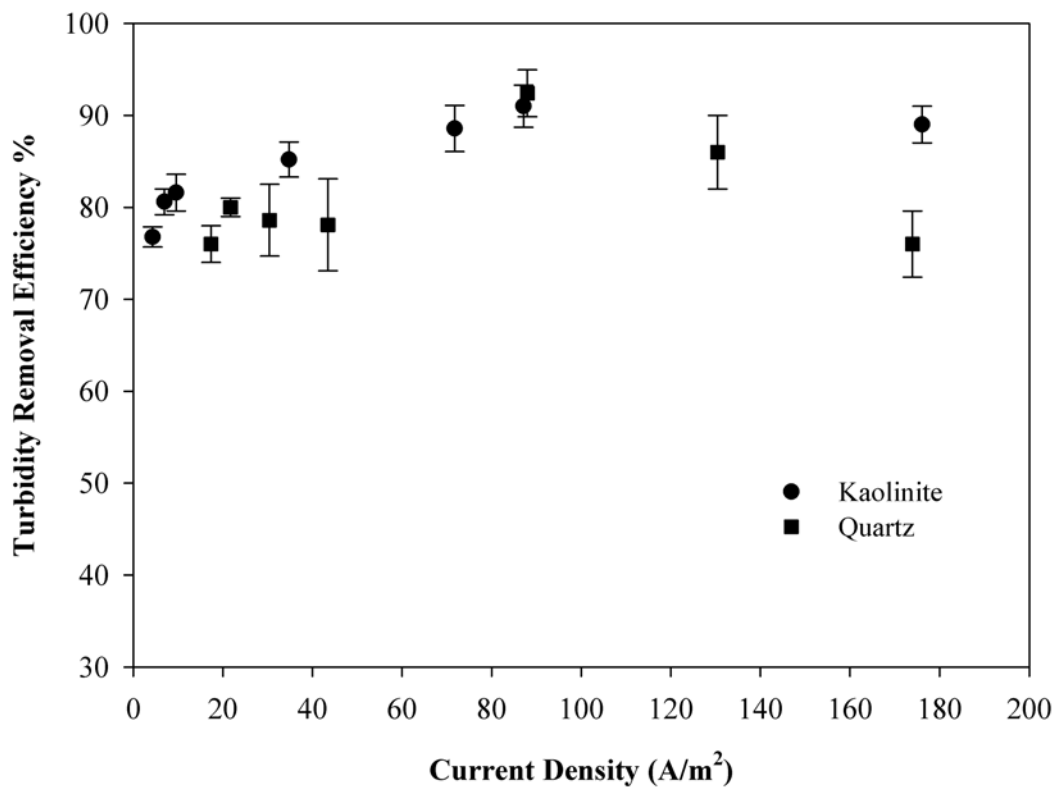


Figure 4.29 The effect of current density on turbidity removal efficiency for kaolinite and quartz suspensions (pH: 9; 40 V; 10 min).

Some of the previous studies showed that in electrocoagulation, current density can influence the removal efficiency, while some other studies have reported that current density has no significant effect on removal efficiency. The study done by Chen et al., 2000 showed that pollutant removal efficiency (oil and grease) does not change while current density changes from 12.50 to 108.9 A/m<sup>2</sup>. Various other studies (Kobyas et al., 2003, Yilmaz et al., 2005, İrdemez et al., 2006) conducted before support our result. The study carried out by Kobyas et al., 2003 showed that removal efficiency of textile wastewater was 35% at 50 A/m<sup>2</sup> and 99% at 150 A/m<sup>2</sup>.

#### **4.5.2 Effect of Time on Electrocoagulation**

To explore the effect of electrocoagulation time on kaolinite and quartz suspensions, turbidity removal efficiency was plotted versus electrocoagulation time starting from 1 min to 60 min (Figures 4.30-4.33) at 20 A/m<sup>2</sup> and 87 A/m<sup>2</sup> current densities. The turbidity removal efficiency increased sharply during 10 minutes, beyond which no significant improvement was observed. In other words, the kaolinite and quartz concentration in suspensions decreased rather sharply within the first 10 minutes of electrocoagulation, approaching a residual level of concentration which did not change appreciably with prolonged electrocoagulation.

To describe the relationship between kaolinite and quartz concentrations and electrocoagulation time, a second-order rate equation was tested. The second-order rate equation for the reduction of concentration in suspension is given in the following equation:

$$\frac{dC}{dt} = -k(C-C_r)^2 \quad (37)$$

where C is the concentration (as g sample/L) of particles in suspension at any time t, C<sub>r</sub> is the residual value of the sample concentration at prolonged times, and k is the second-order rate constant of electrocoagulation. The integrated rate equation takes the form given below:

$$C = \frac{C_o + C_r(C_o - C_r)kt}{1 + (C_o - C_r)kt} \quad (38)$$

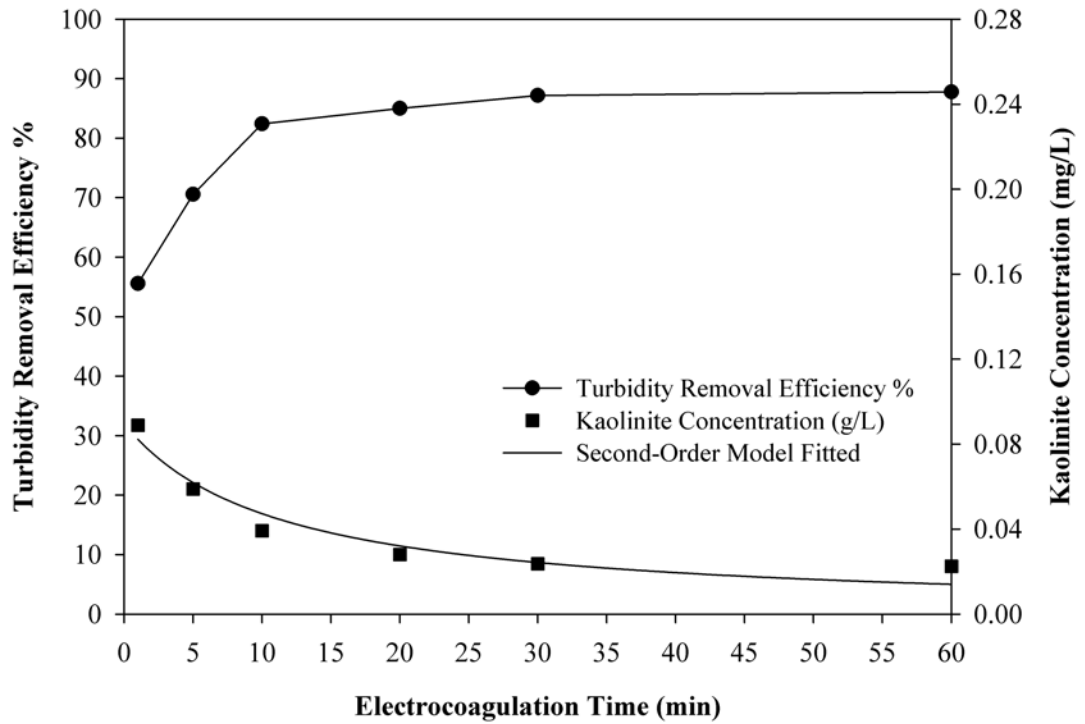


Figure 4.30 The effect of electrocoagulation time on the turbidity removal efficiency of kaolinite from suspension and kaolinite concentration (g/L) in the suspension (pH: 9; 40 V; 20 A/m<sup>2</sup>).

The experimental data showed very good fit to the above kinetic model. In the kaolinite case for 20 A/m<sup>2</sup> current density, the predicted values of the model parameters  $C_r$  and  $k$  from a nonlinear regression analysis were found to be 0.025 g/L and 8.601 min<sup>-1</sup>, respectively, with a corrected sum of squares value of 0.918 in regression. In the quartz case, the predicted values of the model parameters  $C_r$  and  $k$  from a nonlinear regression analysis were found to be 0.037 g/L and

4.444  $\text{min}^{-1}$ , respectively, with a corrected sum of squares value of 0.978 in regression at 20  $\text{A/m}^2$  current density.

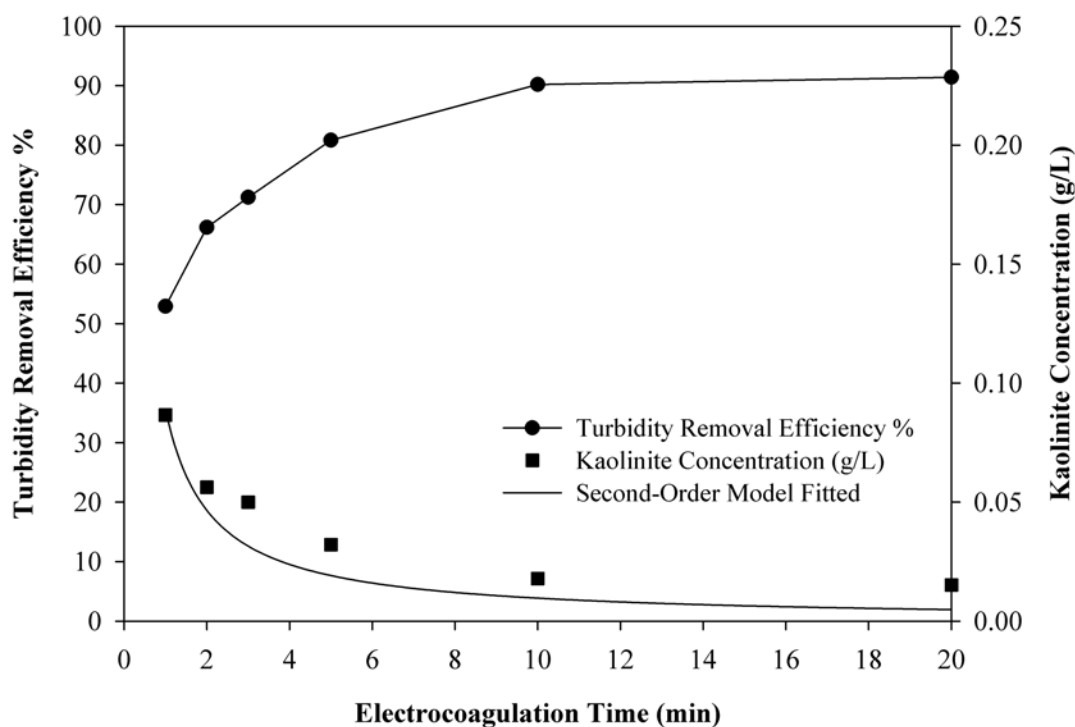


Figure 4.31 The effect of electrocoagulation time on the turbidity removal efficiency of kaolinite from suspension and kaolinite concentration (g/L) in the suspension (pH: 9; 40 V; 87  $\text{A/m}^2$ ).

In the kaolinite case for 87  $\text{A/m}^2$  current density, the predicted values of the model parameters  $C_r$  and  $k$  from a nonlinear regression analysis were found to be 0.008 g/L and 5.969  $\text{min}^{-1}$ , respectively, with a corrected sum of squares value of 0.990 in regression. In the quartz case, the predicted values of the model parameters  $C_r$  and  $k$  from a nonlinear regression analysis were found to be 0.014 g/L and 3.023  $\text{min}^{-1}$ , respectively, with a corrected sum of squares value of 0.946 in regression at 87  $\text{A/m}^2$  current density.

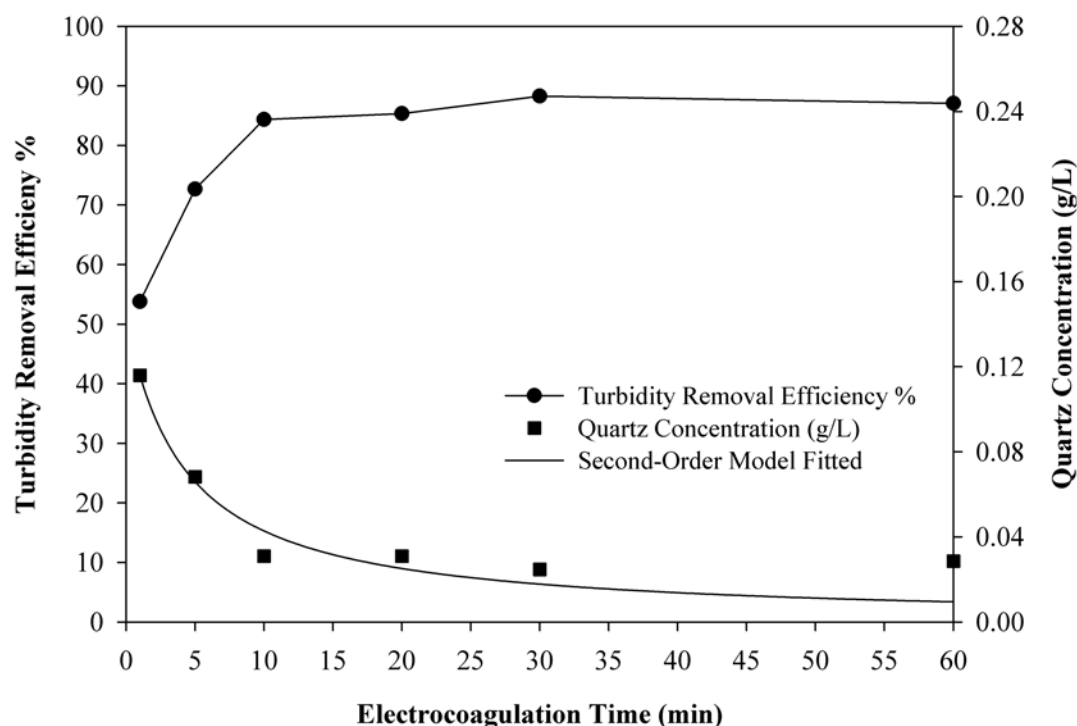


Figure 4.32 The effect of electrocoagulation time on the turbidity removal efficiency of quartz from suspension and quartz concentration (g/L) in the suspension (pH: 9; 40 V; 20 A/m<sup>2</sup>).

The plots show that the correlation coefficient for the second-order kinetic model obtained in all of the studies were above 0.910, and the calculated concentration values agree with the experimental concentration values. These results indicate that the adsorption system studied belongs to the second-order kinetic model. Similar phenomena have been observed in an electrocoagulation process for the removal of iron from drinking water with aluminum alloy as the anode and stainless steel as the cathode (Vasudevan et al., 2009).

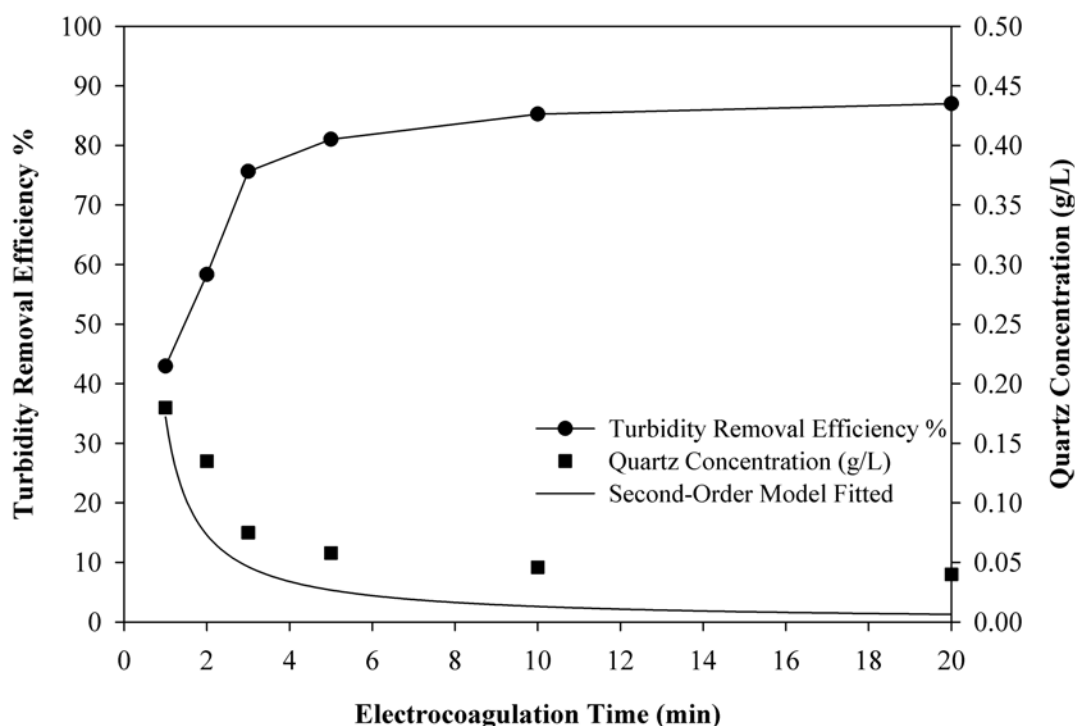


Figure 4.33 The effect of electrocoagulation time on the turbidity removal efficiency of quartz from suspension and quartz concentration (g/L) in the suspension (pH: 9; 40 V; 87 A/m<sup>2</sup>).

Figure 4.31 and Figure 4.33 also display the effect of time on turbidity removal efficiency at 87 A/m<sup>2</sup> which was the optimum current density for kaolinite and quartz suspensions. The turbidity removal efficiency increased from 52% to 72% within 3 min and reached up to 90% at 10 min for kaolinite suspension. For quartz case, turbidity removal efficiency steeply increased from to 75% within 3 min, then to 81% at 5 min. The turbidity removal efficiency reached up to 85% at 10 min electrocoagulation. Turbidity removal efficiencies did not change significantly after 10 minutes of electrocoagulation. At high current density (87 A/m<sup>2</sup>), electrocoagulation or adsorption process was rapid and the process reached the equilibrium with 85% removal efficiency. It is very important to note that very fast

kaolinite or quartz removal took place at a short electrolysis time; this is considered a great advantage of using the electrocoagulation process. Merzouk et al., 2009b stated that the treatment time was shortened with high current. The degree of anodic dissolution of aluminum increases at high current density. This forms a greater amount of precipitate for the removal of pollutants.

#### **4.6 Effect of Aluminum Dosage on Electrocoagulation and Coagulation**

A direct comparison between electrocoagulation and coagulation is not practicable. The systems do not operate on an equivalent basis. In coagulation, coagulant addition is a discrete (shot-fed) event with equilibrium determining aluminum speciation and pH (Holt et al., 2002). Aluminum is generated continuously over the extended area of the anode in electrocoagulation compared with the point addition of aluminum in coagulation. Hence, freshly precipitated flocs are generated and more effectively dispersed in electrocoagulation (Zhu et al., 2005).

In order to compare the electrocoagulation and coagulation processes on the basis of the amount of aluminum, either released from the electrodes or added as aluminum sulfate into the suspension, tests were conducted under the optimum conditions of each process. Figure 4.34 and Figure 4.35 present the experimental conditions and the effects of aluminum dosages on the turbidity removal efficiencies obtained with electrocoagulation and coagulation in kaolinite and quartz suspensions. These data suggest that, as long as the operating conditions are optimized for each process, the source of aluminum does not matter in relation to the turbidity removal. Equal dosages of aluminum in the suspensions lead to similarly effective results in removing the turbidity. Table 4.7 depicts comparison of the electrocoagulation and conventional coagulation in terms of aluminum produced or added and turbidity removal efficiency for kaolinite and quartz suspension.



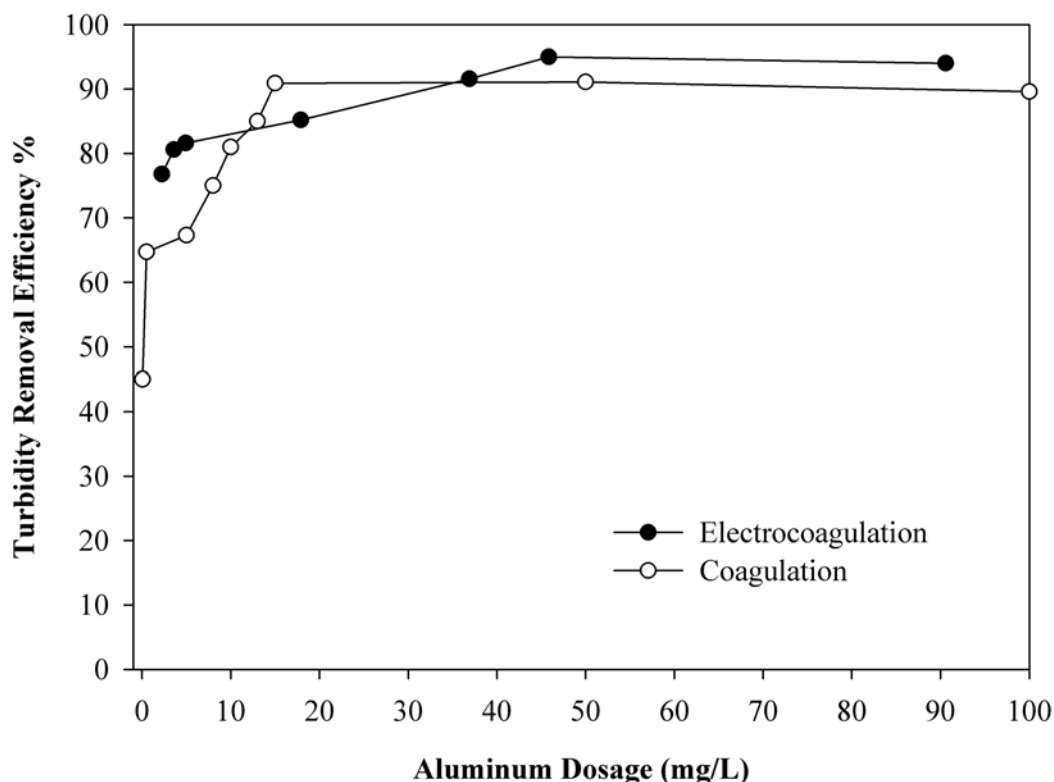


Figure 4.34 The effect of aluminum dosage (mg/L) on kaolinite removal by electrocoagulation (pH: 9; 40 V; 10 min) and coagulation (pH: 6; 10 min).

The effect of  $\text{Al}_2(\text{SO}_4)_3$  dosage (varied from 0.05 mg Al/L to 100 mg Al/L) on kaolinite and quartz removal from the suspensions having an initial pH of 6.5 was studied as given below. The results (Figure 4.34) showed that turbidity removal efficiency for kaolinite suspension increased from 40% at 0.05 mg Al/L to 91% at 50 mg Al/L and then stayed almost constant. 50 mg Al/L produced effective turbidity reduction profiles very similar to the case in quartz suspension. Poor coagulation performance at low aluminum sulfate concentrations suggested insufficient coagulant for pollutant destabilization. Figure 4.36 shows the zeta potential of kaolinite and quartz suspensions at different alum concentrations (0 - 50 mg Al/L). The suspensions (with no aluminum sulfate addition) were stable, with

the particles being negatively charged. Aluminum addition (to 0.05 and 5 mg Al/L) increased the zeta potential. At these concentrations, there was insufficient coagulant to effectively reduce the particles' electric double layer to enable destabilization. At an alum concentration of 15 mg Al/L, particles approached the isoelectric point and coagulation performance improved markedly (Figure 4.36).

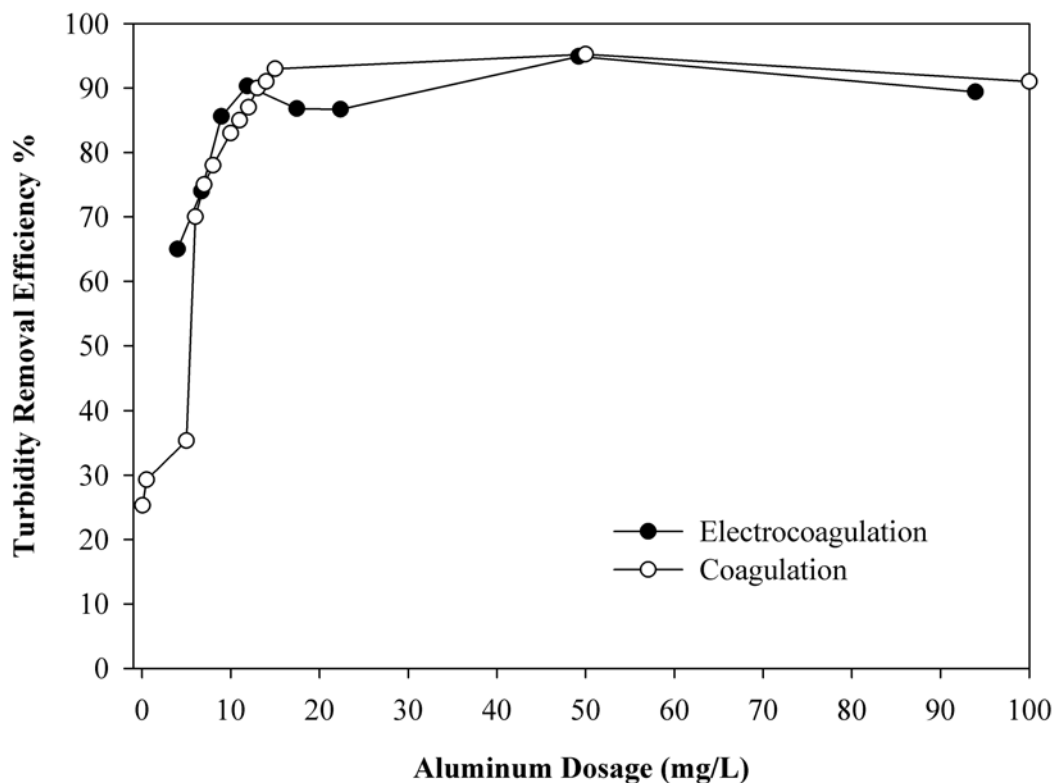


Figure 4.35 The effect of aluminum dosage (mg/L) on quartz removal by electrocoagulation (pH: 9; 40 V; 10 min) and coagulation (pH: 6; 10 min).

High turbidity removal efficiency was recorded for 15 mg Al/L for kaolinite and quartz suspensions. At low aluminum sulfate concentrations (0.05 and 0.5 mg Al/L), the observed poor coagulant performance suggested that the coagulants available for pollutant destabilization were insufficient to accomplish this task.

Gregory (2006) reported that at very low alum dosage, particles were still negative and the turbidity removal was low. As the alum dosage was increased, particles were destabilized and the turbidity removal was significantly more effective.

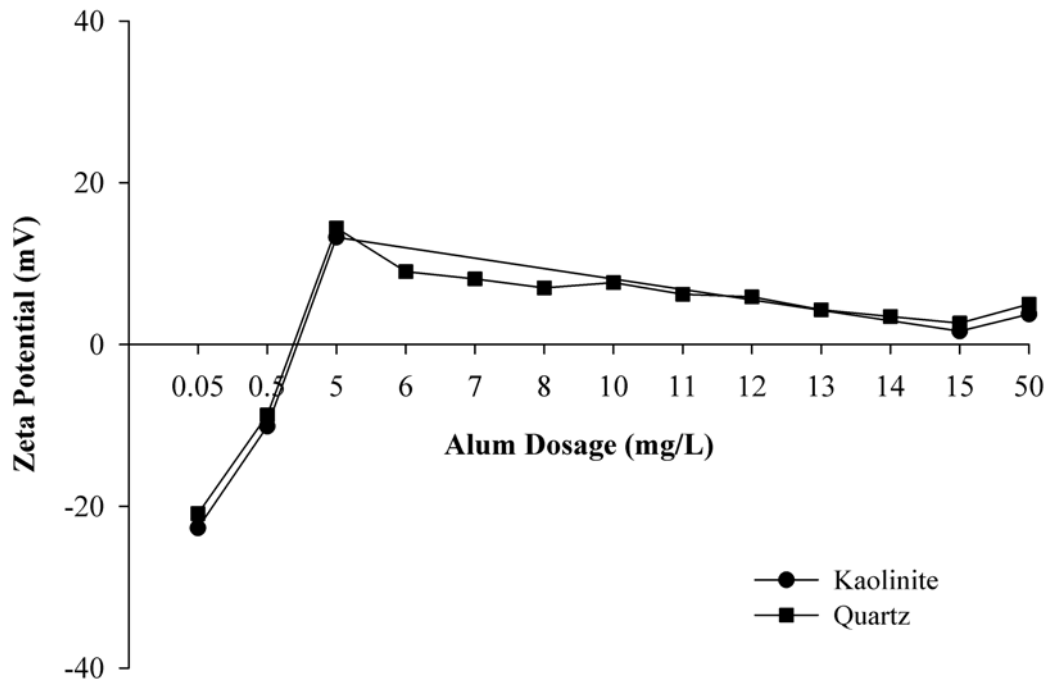


Figure 4.36 Zeta potential measurement after kaolinite and quartz suspension coagulation as a function of aluminum dosage (pH: 6-6.5; coagulation time: 10 min).

Table 4.7 Comparison of electrocoagulation and conventional coagulation in terms of aluminum added or produced and turbidity removal efficiency for kaolinite and quartz suspension.

Kaolinite				Quartz			
Electrocoagulation		Coagulation		Electrocoagulation		Coagulation	
Amount of Aluminum (mg/L)	Turbidity Removal Efficiency %	Amount of Aluminum (mg/L)	Turbidity Removal Efficiency %	Amount of Aluminum (mg/L)	Turbidity Removal Efficiency %	Amount of Aluminum (mg/L)	Turbidity Removal Efficiency %
2.237	76.78	0.05	45.0	4.000	65.0	0.05	25.29
3.579	80.60	0.50	64.7	6.700	74.0	0.50	29.29
4.921	81.60	5.00	67.3	8.947	85.6	5.00	35.35
17.893	85.20	8.00	75.0	11.854	90.3	8.00	78.00
36.905	91.57	10.00	81.0	17.446	86.8	10.00	83.00
45.852	95.00	13.00	85.0	22.367	86.7	13.00	90.00
90.586	94.00	15.00	90.9	49.207	94.9	14.00	91.00
		50.00	91.1	93.941	89.4	15.00	93.00
		100.00	89.6			50.00	95.24
						100.00	91.00

## **CHAPTER 5**

### **CONCLUSIONS AND RECOMMENDATIONS**

Based on the data and discussions presented in this study, the following conclusions are derived:

- The effectiveness of both electrocoagulation and conventional coagulation depends on the initial pH of the suspension. In the electrocoagulation case, the optimum pH for the removal of kaolinite and quartz from the suspension was found to be 9. For electrocoagulation the highest turbidity removal efficiencies were 87% for kaolinite and 89.7% for quartz at pH 9. In the coagulation case, highest turbidity removal efficiencies were 90-95% which occurred within the pH range 5-8 for kaolinite suspension and within the pH range 6-8 for quartz suspension.
- In both the electrocoagulation and coagulation experiments, suspension pHs for optimum turbidity removal were around the isoelectric point of the kaolinite and quartz particles. This suggests similar mechanisms of particle aggregation through charge neutralization and/or enmeshment in aluminum hydroxide precipitates.
- The zeta potential values of electrocoagulated kaolinite and quartz depend mainly on the pH of the suspension. It was found that pHs below 9 lead to

positive values of the zeta potential, whereas higher values of pH caused negative zeta potentials for both kaolinite and quartz. This behavior can be explained in terms of the formation of aluminum hydroxide precipitate, charged positively (due to the adsorption of cations from the solution) under pHs lower than 9. Higher pH values produced a reversal of the charge, leading to negatively charged precipitates (due to anions from the solution) causing negative zeta potentials.

- Electrocoagulation shifted the initial suspension pHs toward neutral pH values during the process whereas aluminum sulfate addition acidifies the water in coagulation.
- In electrocoagulation, when the applied voltage was increased to 40 V, the removal efficiency increased to about 90% as the higher amount of  $\text{Al}^{3+}$  via anodic metal dissolution caused coagulation. When the voltage was increased to 50 V, no further improvement occurred in the removal efficiency. Thus, the optimal applied voltage was decided to be 40 V. This value was the same for both kaolinite and quartz suspensions.
- Turbidity removal efficiency was initially directly proportional to the current density. Optimum current density was  $87 \text{ A/m}^2$  for kaolinite and quartz suspensions. The increase in turbidity removal efficiency with current density can be explained by the formation of higher amount of destabilized particles due to charge neutralization. Since excessive amounts of aluminum were released from the electrodes at higher current densities, the most likely explanation for the decrease in turbidity removal can be regarded as the formation of slow-settling, low-density flocs within the more aluminum hydroxide precipitates.
- The turbidity removal efficiencies for both kaolinite and quartz suspensions increased sharply during 10 min of electrocoagulation time, beyond which

no significant improvement was observed. The rate of electrocoagulation was very fast, leading to an optimum removal of turbidity within 10 min. The kinetics of electrocoagulation could be modeled by a second-order rate equation.

- When the effects of coagulation dosage on removal efficiencies for kaolinite and quartz suspensions were compared, it was found that optimum dosage was 15 mg Al/L for both.
- Electrocoagulation and coagulation removed the turbidity equally well when the same amount of aluminum was introduced into the suspensions, provided that all other operating parameters were optimized specifically for each process.

After the completion of this dissertation, some further studies can be proposed as below:

- Electrocoagulation and coagulation experiments can be conducted with three-layer and mixed-layer clay minerals such as montmorillonite, illite, and chlorite.
- Study can be done with industrial systems to move from laboratory scale to actual scale.
- This study for coagulation was carried out in laboratory scale with a batch operation mode. This would be turned into continuous operation mode since the full scale plants normally operate in a continuous operation mode.
- Some changes can be done in the laboratory-scale system such as electrode connection modes, monopolar parallel, monopolar series, and bipolar series in order to find their effect on the effectiveness of electrocoagulation.
- The effect of temperature needs to be studied since it is an important parameter especially during the electrocoagulation process.

- Utilization of tap water instead of distilled water may be experimented.
- The cost of the process can be evaluated to determine the efficiency of the solution and offer better alternative method for removing particles from wastewaters.
- Electroflotation can be tried instead of sedimentation process after electrocoagulation process.



## REFERENCES

- Abuzaid, N. S., Bukhari, A. A., Al-Hamouz, Z. M. (2002) Ground Water Coagulation Using Soluble Stainless Steel Electrodes, *Advances in Environmental Research*, 6, 325-333.
- Alvarez-Gallegos, A., Pletcher, D. (1999) The Removal of Low Level Organics Via Hydrogen Peroxide Formed in a Reticulated Vitreous Carbon Cathode Cell. Part 2: The Removal of Phenols and Related Compounds from Aqueous Effluents, *Electrochimica Acta*, 44, 2483–2492.
- Bektaş, N., Akbulut, H., Inan, H., Dimoglo, A. (2004) Removal of Phosphate from Aqueous Solutions by Electro-coagulation, *Journal of Hazardous Materials*, 106B, 101-105.
- Bratby, J. (2006) *Coagulation and Flocculation in Water and Wastewater Treatment*, 2nd ed., Seattle, WA : IWA Publishing.
- Butt, H. J., Graf, K., Kappl, M. (2003) *Physic and Chemistry of Interfaces*, Weinheim: Wiley-VCH ; Chichester : John Wiley.
- Can, O. T., Kobya, M., Demirbas, E., Bayramoglu, M. (2006) Treatment of the Textile Wastewater by Combined Electrocoagulation, *Chemosphere*, 62, 181-187.
- Canizares, P., Jimenez, C., Martinez, F., Rodrigo, M. A., Saez, C. (2009) The pH as a Key Parameter in the Choice between Coagulation and Electrocoagulation for the Treatment of Wastewaters, *Journal of Hazardous Materials*, 163, 158-164.

Canizares, P., Martinez, F., Rodrigo, M. A., Jimenez, C., Saez, C., Lobato, J. (2008) Modeling of Wastewater Electrocoagulation Processes: Part I. General Description and Application to Kaolin-Polluted Wastewaters, *Separation and Purification Technology*, 60, 155-161.

Canizares, P., Martinez, F., Jimenez, C., Lobato, J., Rodrigo, M. A. (2007) Coagulation and Electrocoagulation of Wastes Polluted with Colloids, *Separation Science and Technology*, 42, 2157-2175.

Canizares, P., Martinez, F., Jimenez, C., Lobato, J., Rodrigo, M. A. (2006) Comparison of the Aluminum Speciation in Chemical and Electrochemical Dosing, *Industrial and Engineering Chemistry Research*, 45, 8749-8756.

Chen, X., Chen, G., Yue, P. L. (2000) Separation of Pollutants from Restaurant Wastewater by Electrocoagulation, *Separation and Purification Technology*, 19, 65-76.

Chen, G. (2004) Electrochemical Technologies in Wastewater Treatment, *Separation and Purification Technology*, 38, 11-41.

Daneshvar, N., Ashassi-Sorkhabi, H., Tizpar, A. (2003) Decolorization of Orange II by Electrocoagulation Method, *Separation and Purification Technology*, 31, 153-162.

Demirci, Ş. (1973) *Electrical Charge on Colloidal Gold Particles*, PhD. Thesis, METU.

Duan, J., Gregory, J. (2003) Coagulation by Hydrolyzing Metal Salts, *Advances in Colloid and Interface Science*, 100-102, 475-502.

Duan, J., Gregory, J. (1998) The Influence of Silicic Acid on Aluminum Hydroxide Precipitation and Flocculation by Aluminum Salts, *Journal of Inorganic Biochemistry*, 69, 193-201.

Gan, W., Liu, Q. (2008) Coagulation of Bitumen with Kaolinite in Aqueous Solutions Containing  $\text{Ca}^{2+}$ ,  $\text{Mg}^{2+}$  and  $\text{Fe}^{3+}$ : Effect of Citric Acid, *Journal of Colloid and Interface Science*, 324, 85-91.

Golder, A. K., Hridaya, N., Samanta, A. N., Ray, S. (2005) Electrocoagulation of Methylene Blue and Eosin Yellowish Using Mild Steel Electrodes, *Journal of Hazardous Materials*, B127, 134–140.

Gregory, J. (2006) *Particles in Water: Properties and Processes*. London: IWA Pub.: Boca Raton, CRC Press Taylor & Francis.

Gregory, J., Duan, J. (1998) The Effect of Dissolved Silica on the Action of Hydrolysing Metal Coagulants, *Water Science Technology*, 38, 13-120.

Gürses, A., Yalçın, M., Doğar, C. (2002) Electrocoagulation of Some Reactive Dyes: A Statistical Investigation of Some Electrochemical Variables, *Waste Management*, 22, 491-499.

Holt, P. K., Barton, G. W., Wark, M., Mitchell, C. A. (2002) A Quantitative Comparison between Chemical Dosing and Electrocoagulation, *Colloids and Surfaces A: Physicochemical Engineering Aspects*, 211, 233-248.

Holt, P. K., Barton, G. W., Mitchell, C. A. (2004) Deciphering the Science Behind Electrocoagulation to Remove Suspended Clay Particles from Water, *Water Science and Technology*, 50:12, 177-184.

Holt, P. K., Barton, G. W., Mitchell, C. A. (2005) The Future for Electrocoagulation as a Localised Water Treatment Technology, *Chemosphere*, 59, 355-367.

Hunter, R. J. (1981) *Zeta Potential in Colloid Science: Principles and Applications*, Academic Press, London, p. 283.

Hussain, S. A., Demirci, Ş., Özbayoğlu, G. (1996) Zeta Potential Measurements of Three Clays from Turkey and Effects of Clay on Coal Flotation, *Journal of Colloid and Interface Science*, 184, 535-541.

International Union of Pure and Applied Chemistry (IUPAC) (1972) Manual of Symbols and Terminology for Physicochemical Quantities and Units, Appendix II: Definitions, Terminology and Symbols in Colloid and Surface Chemistry, Part I, *Pure and Applied Chemistry*, 31, 577-638.

İrdemez, Ş., Demircioğlu, N., Yıldız, Y. Ş., Bingül, Z. (2006) The Effects of Current Density and Phosphate Concentration on Phosphate Removal from Wastewater by Electrocoagulation Using Aluminum And Iron Plate Electrodes, *Separation and Purification Technology*, 52, 218-223.

Jirgensons, B., Straumanis, M. E. (1962) *A Short Textbook of Colloid Chemistry*, 2nd rev. ed., New York, Macmillan.

Kobya, M., Can, O. T., Bayramoglu, M. (2003) Treatment of the Textile Wastewaters by Electrocoagulation Using Iron and Aluminum Electrodes, *Journal of Hazardous Materials*, B100, 163-178.

Lin, S. H., Peng, C. F. (1994) Treatment of Textile Wastewater by Electrochemical Method, *Water Research*, 28, 277-282.

Lu, S., Pugh, R. J., Forssberg, E. (2005) *Interfacial separation of particles*, Elsevier, Amsterdam, p. 336.

Marel, H. W., Beutelspacher, H. (1976) *Atlas of Infrared Spectroscopy of Clay Minerals and their Admixtures*, Elsevier Scientific Publishing Company, Amsterdam.

Matteson, M. J., Dobson, R. L., Glenn, Jr. R. W., Kukunoor, N. S., Waits III, W. H., Clayfield, E. J., (1995) Electrocoagulation and Separation of Aqueous Suspensions of Ultrafine Particles, *Colloids and Surfaces A: Physicochemical and Engineering Aspects*, 104, 101-109.

McFarlane, A., Bremmell, K., Addai-Mensah, J. (2006) Improved Dewatering Behavior of Clay Minerals Dispersions via Interfacial Chemistry and Particle Interactions Optimization, *Journal of Colloid and Interface Science*, 293, 116-127.

Merzouk, B., Gourich, B., Sekki, A., Madani, K., Vial, Ch., Barkaoui, M. (2009a) Studies on the Decolorization of Textile Dye Wastewater by Continuous Electrocoagulation Process, *Chemical Engineering Journal*, 149, 2007-214.

Merzouk, B., Gourich, B., Sekki, A., Madani, K., Chibane, M. (2009b) Removal Turbidity and Separation of Heavy Metals using Electrocoagulation-Electroflotation Technique A Case Study, *Journal of Hazardous Materials*, 164, 215-222.

Mollah, M. Y. A., Schennach, R., Parga. J. R., Cocke, D. L. (2001) Electrocoagulation (EC) – Science and Applications, *Journal of Hazardous Materials*, B84, 29-41.

Mollah, M. Y. A., Morkovsky, P., Gomes, J. A. G., Kesmez, M., Parga, J., Cocke, D. L. (2004) Fundamentals, Present and Future Perspectives of Electrocoagulation, *Journal of Hazardous Materials*, B114, 199-210.

Mouedhen, G., Feki, M., De Petris Wery, M., Ayedi, H. F. (2008) Behavior of Aluminum Electrodes in Electrocoagulation Process, *Journal of Hazardous Materials*, 150, 124-135.

Mpofu, P., Addai-Mensah, J., Ralston, J. (2005) Interfacial Chemistry, Particle Interactions and Improved Dewatering Behaviour of Smectite Clay Dispersions, *International Journal of Mineral Processing*, 75, 155-171.

Nayak, P. S., Singh, B. K. (2007) Instrumental Characterization of Clay by XRF, XRD and FTIR, *Bulletin of Materials Science*, 30:3, 235–238.

Nemerow, N. L., Agardy, F. J. (1998) *Strategies of Industrial and Hazardous Waste Management*, 2nd ed., John Wiley and Sons.

Niimi, N., Aikawa, N., Shinoda, K., (1999) The Infrared Absorption Band at 3596  $\text{cm}^{-1}$  of the Recrystallized Quartz from Mt. Takamiyama, Southwest Japan, *Mineralogical Magazine*, 63:5, 693-701.

Ölmez, T. (2009) The Optimization of Cr(VI) Reduction and Removal by Electrocoagulation Using Response Surface Methodology, *Journal of Hazardous Materials*, 162, 1371-1378.

Rubio, J., Souza, M. L., Smith, R.W. (2002) Overview of Flotation as a Wastewater Treatment Technique, *Minerals Engineering*, 15, 139-155.

Sabah, E., Yüzer, H., Çelik, M. S. (2004) Characterization and Dewatering of Fine Coal Tailings by Dual-Flocculant Systems, *International Journal of Mineral Processing*, 74, 303-315.

Seyrankaya, A., Malayoğlu, U., Akar, A. (2000) Flocculation Conditions of Marble from Industrial Wastewater and Environment Consideration, *Mineral Processing on the Verge of the 21st Century*, Balkema, Rotterdam, 645-652.

Shaw, D. J. (1966) *Introduction to Colloid and Surface Chemistry*, London, Butterworths.

Sincero Arcadio P., Sincero Gregoria A. (2003) *Physical-Chemical Treatment of Water and Wastewater*, London: IWA Pub.; Boca Raton, Fla.: CRC Press.

Sparks, D. L. (2002) *Environmental Soil Chemistry*, 2nd ed., Academic Press, p 273.

Sposito, G. (1996) *The Environmental Chemistry of Aluminum*, 2nd ed., CRC Press.

Stumm, W., Morgan, J. J. (1996) *Aquatic Chemistry – Chemical Equilibria and Rates in Natural Waters*. New York: Wiley.

Szynkarczuk, J., Kan, J., Hassan, T. A. T., Donini, J. C. (1994) Electrochemical Coagulation of Clay Suspensions, *Clay and Clay Minerals*, 42, 667-673.

Şener, S. (2007) Removal of Suspended Solid Materials from the Wastewater of Natural Dimension Stone Cutting Plants by Flocculation, *Journal of Science and Technology*, 1 (2), 234-244.

Tchobanoglous, G., Burton, F. L., Stensel, H. D. (2003) *Wastewater engineering: treatment and reuse*, 4th ed., Metcalf & Eddy, Inc., Boston: McGraw-Hill.

Thiele, E. S., French, R. H. (1998) Light-Scattering Properties of Representative, Morphological Rutile Titania Particles Studied Using a Finite-Element Method, *Journal of the American Ceramic Society*, 81, 3, 469-479.

Van Olphen, H. (1977) *An Introduction to Clay Colloid Chemistry: for clay technologists, geologists, and soil scientists*, 2d ed., New York: Wiley.

Vasudevan, S., Jayaraj, J., Lakshmi, J., Sozhan, G. (2009) Removal of iron from drinking water by electrocoagulation: Adsorption and kinetics studies, *Korean Journal of Chemical Engineering*, 26, 1058-1064.

Vik, E. A., Carlson, D. A., Eikum, A. S., Gjessing, E. T. (1984) Electrocoagulation of Potable Water, *Water Research*, 18, 1355-1360.

Yılmaz, A. E., Boncukcuoğlu, R., Kocakerim, M. M. (2007) A Quantitative Comparison between Electrocoagulation and Chemical Coagulation for Boron Removal from Boron-Containing Solution, *Journal of Hazardous Materials*, 149, 475-481.

Yılmaz, M. T., Boncukcuoğlu, R., Yılmaz, A. E. (2006) Removal of Suspended Solids from Boron Industry Wastewater by Coagulation, *III: International Boron Symposium*, 533-538.

Yılmaz, A. E., Boncukcuoğlu, R., Kocakerim, M. M., Keskinler, B. (2005) The Investigation of Parameters Affecting Boron Removal by Electrocoagulation Method, *Journal of Hazardous Materials*, B125, 160-165.

Wang, C. T., Chou, W. L., Chen, L. S., Chang, S. Y. (2009) Silica Particles Settling Characteristics and Removal Performances of Oxide Chemical Mechanical Polishing Wastewater Treated by Electrocoagulation Technology, *Journal of Hazardous Materials*, 161, 344-350.

Zhu, B., Clifford, D. A., Chellam, S. (2005) Comparison of electrocoagulation and chemical coagulation pretreatment for enhanced virus removal using microfiltration membranes, *Water Research*, 39, 3098-3108.



## **APPENDIX A**

### **PHYSICAL, CHEMICAL AND BIOLOGICAL CONSTITUENTS OF WASTEWATER**

Table A.1 Common analyses used to assess the constituents found in wastewater (Tchobanoglous, 2003).

Test	Abbreviation/ Definition	Use or significance of test results
<b>Physical characteristics</b>		
Total solids	TS	To assess the reuse potential of a wastewater and to determine the most suitable type of operations and processes for its treatment
Total volatile solids	TVS	
Total fixed solids	TFS	
Total suspended solids	TSS	
Volatile suspended solids	VSS	
Fixed suspended solids	FSS	
Total dissolved solids	TDS (TS - TSS)	
Volatile dissolved solids	VDS	
Total fixed dissolved solids	FDS	
Settleable solids		To determine those solids that will settle by gravity in a specified time period
Particle size distribution	PSD	To assess the performance of treatment processes
Turbidity	NTU	Used to assess the quality of treated wastewater
Color	light brown, gray, black	To assess the condition of wastewater (fresh or septic)
Transmittance	%T	Used to assess the suitability of treated effluent for UV disinfection
Odor		To determine if odors will be a problem
Temperature	°C or °F	Important in the design and operation of biological processes in treatment facilities
Density	P	Used to assess the suitability of treated effluent for agricultural applications
Conductivity	EC	

Table A.1 cont'd

Test	Abbreviation/ Definition	Use or significance of test results
<b>Inorganic chemical characteristics</b>		
Free ammonia	$\text{NH}_4^+$	Used as a measure of the nutrients present and the degree of decomposition in the wastewater; the oxidized forms can be taken as a measure of the degree of oxidation.
Organic nitrogen	Org N	
Total Kjeldahl nitrogen	TKN (Org N + $\text{NH}_4^+\text{-N}$ )	
Nitrites	$\text{NO}_2^-$	
Nitrates	$\text{NO}_3^-$	
Total nitrogen	TN	
Inorganic phosphorus	Inorg P	
Total phosphorus	TP	
Organic phosphorus	Org P	
pH	$\text{pH} = -\log [\text{H}^+]$	A measure of the acidity or basicity of an aqueous solution
Alkalinity	$\Sigma \text{HCO}_3^- + \text{CO}_3^{2-} + \text{OH}^- - \text{H}^+$	A measure of the buffering capacity of the wastewater
Chloride	$\text{Cl}^-$	To assess the suitability of wastewater for agricultural reuse
Sulfate	$\text{SO}_4^{2-}$	To assess the potential for the formation of odors and may impact the treatability of the waste sludge
Metals	As, Cd, Ca, Cr, Co, Cu, Pb, Mg, Hg, Mo, Ni, Se, Na, Zn	To assess the suitability of the wastewater for reuse and for toxicity effects in treatment. Trace amounts of metals are important in biological treatment
Specific inorganic elements and compound		To assess presence or absence of a specific constituent
Various gases	$\text{O}_2$ , CO, $\text{NH}_3$ , $\text{H}_2\text{S}$ , $\text{CH}_4$	The presence or absence of specific gases

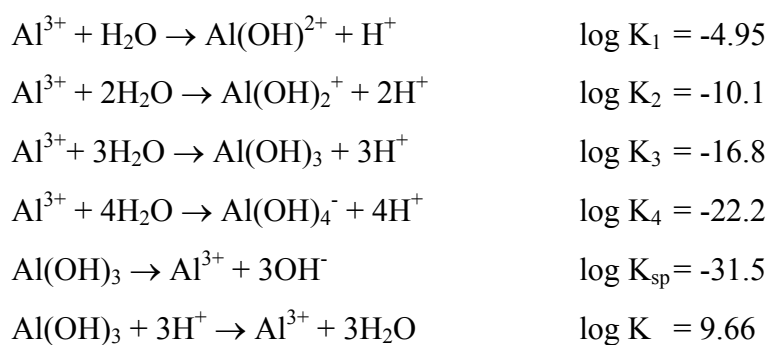
Table A.1 cont'd

Test	Abbreviation/ Definition	Use or significance of test results
<b>Organic chemical characteristics</b>		
Five day carbonaceous biochemical oxygen demand	CBOD <sub>5</sub>	A measure of the amount of oxygen required to stabilize a waste biologically
Ultimate carbonaceous biochemical oxygen demand	UBOD (also BOD <sub>u</sub> , BOD <sub>L</sub> )	A measure of the amount of oxygen required to stabilize a waste biologically
Nitrogenous oxygen demand	NOD	A measure of the amount of oxygen required to oxidize biologically the nitrogen in the wastewater to nitrate
Chemical oxygen demand	COD	Often used as a substitute for the BOD test
Total organic carbon	TOC	Often used as a substitute for the BOD test
Specific organic compounds and classes of compounds	MBAS <sup>e</sup> , CTAS <sup>f</sup>	To determine presence of specific organic compounds and to assess whether special design measures will be needed for removal
<b>Biological characteristics</b>		
Coliform organisms	MPN (most probable number)	To assess presence of pathogenic bacteria and effectiveness of disinfection process
Specific microorganisms	Bacteria, protozoa, helminths, viruses	To assess presence of specific organisms in connection with plant operation and for reuse
Toxicity	TUa and TUc	Toxic unit acute, Toxic unit chronic

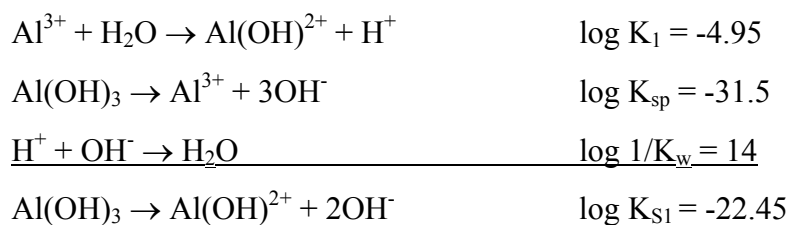
## APPENDIX B

### THE HYDROLYSIS OF ALUMINUM

K values are taken from the "Environmental Chemistry of Aluminum" (Sposito, 1996).



#### ***First Reaction;***



$$K_{\text{S1}} = [\text{Al}(\text{OH})^{2+}] [\text{OH}^-]^2$$

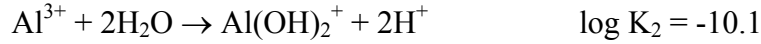
$$\log K_{\text{S1}} = \log[\text{Al}(\text{OH})^{2+}] + 2\log[\text{OH}^-]$$

$$\log[\text{Al}(\text{OH})^{2+}] = 2\text{pOH} - 22.45$$

$$\text{pH} + \text{pOH} = 14$$

$$\log[\text{Al}(\text{OH})^{2+}] = 2(14 - \text{pH}) - 22.45 = 5.55 - 2\text{pH}$$

**Second Reaction;**



$$K_{\text{S2}} = [\text{Al}(\text{OH})_2^+] [\text{OH}^-]$$

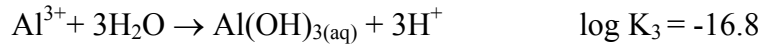
$$\log K_{\text{S2}} = \log[\text{Al}(\text{OH})_2^+] + \log[\text{OH}^-]$$

$$\log[\text{Al}(\text{OH})_2^+] = \text{pOH} - 13.6$$

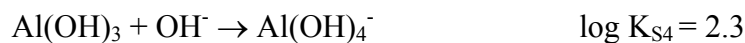
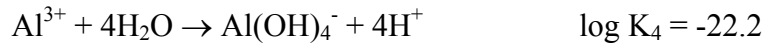
$$\text{pH} + \text{pOH} = 14$$

$$\log[\text{Al}(\text{OH})_2^+] = (14 - \text{pH}) - 13.6 = 1.03 - \text{pH}$$

**Third Reaction;**



**Fourth Reaction;**



$$K_{\text{S4}} = [\text{Al}(\text{OH})_4^-] / [\text{OH}^-]$$

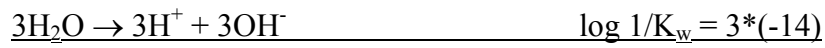
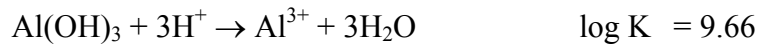
$$\log K_{s4} = \log[\text{Al}(\text{OH})_4^-] - \log[\text{OH}^-]$$

$$\log[\text{Al}(\text{OH})_4^-] = 2.3 - \text{pOH}$$

$$\text{pH} + \text{pOH} = 14$$

$$\log[\text{Al}(\text{OH})_4^-] = 2.3 - (14 - \text{pH}) = -11.7 + \text{pH}$$

***Fifth Reaction;***



$$K_s = [\text{Al}^{3+}] [\text{OH}^-]^3$$

$$\log K_s = \log[\text{Al}^{3+}] + 3\log[\text{OH}^-]$$

$$\log[\text{Al}^{3+}] = 3\text{pOH} - 32.34$$

$$\text{pH} + \text{pOH} = 14$$

$$\log[\text{Al}^{3+}] = 3(14 - \text{pH}) - 32.34 = 9.66 - 3\text{pH}$$

$\log[\text{Al}^{3+}]$	$= 9.66 - 3\text{pH}$
$\log[\text{Al}(\text{OH})^{2+}]$	$= 5.55 - 2\text{pH}$
$\log[\text{Al}(\text{OH})_2^+]$	$= 1.03 - \text{pH}$
$\log[\text{Al}(\text{OH})_3]$	$= -6.3$
$\log[\text{Al}(\text{OH})_4^-]$	$= -11.7 + \text{pH}$

Table B.1 Calculation log concentration of aluminum species.

pH	$\log \text{Al}^{3+}$	$\log \text{Al(OH)}^{2+}$	$\log \text{Al(OH)}_2^+$	$\log \text{Al(OH)}_3$	$\log \text{Al(OH)}_4^-$
0.0	9.66	5.55	1.03	-6.3	-11.7
0.2	9.06	5.15	0.83	-6.3	-11.5
0.4	8.46	4.75	0.63	-6.3	-11.3
0.6	7.86	4.35	0.43	-6.3	-11.1
0.8	7.26	3.95	0.23	-6.3	-10.9
1.0	6.66	3.55	0.03	-6.3	-10.7
1.2	6.06	3.15	-0.17	-6.3	-10.5
1.4	5.46	2.75	-0.37	-6.3	-10.3
1.6	4.86	2.35	-0.57	-6.3	-10.1
1.8	4.26	1.95	-0.77	-6.3	-9.9
2.0	3.66	1.55	-0.97	-6.3	-9.7
2.2	3.06	1.15	-1.17	-6.3	-9.5
2.4	2.46	0.75	-1.37	-6.3	-9.3
2.6	1.86	0.35	-1.57	-6.3	-9.1
2.8	1.26	-0.05	-1.77	-6.3	-8.9
3.0	0.66	-0.45	-1.97	-6.3	-8.7
3.2	0.06	-0.85	-2.17	-6.3	-8.5
3.4	-0.54	-1.25	-2.37	-6.3	-8.3
3.6	-1.14	-1.65	-2.57	-6.3	-8.1
3.8	-1.74	-2.05	-2.77	-6.3	-7.9
4.0	-2.34	-2.45	-2.97	-6.3	-7.7
4.2	-2.94	-2.85	-3.17	-6.3	-7.5
4.4	-3.54	-3.25	-3.37	-6.3	-7.3
4.6	-4.14	-3.65	-3.57	-6.3	-7.1
4.8	-4.74	-4.05	-3.77	-6.3	-6.9
5.0	-5.34	-4.45	-3.97	-6.3	-6.7
5.2	-5.94	-4.85	-4.17	-6.3	-6.5
5.4	-6.54	-5.25	-4.37	-6.3	-6.3
5.6	-7.14	-5.65	-4.57	-6.3	-6.1
5.8	-7.74	-6.05	-4.77	-6.3	-5.9
6.0	-8.34	-6.45	-4.97	-6.3	-5.7
6.2	-8.94	-6.85	-5.17	-6.3	-5.5
6.4	-9.54	-7.25	-5.37	-6.3	-5.3



Table B.1 cont'd

pH	$\log \text{Al}^{3+}$	$\log \text{Al(OH)}^{2+}$	$\log \text{Al(OH)}_2^+$	$\log \text{Al(OH)}_3$	$\log \text{Al(OH)}_4^-$
6.6	-10.14	-7.65	-5.57	-6.3	-5.1
6.8	-10.74	-8.05	-5.77	-6.3	-4.9
7.0	-11.34	-8.45	-5.97	-6.3	-4.7
7.2	-11.94	-8.85	-6.17	-6.3	-4.5
7.4	-12.54	-9.25	-6.37	-6.3	-4.3
7.6	-13.14	-9.65	-6.57	-6.3	-4.1
7.8	-13.74	-10.05	-6.77	-6.3	-3.9
8.0	-14.34	-10.45	-6.97	-6.3	-3.7
8.2	-14.94	-10.85	-7.17	-6.3	-3.5
8.4	-15.54	-11.25	-7.37	-6.3	-3.3
8.6	-16.14	-11.65	-7.57	-6.3	-3.1
8.8	-16.74	-12.05	-7.77	-6.3	-2.9
9.0	-17.34	-12.45	-7.97	-6.3	-2.7
9.2	-17.94	-12.85	-8.17	-6.3	-2.5
9.4	-18.54	-13.25	-8.37	-6.3	-2.3
9.6	-19.14	-13.65	-8.57	-6.3	-2.1
9.8	-19.74	-14.05	-8.77	-6.3	-1.9
10.0	-20.34	-14.45	-8.97	-6.3	-1.7
10.2	-20.94	-14.85	-9.17	-6.3	-1.5
10.4	-21.54	-15.25	-9.37	-6.3	-1.3
10.6	-22.14	-15.65	-9.57	-6.3	-1.1
10.8	-22.74	-16.05	-9.77	-6.3	-0.9
11.0	-23.34	-16.45	-9.97	-6.3	-0.7
11.2	-23.94	-16.85	-10.17	-6.3	-0.5
11.4	-24.54	-17.25	-10.37	-6.3	-0.3
11.6	-25.14	-17.65	-10.57	-6.3	-0.1
11.8	-25.74	-18.05	-10.77	-6.3	0.1
12.0	-26.34	-18.45	-10.97	-6.3	0.3
12.2	-26.94	-18.85	-11.17	-6.3	0.5

Table B.1 cont'd

pH	$\log \text{Al}^{3+}$	$\log \text{Al(OH)}^{2+}$	$\log \text{Al(OH)}_2^+$	$\log \text{Al(OH)}_3$	$\log \text{Al(OH)}_4^-$
12.4	-27.54	-19.25	-11.37	-6.3	0.7
12.6	-28.14	-19.65	-11.57	-6.3	0.9
12.8	-28.74	-20.05	-11.77	-6.3	1.1
13.0	-29.34	-20.45	-11.97	-6.3	1.3
13.2	-29.94	-20.85	-12.17	-6.3	1.5
13.4	-30.54	-21.25	-12.37	-6.3	1.7
13.6	-31.14	-21.65	-12.57	-6.3	1.9
13.8	-31.74	-22.05	-12.77	-6.3	2.1
14.0	-32.34	-22.45	-12.97	-6.3	2.3

## **APPENDIX C**

### **ASTM C-837-81- STANDARD TEST METHOD FOR METHYLENE BLUE INDEX OF CLAY**

This test method covers the measurement of the adsorption of methylene blue dye by clay, which is calculated as a methylene blue index for clay.

#### **Apparatus**

1. Balance, accurate to 0.01 g.
2. Mixer
3. pH meter
4. Beaker, 600 mL
5. Buret, 25 mL
6. Medicine Dropper or Glass Stirring Rod
7. Filter Paper, Baroid No. 987

#### **Reagents**

1. Methylene Blue Solution (1mL = 0.01 meq) – Store in darkness
2. Sulfuric Acid (0.1 N)

#### **Procedure**

1. Weight out 2.00 g of dried clay and place in the 600 mL beaker. If the clay cannot be tested immediately after drying it should be stored in a suitable desiccator.

2. Add 300 mL of distilled water to the beaker and stir with the mixer until the clay is uniformly dispersed.
3. Determine the pH of the slurry and add sufficient sulfuric acid to bring the pH within the range from 2.5 to 3.8. Continue stirring while the pH is being adjusted and continue stirring for 10 to 15 min after the last addition of acid.
4. Again test the slurry for pH, adding additional acid if necessary to restore the pH to the 2.5 to 3.8 range.
5. With the slurry still under the mixer, fill the buret with the methylene blue solution, add 5 mL of the solution to the slurry, and stir 1 to 2 min.
6. Remove a drop of the slurry, using the dropper or the glass stirring rod, and place on the edge of the filter paper.
7. Observe the appearance of the drop on the filter paper. The end point is indicated by the formation of a light blue halo around the drop. Continue adding the methylene blue solution to the slurry in 1.0 mL increments with 1 to 2 min of stirring after each addition, then testing, until the end point is reached.
8. After the end point is reached, continue stirring for 2 min and retest.

### Calculation

1. Calculate the methylene blue index as follows:

$$\text{MBI} = \frac{E \times V}{W} \times 100$$

where MBI is methylene blue index for clay in meq/100g clay, E is milliequivalents of methylene blue per milliliter (1mL = 0.01 meq), V is milliliters of methylene blue solution required for the titration, and W is grams of dry material.

2. The calculations may be facilitated by using a multiplication factor where the specimen size is 2.00 g and the methylene blue titrating solution is 0.01 N:

$$\text{MBI} = \frac{0.01 \times V}{2} \times 100 = 0.5 V$$

3. Record the methylene blue index for the clay.

## **APPENDIX D**

### **PARTICLE SIZE DISTRIBUTION, XRD AND ZETA POTENTIAL DATA**

Table D.1 Particle size distribution data for kaolinite sample.

<b>Size (micron)</b>	<b>Volume %</b>	<b>Size (micron)</b>	<b>Volume %</b>	<b>Size (micron)</b>	<b>Volume %</b>
0.020	0.00	1.002	21.91	50.238	100.00
0.022	0.00	1.125	26.62	56.368	100.00
0.025	0.00	1.262	31.71	63.246	100.00
0.028	0.00	1.416	37.15	70.963	100.00
0.032	0.00	1.589	42.89	79.621	100.00
0.036	0.00	1.783	48.82	89.337	100.00
0.040	0.00	2.000	54.83	100.237	100.00
0.045	0.00	2.224	60.75	112.468	100.00
0.050	0.00	2.518	66.42	126.191	100.00
0.056	0.00	2.852	71.72	141.589	100.00
0.063	0.00	3.170	76.55	158.866	100.00
0.071	0.00	3.557	80.83	178.250	100.00
0.080	0.00	3.991	84.55	200.000	100.00
0.089	0.00	4.447	87.73	224.404	100.00
0.100	0.00	5.024	90.40	251.785	100.00
0.112	0.00	5.637	92.62	282.508	100.00
0.126	0.00	6.325	94.46	316.979	100.00
0.142	0.00	7.096	95.97	355.656	100.00
0.159	0.00	7.962	97.20	399.052	100.00
0.178	0.00	8.934	98.19	447.744	100.00
0.200	0.00	10.024	98.95	502.377	100.00
0.224	0.00	11.247	99.49	563.677	100.00
0.252	0.00	12.619	99.85	632.456	100.00
0.283	0.00	14.159	99.97	709.627	100.00
0.317	0.02	15.887	100.00	796.214	100.00
0.356	0.15	17.825	100.00	893.367	100.00
0.399	0.64	20.000	100.00	1002.374	100.00
0.448	1.63	22.440	100.00	1124.683	100.00
0.502	3.05	25.179	100.00	1261.915	100.00
0.564	4.99	28.251	100.00	1415.892	100.00
0.632	7.43	31.698	100.00	1588.656	100.00
0.710	10.36	35.566	100.00	1782.502	100.00
0.796	13.76	39.905	100.00	2000.000	100.00
0.893	17.62	44.774	100.00		

Table D.2 Kaolinite XRD data and ICDD card.

<b>OBSERVED DATA</b>		<b>ICDD CARD 75-1593 (Kaolinite)</b>				
$d_{\text{obs}}$	$I/I_0$	$d$	$I/I_0$	$h$	$k$	$l$
7.019	85	7.131	100	0	0	1
4.403	8	4.463	11	0	2	0
4.312	15	4.361	31	-1	1	0
4.129	16	4.158	29	-1	-1	1
3.811	12	3.839	23	0	-2	1
3.695	9	3.729	12	0	2	1
3.538	100	3.566	42	0	0	2
2.547	10	2.544	7	1	3	0
2.479	14	2.488	12	2	0	0
2.369	14	2.377	6	0	0	3
2.328	23	2.326	16	-1	-1	3
2.279	15	2.286	23	1	3	1
1.980	9	1.988	6	1	-3	2
1.779	9	1.782	2	-1	1	4
1.660	13	1.667	2	-2	4	0
1.613	8	1.615	6	1	3	3
1.539	7	1.537	4	-1	3	4
1.484	18	1.484	12	-3	3	1

Table D.3 Kaolinite zeta potential data.

<b>pH</b>	<b>Zeta Potential (mV)</b>
2.10	-10.80
3.80	-14.20
4.20	-15.00
4.70	-17.20
5.50	-19.80
6.20	-22.00
7.35	-27.20
7.60	-28.10
8.00	-30.00
8.50	-32.10
9.10	-35.60
9.40	-37.60
10.20	-38.50



Table D.4 Particle size distribution data for quartz sample.

Size (micron)	Volume %	Size (micron)	Volume %	Size (micron)	Volume %
0.020	0.00	1.002	4.38	50.238	100.00
0.022	0.00	1.125	5.57	56.368	100.00
0.025	0.00	1.262	6.93	63.246	100.00
0.028	0.00	1.416	8.49	70.963	100.00
0.032	0.00	1.589	10.30	79.621	100.00
0.036	0.00	1.783	12.42	89.337	100.00
0.040	0.00	2.000	14.87	100.237	100.00
0.045	0.00	2.224	17.68	112.468	100.00
0.050	0.00	2.518	20.89	126.191	100.00
0.056	0.00	2.852	24.49	141.589	100.00
0.063	0.00	3.170	28.53	158.866	100.00
0.071	0.00	3.557	32.99	178.250	100.00
0.080	0.00	3.991	37.90	200.000	100.00
0.089	0.00	4.447	43.24	224.404	100.00
0.100	0.00	5.024	48.97	251.785	100.00
0.112	0.00	5.637	55.01	282.508	100.00
0.126	0.00	6.325	61.24	316.979	100.00
0.142	0.00	7.096	67.50	355.656	100.00
0.159	0.00	7.962	73.60	399.052	100.00
0.178	0.00	8.934	79.33	447.744	100.00
0.200	0.00	10.024	84.49	502.377	100.00
0.224	0.00	11.247	88.92	563.677	100.00
0.252	0.00	12.619	92.54	632.456	100.00
0.283	0.00	14.159	95.32	709.627	100.00
0.317	0.00	15.887	97.31	796.214	100.00
0.356	0.00	17.825	98.62	893.367	100.00
0.399	0.00	20.000	99.39	1002.374	100.00
0.448	0.04	22.440	99.81	1124.683	100.00
0.502	0.16	25.179	99.97	1261.915	100.00
0.564	0.48	28.251	100.00	1415.892	100.00
0.632	0.97	31.698	100.00	1588.656	100.00
0.710	1.61	35.566	100.00	1782.502	100.00
0.796	2.40	39.905	100.00	2000.000	100.00
0.893	3.32	44.774	100.00		

Table D.5 Quartz XRD data and ICDD card.

OBSERVED DATA		ICDD CARD 46-1045 (Quartz)				
$d_{\text{obs}}$	$I/I_0$	d	$I/I_0$	h	k	l
4.187	17	4.255	16	1	0	0
3.299	100	3.343	100	1	0	1
2.433	10	2.457	9	1	1	0
2.262	9	2.281	8	1	0	2
2.217	5	2.236	4	1	1	1
2.113	7	2.128	6	2	0	0
1.965	6	1.980	4	2	0	1
1.807	20	1.818	13	1	1	2
1.662	7	1.672	4	2	0	2
1.534	16	1.542	9	2	1	1
1.447	3	1.453	2	1	1	3
1.376	11	1.375	7	2	0	3

Table D.6 Quartz zeta potential data.

pH	Zeta Potential (mV)
2.30	-13.00
3.80	-15.00
4.60	-17.30
5.30	-19.00
6.90	-23.50
7.40	-26.00
8.40	-31.00
9.60	-33.00
10.10	-34.40

## CURRICULUM VITAE

### PERSONAL INFORMATION

**Surname, Name:** Gülsün Kılıç, Mehtap

**Nationality:** Turkish (TC)

**Date and Place of Birth:** 01 March 1976, Diyarbakır

**Marital Status:** Married

**Phone:** +90 312 281 13 59

**E-mail:** mgulsum@hotmail.com

### EDUCATION

Degree	Institution	Year of Graduation
PhD	METU Mining Engineering Department	2009
MS	METU Mining Engineering Department	2003
BS	Dicle University	1996

### WORK EXPERIENCE

Year	Place	Enrolment
1999-2000	Dicle University	Research Assistant
2000-Present	METU Mining Engineering Department	Research Assistant

### FOREIGN LANGUAGES

English

### PUBLICATIONS

1. Hoşten, Ç., Gülsün, M. (2002) Reactivity of limestones of different sources for flue gas desulfurization application, *International Mineral Processing Symposium, Kapadokya, Turkey*.

2. Hoşten Ç., Gülsün M. (2004) Reactivity of limestones from different sources of Turkey, *Minerals Engineering*, 17, 97-99.
3. Kılıç, M. G., Hoşten, Ç. (2008) The effect of grinding mode (dry/wet) and particle size on the reactivity of Kemerköy limestone for wet flue gas desulfurization application, *12<sup>th</sup> Conference on Environment and Mineral Processing, Ostrava, Czech Republic*, 199-203.
4. Kılıç, M. G., Hoşten, Ç. (2008) Electrocoagulation of clay suspensions, *The 11<sup>th</sup> International Mineral Processing Symposium, Antalya, Turkey*, 847-854.
5. Kılıç, M. G., Hoşten, Ç. (2009) Electrocoagulation of ultrafine quartz using aluminum electrodes, *The XIII<sup>th</sup> Balkan Mineral Processing Congress, Bucharest, Romania*, 785-791.
6. Kılıç, M. G., Hoşten, Ç., Demirci, Ş. (2009) A parametric comparative study of electrocoagulation and coagulation using ultrafine quartz suspensions, *Journal of Hazardous Material*, 171, 247-252.
7. Kılıç, M. G., Hoşten, Ç. (2010) A comparative study of electrocoagulation and coagulation of aqueous suspensions of kaolinite powders, *Journal of Hazardous Material*, In Press, Accepted Manuscript.